4
N-73-4
.3

US-CE-C

DISPOSITION OF THIS DOCUMENT MAY BE MADE BY ANY AGENCY OF THE UNITED STATES GOVERNMENT

TECHNICAL REPORT N-73-4

OPERATION DIAL PACK
PROJECT LN 305: EARTH MOTION AND STRESS MEASUREMENTS IN THE OUTRUNNING REGION

by

D. W. Murrell AD 762 172

LIBRARY BRANCH
TECHNICAL INFORMATION CENTER
US ARMY ENGINEER WATERWAYS EXPERIMENT STATION
VICKSBURG, MISSISSIPPI

May 1973

Sponsored by U. S. Army Engineer Division, Huntsville

Conducted by U. S. Army Engineer Waterways Experiment Station
Weapons Effects Laboratory
Vicksburg, Mississippi

APPROVED FOR PUBLIC RELEASE; DISTRIBUTION UNLIMITED

TECHNICAL REPORT N-73-4

OPERATION DIAL PACK
PROJECT LN 305: EARTH MOTION AND STRESS MEASUREMENTS IN THE OUTRUNNING REGION

by

D. W. Murrell AD 762 172

May 1973

Sponsored by U. S. Army Engineer Division, Huntsville

Conducted by U. S. Army Engineer Waterways Experiment Station
Weapons Effects Laboratory
Vicksburg, Mississippi

ARMY-MRC VICKSBURG, MISS

APPROVED FOR PUBLIC RELEASE; DISTRIBUTION UNLIMITED

W34
no. N-73-4
cop. 3

THE CONTENTS OF THIS REPORT ARE NOT TO BE USED FOR ADVERTISING, PUBLICATION, OR PROMOTIONAL PURPOSES. CITATION OF TRADE NAMES DOES NOT CONSTITUTE AN OFFICIAL ENDORSEMENT OR APPROVAL OF THE USE OF SUCH COMMERCIAL PRODUCTS.

76706

ABSTRACT

The objective of this project was to measure and analyze ground shock in the outrunning region produced by the 500-ton Dial Pack detonation.

Motions and stresses were measured at 645- and 840-foot ground ranges at depths of 1.5, 5, 10, and 20 feet. Thirty-one of thirty-two gages produced good records; time histories are included in Appendixes A and B, and frequency response spectra are presented in Appendix C.

Peak outrunning accelerations and velocities showed little attenuation over the instrumented range. The vertical peaks did not show any consistent relationship with depth, but the horizontal motions increased with depth. Since the deeper gages were close to the refractive layer, the motions emanating therefrom were stronger at depth. Vertical accelerations were greater than horizontal accelerations by a factor of 4, and vertical velocities showed a tenfold increase over horizontal velocities. Similar patterns of attenuation were noted for the displacements. However, due to additive effects of the airblast-induced motion, horizontal displacements were greater than vertical displacements by a factor of 1.9.

Airblast-induced accelerations and velocities were compared with the outrunning motions and were found to be dominant at the 1.5- and 5-foot depths. At the 10- and 20-foot depths, accelerations and velocities from the two sources were about equal.

PREFACE

This report describes an experiment conducted by the U. S. Army Engineer Waterways Experiment Station (WES) as a part of Operation Dial Pack. This study was sponsored by the Research Branch of the Huntsville Division, U. S. Army Corps of Engineers. Operation Dial Pack was conducted under the auspices of the Defense Nuclear Agency in conjunction with the Defence Research Board of Canada at the Defence Research Establishment, Suffield, Alberta, Canada.

This study, designated Project LN 305, was conducted under the supervision of Messrs. G. L. Arbuthnot, Jr., Chief, Weapons Effects Laboratory (WEL), L. F. Ingram, Chief, Physical Sciences Branch, and J. D. Day, Chief, Blast and Shock Section. Project personnel were Messrs. D. W. Murrell and C. M. Wright of the Blast and Shock Section, WEL, and L. T. Watson, G. P. Bonner, G. H. Williams, and S. Bell of the Instrumentation Services Division, WES.

COL Levi A. Brown, CE, and COL Ernest D. Peixotto, CE, were Directors of WES during the conduct of the investigation and the preparation of this report. Mr. F. R. Brown was Technical Director.

CONTENTS

CONVERSION FACTORS, BRITISH TO METRIC UNITS OF MEASUREMENT

British units of measurement used in this report can be converted to metric units as follows:

Multiply	By	To Obtain
feet	0.3048	meters
tons (2,000 pounds)	0.907185	megagrams
pounds (force) per square inch	0.6894757	newtons per square centimeter
pounds (mass) per cubic foot	16.0185	kilograms per cubic meter
feet per second	0.3048	meters per second

CHAPTER 1

INTRODUCTION

1.1 OBJECTIVE

The objective of this project was to measure and analyze ground shock in the outrunning region, i.e., the region where ground shock arrives prior to airblast. The results attained provide engineering information for analysis of the response of specific Army structures and will be used as input to drive analytical free-field and target-response computer codes.

1.2 BACKGROUND AND THEORY

Knowledge of the free-field ground shock environment experienced by structural systems is necessary in determining the required degree of hardness of the system and the requirements for shock-mounting vital components. The limited amount of outrunning ground shock data available indicates predominance of much lower frequencies than are generated by airblast. The implications of this on system components (either not shock-mounted at all or protected only against high-frequency shocks) are obvious and clearly indicate a need for further investigation. Outrunning ground shock data are especially needed for greater depths than previously instrumented in order to completely define the ground shock loading of structures in the region of interest.

Historically, outrunning ground motion was observed during the Tumbler-Snapper Series in 1952 and Upshot-Knothole in 1953, both conducted at the Nevada Test Site, and during numerous operations at Eniwetok Proving Ground such as Ivy, Castle, and Redwing (Reference 1). More recently, outrunning was observed during Operation Snowball at the Defence Research Establishment, Suffield (DRES), Alberta, Canada, where the shallow water table (at approximately a 23-foot[1] depth) produced a

---

[1] A table of factors for converting British units of measurement to metric units is presented on page 8.

strong refraction (Reference 2). As a follow-up to Snowball, the Distant Plain Event 6 (Reference 3) and Prairie Flat (Reference 4) experiments were planned, with documentation of outrunning motion as an objective--both from a phenomenological standpoint and in response to the great amount of interest expressed by persons concerned with target-response projects. Data acquired from these events emphasized the importance of outrunning motions, and inclusion of an Army structural response project in the outrunning region on Dial Pack dictated their documentation.

CHAPTER 2

PROCEDURE

2.1 DESCRIPTION OF TEST SITE

The charge for the Dial Pack Event was detonated on the Watching Hill Blast Range at DRES. Over the area instrumented for this project, the ground surface was essentially flat, with an elevation of approximately 2,160 feet above mean sea level. Geologically, the test site lies in the southern end of the Ross Depression, which apparently was once covered by a large lake. The soils to a depth of 200 feet are lacustrine deposits consisting of fairly uniform beds of clays and silts with occasional sand lenses (Reference 5).

Detailed accounts of the soil survey and testing for the Distant Plain Series are given in References 6 and 7. Briefly, Project 3.10, "Soil Sampling and Testing" (References 6 and 7), reported the upper 5.5 feet of soil at the Watching Hill Range to be a tan, sandy, silty clay. From this point to a depth of about 30 feet, the soil consisted of thin interbedded layers of sand, silt, and clay. The groundwater table was at a depth of approximately 23 feet.

2.2 INSTRUMENTATION LAYOUT

A total of 32 earth motion and stress gages, including 8 particle velocity gages, 16 accelerometers, and 8 soil stress gages, were installed 645 and 840 feet from GZ along an extension of the close-in ground shock project (Reference 8) gage line. Depths of 1.5, 5, 10, and 20 feet were instrumented. Since outrunning ground motion was expected to commence about 560 feet from GZ, based on results from Prairie Flat (Reference 4), this layout was adequate for assessing motions well into the outrunning region. The gage layout is shown in Figure 2.1, and a plan view is shown in Figure 2.2.

2.3 INSTRUMENTATION

2.3.1 Gages and Calibration. All particle motion gages used for

this project were commercially available units that have been proved reliable in numerous field and laboratory soil motion experiments. The particle velocity gages were the Sparton Southwest, Inc., Model 601. This gage was developed under a Defense Atomic Support Agency (now Defense Nuclear Agency) contract by Stanford Research Institute and modified by Sandia Corporation. The Model 601 is a variable-reluctance gage of the highly overdamped accelerometer design. Endevco Corporation semiconductor strain gage accelerometers were used at all locations.

The soil stress gages were designed and constructed by personnel of the U. S. Army Engineer Waterways Experiment Station (WES). Basically, the gage is a dual-diaphragm gage with two arms of a full semiconductor strain gage bridge bonded to each diaphragm. Reference 9 gives a detailed account of the development and testing of this gage.

All velocity gages were calibrated by using the free-fall-of-the-pendulum method. The accelerometers were dynamically calibrated with a dynamic shock calibrator of the impacting ball type. The soil stress gages were calibrated statically in a small pressure chamber.

All gages were electrically calibrated just prior to shot time by shunting a resistor across one arm of the bridge circuit, thus producing a circuit imbalance of a known motion or stress equivalence.

2.3.2 Gage Canisters and Placement. Those motion gages installed at a single location were mounted in an aluminum canister along with associated calibration and line-matching electronics. All canisters were potted with paraffin in order to resist water leakage and damp high-frequency vibrations. The final density of the assembled canister was about 100 pcf, which provided a good match with the in situ soil. Stress gages placed at the 1.5-foot depth were placed by hand, and soil was hand-tamped around them. The stress gages at depths of 5 feet and greater were cast in soil-cement plugs consisting of in situ soil, about 3 percent portland cement, and about 10 percent water to enable compaction.

In all cases, the instrument holes were backfilled with the same soil-cement mixture used for the stress gage plugs. This mixture, though perhaps slightly stiffer than the in situ soil, provided a good

density match and was considered to be a significant improvement over dry sand or cement grout for matching alluvial soils.

2.3.3 Recording System. Signal conditioning equipment for the accelerometers and stress gages consisted of operational amplifiers designed and built at WES. These are solid-state units having a frequency response of 0 to 10 kHz.

CEC 1-113B (System D) carrier-demodulator amplifiers were used with velocity gages. These units have a frequency response of 0 to 600 Hz. All data were recorded on CEC VR-3300 magnetic-tape recorders. Twelve channels of data were recorded on each machine, along with a reference track and a combination IRIG B time code/zero time track.

Signal conditioning and recording equipment was housed in a blast-resistant wooden bunker about 4,000 feet from GZ.

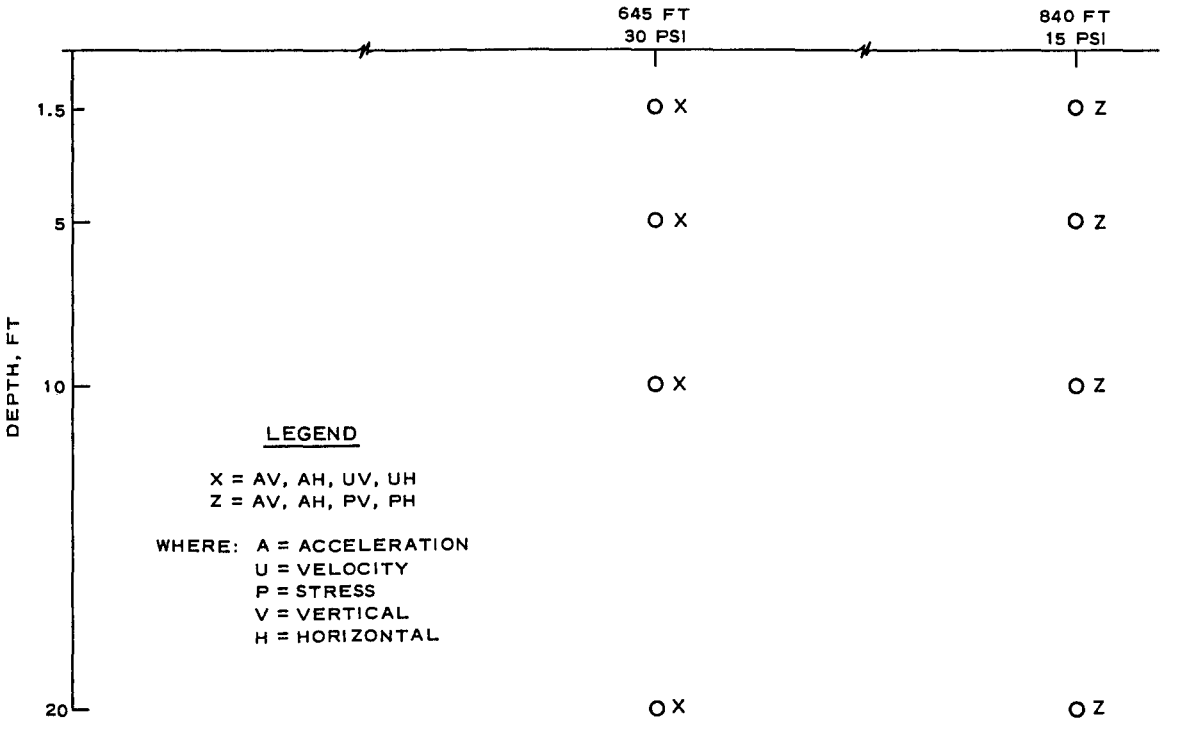

Figure 2.1 Instrumentation layout.

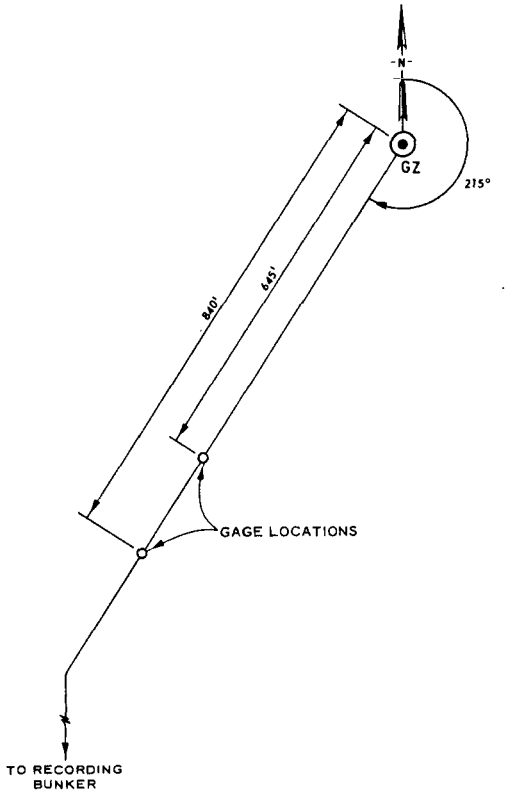

Figure 2.2 Plan view of project layout.

CHAPTER 3

RESULTS AND DISCUSSION

3.1 INSTRUMENT PERFORMANCE

Thirty-one of the thirty-two gages installed for this project were operable at shot time, and all yielded high-quality data. The one inoperable gage was the horizontal accelerometer at the 840-foot range and 10-foot depth. It had developed electrical leakage and was disconnected preshot.

The calibration and sequence-initiating signals from DRES control were properly received, and all equipment operated as programmed.

3.2 DATA REDUCTION

The ground shock data for this project were recorded in the form of analog magnetic tapes. These were converted to a digital format on the WES high-speed, analog-to-digital conversion facility at a rate of 24 kHz for the acceleration data and 12 kHz for velocity and stress data. The digitized records were then processed on the WES digital computer where integrations and base-line shifting were accomplished. Computer outputs were then plotted to a page-size format.

3.3 GENERAL GROUND SHOCK CHARACTERISTICS

Ground motions lasted more than 2 seconds. The records were marked by several distinct pulse arrivals of importance, beginning with the onset of outrunning motion and continuing with the airblast-induced pulse and subsequent oscillatory motions.

Figure 3.1 shows horizontal and vertical velocity records from the 645-foot range and 5-foot depth, which are representative of motion records in the outrunning region at DRES. The very early-time motions are shown on a greatly expanded time scale in the insets for each record in order to facilitate identification of the several peaks. The initial motion at this location, Peak 1 on the insets, is the true outrunning motion, producing an outward- and upward-directed motion prior to

arrival of the airblast, and is attributable to energy refracted through the saturated material below the water table. Peak 2 on the insets is the airblast-induced motion, directed outward and downward. It is easily identifiable by its direction, its characteristic single spike, and its time correlation with passage of the airblast. The airblast arrival at the surface at this location occurred 169 msec after detonation (Reference 10). Peak 3 in Figure 3.1 (upward and outward) is more difficult to identify. Its initial occurrence at about 200 msec is too early to indicate the direct transmission of energy through the overburden, since velocities in excess of 3,000 ft/sec would be required. This, then, points toward a refractive origin, similar to Peak 1, with the result being that the airblast-induced motion is superposed on a refracted wave train. Individual components of this wave train may have different sources, i.e., refracted directly induced energy or refracted airblast-induced energy, but positive association of particular peaks with a specific source is not possible. The refracted wave train will consequently be treated simply as an entity with an early outrunning portion and subsequent peak.

The fourth peak identified in Figure 3.1 is the major excursion of a series of oscillations that commences 600 to 800 msec after detonation. This peak is of considerably longer duration than earlier motions, and, although it is quite prominent on velocity and displacement records, accelerations associated with it are low. The origin of this motion is unknown, although it is probably a Rayleigh-type disturbance. This peak will consequently be referred to herein simply as late-time ground motion.

An effect of these several peaks is that displacement data are, in many cases, a conglomerate of motion from several sources, and the individual contributions may not be identifiable. For example, in Figure 3.1a, Peaks 1, 2, and 3 combine to give a single, rather smooth outward displacement pulse.

Table 3.1 is a data summary listing peak measured values, integrals, and arrival times for all motion gages. Three peaks are tabulated for accelerations, i.e., the initial outrunning motion, the

airblast-induced motion, and the secondary refracted motion. Four peaks are listed for velocities, including the three motions mentioned above plus the late-time motion. For displacements, the initial positive motion (upward or outward), the initial negative motion (downward or inward), and the positive late-time motion are tabulated. In several instances, one or more of the integration peaks is not discernible or is not reliable due to base-line instability on the gaged parameter. Table 3.2 presents a similar listing of soil stress measurements.

Time histories for all data are presented in Appendix A, where records are shown for 4 seconds after detonation. The initial 500 msec of each record is shown on an expanded time scale in Appendix B, which facilitates inspection of the early-time wave structure.

Most of the data show a burst of noise 2.75 seconds after detonation. This corresponds to airblast arrival at the recording bunker.

3.4 ARRIVAL TIMES

Shock arrival times were established for all successfully recorded gages. Propagation velocities for the initial arrivals at the 20-foot depth were calculated as 5,100 and 5,150 ft/sec for the 645- and 840-foot ranges, respectively. These values are about 16 percent lower than the 6,100-ft/sec velocities noted during Operation Prairie Flat (Reference 4) but are in much better agreement with the 5,500-ft/sec velocities reported for Distant Plain, Event 6 (Reference 3). These velocities correspond to the shock propagation velocity of the saturated layer (below about 23 feet) and are indicative of a shock front refracted along this layer.

Figure 3.2 is a shock front profile based on the arrival times and propagation velocities mentioned above and on arrival times of ground shock (Reference 8) and airblast (Reference 10) measured during other projects. Development of refracted energy is obvious; as the airblast itself slows, the refracted pulse overtakes and passes the airblast. The refracted shock produces an upward moving wave in the overburden, and at a ground range of about 600 feet the refracted motion is the initial disturbance at the ground surface. The onset of outrunning conditions

thus occurs at a horizontal range of 600 feet. At all points beyond this range, the initial motions are due to upward and outward directed refracted energy. Outrunning conditions were observed at a horizontal range of about 560 feet for an identical Prairie Flat (Reference 4) experiment. The difference in the ranges, i.e., 600 feet for this study and 560 feet for the Prairie Flat study, is attributable to the somewhat higher Prairie Flat transmission velocities mentioned previously and to the uncertainties introduced by the large spacing of the instrument grid for both events.

3.5 OUTRUNNING ACCELERATION

Figure 3.3 shows typical vertical and horizontal acceleration-time histories for the 840-foot range and 1.5- and 20-foot depths. Outrunning motions are evident on all four records, with initial motions occurring more than 100 msec prior to the arrival of airblast. Airblast-induced accelerations are dominant at the 1.5-foot depth for both vertical and horizontal motions. At the 20-foot depth, however, the airblast-induced motions have attenuated in magnitude to the extent that the airblast-induced and outrunning motions are roughly equal. The airblast-induced peak also broadens significantly at the 20-foot depth. The wave train characteristic of outrunning motions is readily apparent on the acceleration-time plot for the 20-foot depth; it is also present on the plot for the 1.5-foot depth, but is somewhat less discernible due to the larger scales.

3.5.1 Vertical Acceleration. Peak upward outrunning acceleration is plotted versus range in Figure 3.4 for both the Dial Pack and Prairie Flat Events. Data scatter precludes a quantitative statement about attenuation with range, although there is a trend toward attenuation. In addition, there is a lack of effect of depth, which is noticeable in Figure 3.4. Data acquired at a particular depth were neither systematically high nor low. Vertical outrunning accelerations from the two events correlate quite well, indicating reproducibility of this aspect of outrunning motions.

Figure 3.5 shows peak upward outrunning accelerations plotted

versus scaled range ($R/kt^{1/3}$) for the Dial Pack and Prairie Flat Events (conducted at DRES) and for the Mineral Rock, Mine Under, and Mine Ore Events of the Mine Shaft Series. All data are plotted undifferentiated as to depth. The striking feature in Figure 3.5 is the significantly greater magnitude (by a factor of about 5) of the DRES data. This suggests an inverse relationship between vertical acceleration and compressional wave velocity since the ratio of compressional velocities for DRES alluvium to the Mine Shaft granite is about 1 to 10. This inverse relationship has been suggested previously (Reference 1).

3.5.2 Horizontal Acceleration. Peak horizontal outward outrunning accelerations are plotted versus range in Figure 3.6. A lack of attenuation with depth is obvious; in fact, the accelerations increase with depth. Since the energy is being refracted, it was expected that it would be stronger nearer the source, i.e., those gages nearer the refractive boundary should record the stronger signal.

Generally, horizontal outrunning accelerations were significantly smaller than the vertical accelerations, i.e., by an average factor of about 4. This is in contrast with data in Reference 1 for the outrunning region. In Reference 1, equality of horizontal and vertical components is suggested. In spite of this inconsistency, agreement between Dial Pack and Prairie Flat horizontal accelerations is considered good.

3.6 OUTRUNNING PARTICLE VELOCITY

Figures 3.7 and 3.8 show the vertical and horizontal particle velocity-time histories for the 645-foot range. The onset of airblast-induced motion is denoted on all traces. In the case of vertical velocities (Figure 3.7), the relative influence of the airblast pulse diminishes with increasing depth and is nearly nonexistent at the 20-foot depth. Also, a double peak in the outrunning pulse occurs as depth increases. It should not be inferred that the double peak is absent at the shallow depths, but rather that the airblast pulse is possibly masking the second peak at these locations.

The most significant feature exhibited by the horizontal velocities (Figure 3.8) is a secondary refracted outward pulse that follows

the airblast-induced motion (Peak 3 in Figure 3.1). It is quite dominant at the 1.5- and 5-foot depths and is still significant at the 10-foot depth. It has declined in importance, however, at the 20-foot depth where it is about one-third of the airblast-induced peak. Generally, the true outrunning horizontal motions show the same tendency toward multiple peaks that the vertical motions showed.

3.6.1 Vertical Velocity. Figure 3.9 presents peak upward outrunning particle velocity versus range for both the Dial Pack and Prairie Flat Events. The spread of data at each instrumented ground range is small, with the data maxima at each range being on the order of 50 percent greater than the minima. The velocity data show a general decrease with increasing range, although the decay is not steep. Prairie Flat data at the 560-foot range are noted to depart from the curve. This is a function of location, since the 560-foot range was very nearly the point of onset of outrunning motion and outrunning peaks were clipped by airblast-induced motion before they had fully developed.

3.6.2 Horizontal Velocity. Peak outward horizontal velocities are plotted versus range in Figure 3.10. There is considerably greater spread in these data than was found for the vertical velocities. This is at least partially attributable to a velocity variation with depth. The velocity data tend to increase with depth, much as the horizontal accelerations did. Attenuation with range is not well-defined. In fact, in Figure 3.10 attenuation with range appears to be negligible. Horizontal outrunning velocities from the two events are again in good agreement. Horizontal velocities are consistently less than the vertical velocities by an average of about 9. Thus, a much greater difference in horizontal and vertical velocities was observed than was observed for horizontal and vertical accelerations.

3.6.3 Late-Time Motions. The late-time ground motion mentioned in Section 3.3 is of considerable significance due to its magnitude and duration. This motion is not readily shown to be a part of the outrunning wave train due to its considerable separation in time from the initial portions of the record. However, it is evidently not associated with the airblast, so it will be discussed along with outrunning motions

in this report. This motion is especially predominant on the horizontal motion plots and, in several cases, is the largest peak occurring in the entire time history. It takes the form of damped oscillations with a period of about 0.67 second (frequency $\approx$ 1.5 Hz). Figure 3.11 is a plot of the initial outward peak of late-time horizontal velocity versus distance for data recorded for this project, LN 305, and the close-in ground motion project, LN 302 (Reference 8). This motion was first noted at a range of 270 feet from GZ and had become well-developed at a range of 425 feet. Its magnitude shows no discernible dependency on distance or depth over the range instrumented. Precision of the data points is good, and a value of 0.4 ft/sec $\pm$ 30 percent covers all the data points for ranges of 400 to 840 feet and depths of 1.5 to 20 feet.

3.7 DISPLACEMENT

Figure 3.12 is a plot of both horizontal and vertical initial displacement peaks versus range. A direct relationship between peak data and depth can be noted, with the largest peaks generally occurring at the greatest depths. No significant decrease in either parameter was observed with increasing range; however, the range of distances covered by the data was relatively small. The maximum and minimum displacements occurred at the 645-foot range for both horizontal and vertical measurements. Horizontal peaks varied from 0.019 to 0.051 foot, and vertical peaks ranged from 0.012 to 0.024 foot.

The horizontal peaks are consistently higher than their vertical counterparts by an average factor of 1.9. The initial vertical displacement peaks are positive (upward), however, and are due to purely outrunning pulses. Thus, a direct empirical comparison of initial horizontal and vertical displacements would be of limited value.

3.8 SOIL STRESS

Soil stress measurements for this project were made only at the 840-foot range. Both horizontal and vertical outrunning stresses are plotted in Figure 3.13 to define the stress field with depth and to compare horizontal and vertical stresses. As shown in Figure 3.13, the

vertical stress peaks increased with increasing depth. The nearly five-fold scatter in horizontal measurements, coupled with the random nature of the data when differentiated by depth, limits the usefulness of peak stress data per se, although the waveforms themselves are of significance. This scatter was caused by the extreme sensitivity of stress measurements to gage placement procedures, especially backfilling of instrument holes. A comparison of vertical and horizontal stress and particle velocity waveforms is presented in Figure 3.14. The stress and velocity waveforms correlate well, with the stress records showing generally higher frequency components due to the inherent higher frequency capabilities of the stress gage. For the vertical data, it is noted that the airblast produces a negative (downward) velocity, which appears as a positive (compressive) stress. All pulses are positive (outward and compressive) for horizontal data.

3.9 AIRBLAST-INDUCED MOTIONS

3.9.1 Airblast-Induced Acceleration. Peak downward airblast-induced vertical accelerations are generally correlatable with the airblast overpressure directly above the point of interest. This correlation has been found to hold true both at higher pressures (superseismic conditions) and in the region of outrunning motion. Figure 3.15 presents the ratio of near-surface acceleration to overpressure as a function of overpressure for several events at DRES. The ratio decreases with increasing pressure. This trend is normal and extends well into the superseismic region. For example, at the 2,000-psi overpressure level, the average ratio is about 0.4 (Reference 4). In Figure 3.15, one of the Dial Pack data points seems rather low, resulting in the anomaly of greater acceleration at greater distance. Further evidence of anomalous behavior at this location is noted when attenuation of vertical acceleration with depth is considered. At the overpressure levels of interest (≈10 to 30 psi), data from previous events (Reference 4) indicate that vertical accelerations at the 5-foot depth will average 30 percent of those at the 15-foot depth. For the 645-foot range on Dial Pack, the ratio was 58 percent. These factors point

toward a lower acceleration at the 645-foot range and 1.5-foot depth than might be expected.

Horizontal airblast-induced accelerations did not attenuate significantly with either range or depth. For example, with one exception, these accelerations were all between 1.65 and 3.0 g. This is a significantly smaller data spread than occurred with vertical measurements. Horizontal airblast-induced accelerations were only a small portion of the vertical peaks for the 1.5- and 5-foot depths, but at the 10- and 20-foot depths, they were about half of the vertical motions.

3.9.2 Comparison of Outrunning and Airblast-Induced Accelerations. Figure 3.16 presents a comparison of outrunning and airblast-induced vertical accelerations. The dominance of airblast-induced motions is apparent at the 1.5-foot depth. At increasing depth, however, attenuation of the airblast-induced acceleration diminishes its relative effect until at a depth of 10 feet and greater the outrunning and airblast-induced motions are virtually equal. Apparently, range does not affect the motions, as ratios for the two ranges are essentially identical at the 5-, 10-, and 20-foot depths. The previously mentioned anomaly at the 645-foot range and 1.5-foot depth produced a lower airblast motion, and hence a higher ratio. Therefore, the 0.12 ratio for the 840-foot range and 1.5-foot depth is probably the more representative.

3.9.3 Airblast-Induced Velocity. Figure 3.17 is a correlation of vertical, near-surface, airblast-induced velocities in the outrunning region with overpressure. The trend toward lower ratios of motion to pressure noted for accelerations is much less pronounced in this figure. This is consistent with data published for previous events at DRES (Reference 4), which indicated that decay of the motion-to-overpressure ratios at higher pressures was more pronounced for accelerations than for velocities. This is a result of the greater sensitivity of acceleration to the shape of the air shock, which varies with pressure.

Horizontal airblast-induced velocities are easily correlated with the vertical velocities. Ratios of horizontal to vertical airblast-induced velocities varied from 0.037 to 1.04, with a very consistent

increase with depth. Two factors contribute to this: first, the vertical velocities attenuate rapidly with depth, and second, the horizontal velocities increase with depth, possibly due to reinforcement of the airblast motion by a portion of the outrunning wave train.

3.9.4 Comparison of Outrunning and Airblast-Induced Velocities. Figure 3.18 presents a comparison of outrunning and airblast-induced vertical velocities. Here the airblast-induced motion is again predominant (see Figure 3.16) at the shallow depths, as indicated by ratios of 0.4 and 0.5. The two motions are about equal at depths of 10 feet and greater, however. The dominance of the airblast-induced motion appears to be more pronounced at the 645-foot range, where, for the 1.5-, 5-, and 10-foot depths, ratios are uniformly smaller. This indicates a more rapid decay with distance of airblast, or at least its associated motions, than of the outrunning pulse.

TABLE 3.1 SUMMARY OF MOTION MEASUREMENTS, PROJECT LN 305

Range	Depth	Parameter and Orientation[a]	Motion Arrival Time	Peak Acceleration			Peak Velocity				Peak Displacement		
				Initial Outrunning	Airblast-Induced	Secondary Refracted	Initial Outrunning	Airblast-Induced	Secondary Refracted	Late-Time Motion	Initial Positive	Initial Negative	Late-Time Positive
feet	feet		msec	g	g	g	ft/sec	ft/sec	ft/sec	ft/sec	feet	feet	feet
645	1.5	AV	145.0	+4.9[b]	-13.7[b]	+3.1	+0.87	-2.18	+0.36	+0.65	0.011	c	c
		UV	145.0	--	--	--	+0.70	-1.65	+0.48	+0.04	0.010	c	c
		AH	145.0	+0.5	+1.65	+1.2	+0.08	+0.08	+0.52	+0.44	0.019	0.096	d
		UH	145.9	--	--	--	+0.07	+0.07	+0.40	+0.41	0.034	0.037	0.04
645	5	AV	138.0	+4.8	-8.0	+7.2	+0.80	-1.71	+0.46	+0.17	0.016	c	c
		UV	138.9	--	--	--	+0.56	-1.0	+0.28	+0.10	0.011	0.01	0.013
		AH	139.0	+0.5	+2.4	+1.2	+0.06	+0.38	+0.49	+0.53	0.029	0.082	0.016
		UH	138.3	--	--	--	+0.05	+0.21	+0.35	+0.35	0.025	0.037	0.028
645	10	AV	134.0	+6.3	-6.4	+6.5	+1.0	-1.1	+0.30	+0.08	0.017	0.012	c
		UV	136.8	--	--	--	+0.47	-0.63	+0.10	+0.05	0.008	0.01	0.007
		AH	136.0	+0.8	+3.0	+0.9	+0.12	+0.61	+0.44	+0.48	0.051	0.053	0.031
		UH	137.2	--	--	--	+0.075	+0.32	+0.25	+0.31	0.024	0.028	0.028
645	20	AV	126.0	+3.44	-3.76	+1.44	+0.77	-0.89	e	+0.25	0.024	c	c
		UV	130.2	--	--	--	+0.35	-0.42	e	+0.08	0.010	0.011	0.010
		AH	126.0	+0.75	+2.70	+0.45	+0.12	+0.85	+0.30	+0.33	0.050	0.029	0.029
		UH	131.1	--	--	--	+0.06	+0.51	+0.19	+0.27	0.023	0.021	0.028
840	1.5	AV	177.0	+2.7	-20.0	+3.5	+0.63	-1.20	+1.12	c	c	c	c
		AH	177.0	--	+5.5	--	c	c	c	c	c	c	c
840	5	AV	173.2	+2.3	-4.3	+2.2	+0.51	-0.74	+0.24	c	0.019	c	--
		AH	174.0	+0.5	+2.3	+0.90	+0.04	+0.40	+0.33	+0.42	0.021	0.072	e
840	10	AV	170.8	+3.9	-3.0	+0.8	+0.64	-0.42	e	+0.12	0.022	0.014	c
		AH[f]	--	--	--	--	--	--	--	--	--	--	--
840	20	AV	164.0	+4.2	-3.70	+2.3	+0.58	-0.69	e	c	0.017	c	c
		AH	163.9	+0.58	+1.73	+0.91	+0.15	+0.72	+0.29	+0.34	0.034	0.025	0.040

[a] A = acceleration, U = velocity, V = vertical, H = horizontal.
[b] A plus sign denotes upward, outward motion; a minus sign denotes downward, inward motion.
[c] Peak not reliable due to base-line shift.
[d] No negative peak indicated.
[e] No positive peak indicated.
[f] No data--gage was inoperable at shot time.

EG&G 6709

TABLE 3.2 SUMMARY OF STRESS MEASUREMENTS, PROJECT LN 305

Range	Depth	Parameter and Orientation[a]	Arrival Time	Peak Stress	
				Outrunning	Airblast-Induced
feet	feet		msec	psi	psi
840	1.5	PV	176.8	0.63	2.7
		PH	177.1	0.3	1.2
	5	PV	174.5	--	1.0
		PH	174.5	0.80	1.90
	10	PV	170.5	0.95	1.1
		PH	172.0	0.17	0.8
	20	PV	162.8	1.3	1.7
		PH	163.1	0.6	1.3

[a] P = stress, V = vertical, H = horizontal.

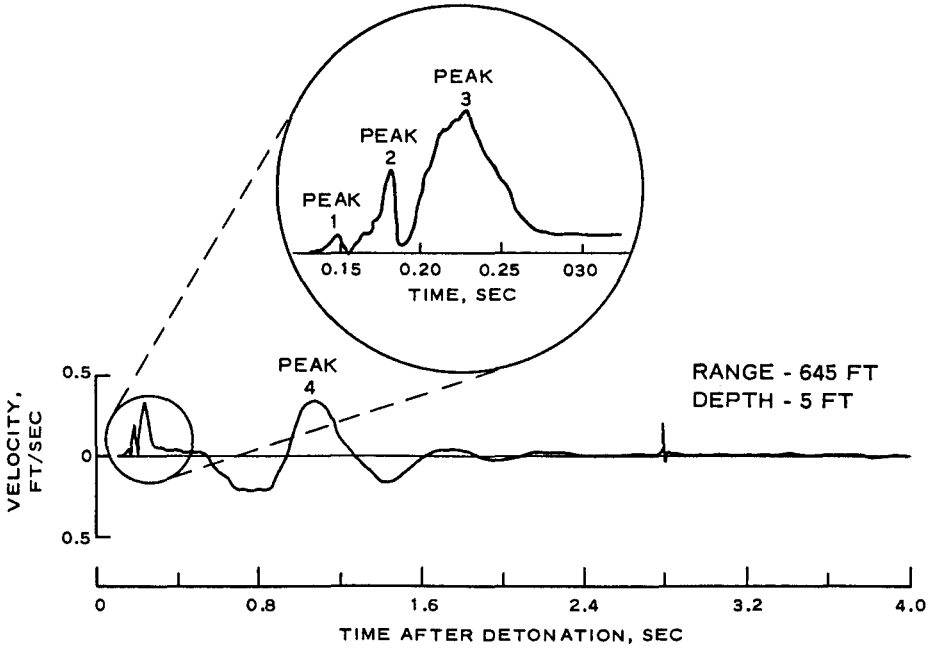

a. HORIZONTAL VELOCITY

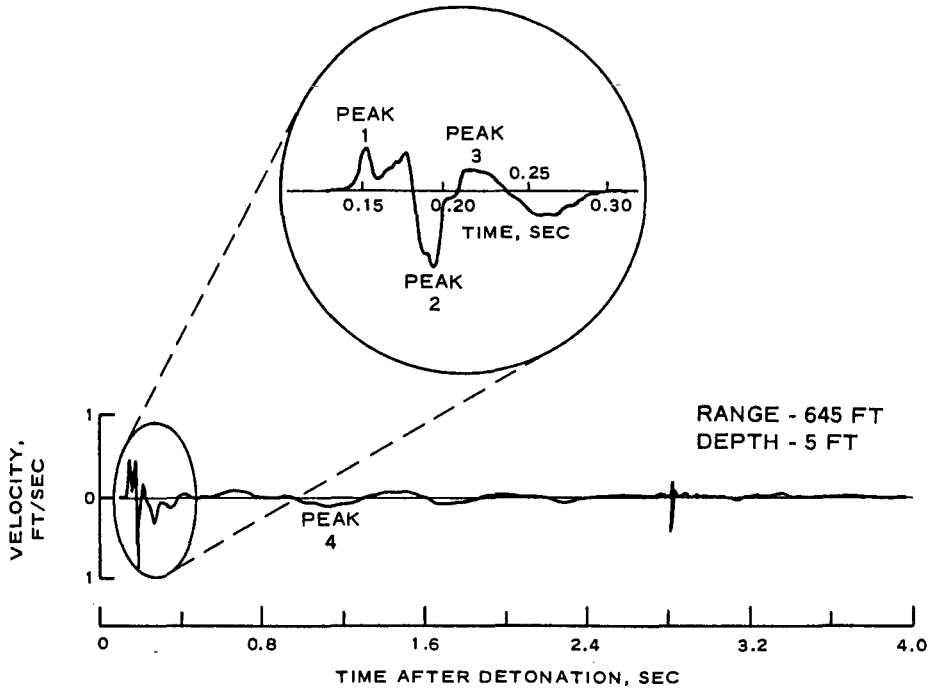

b. VERTICAL VELOCITY

Figure 3.1 Typical particle velocity waveforms.

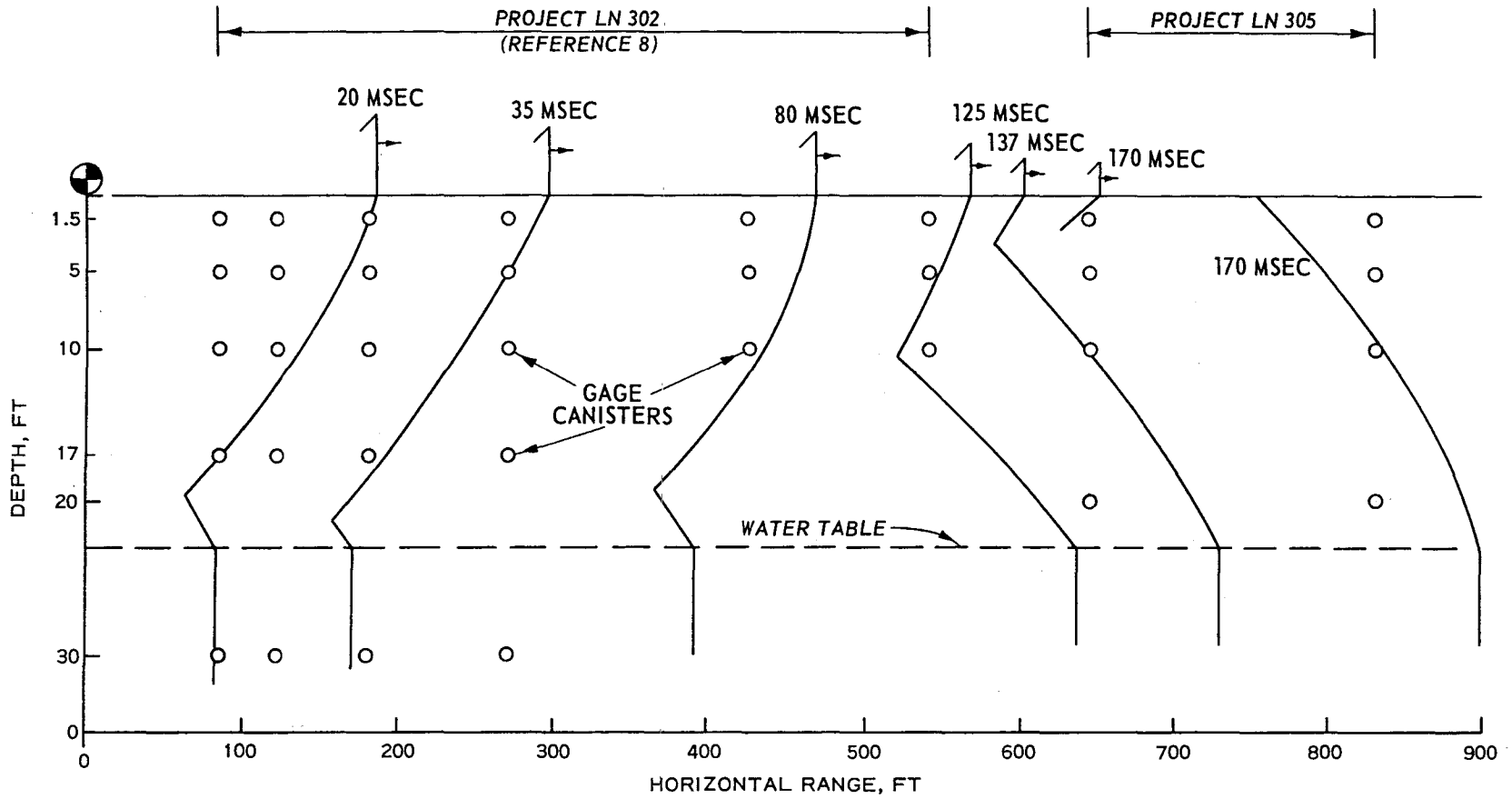

Figure 3.2 Shock front profile.

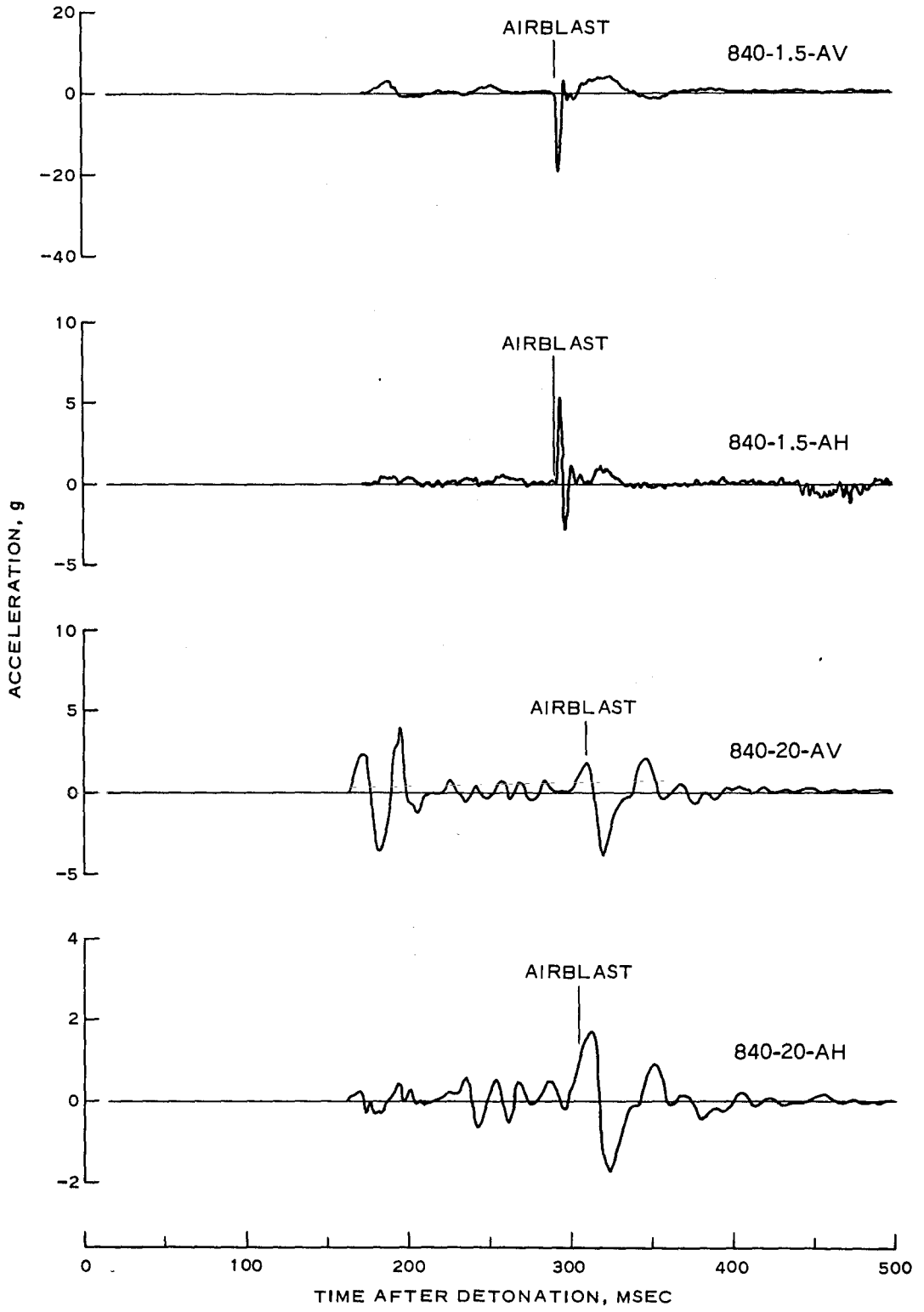

Figure 3.3 Typical acceleration-time histories for 840-foot range and 1.5- and 20-foot depths.

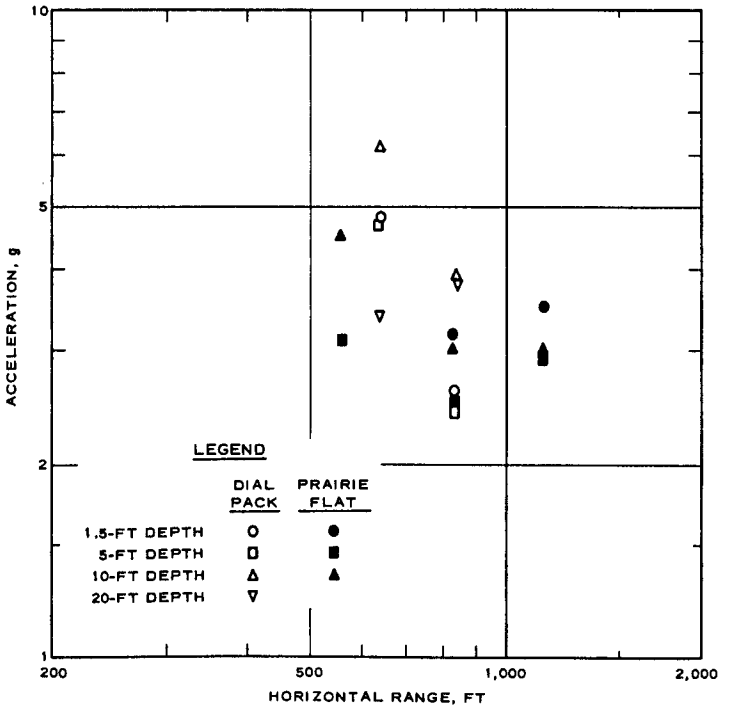

Figure 3.4 Peak upward outrunning acceleration versus horizontal range.

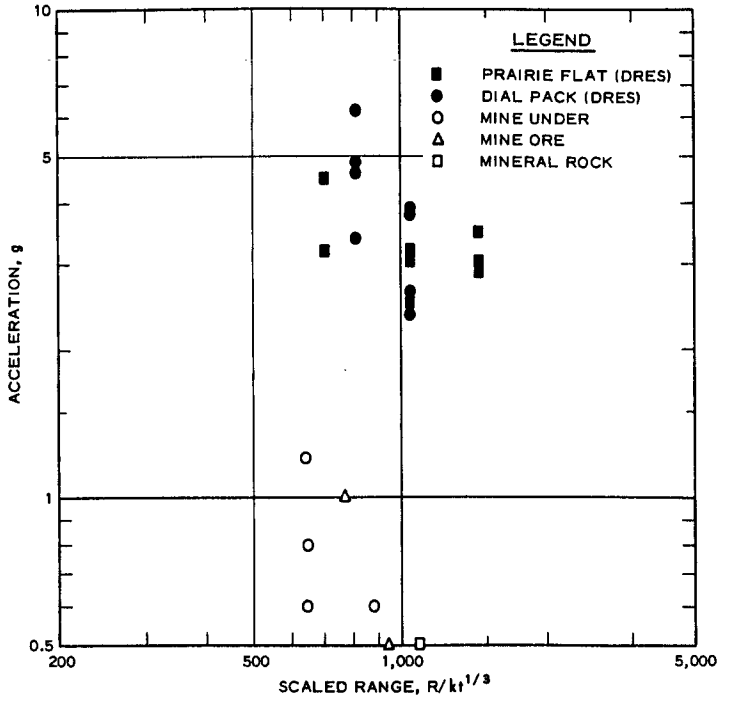

Figure 3.5 Peak upward outrunning acceleration versus scaled range ($R/kt^{1/3}$).

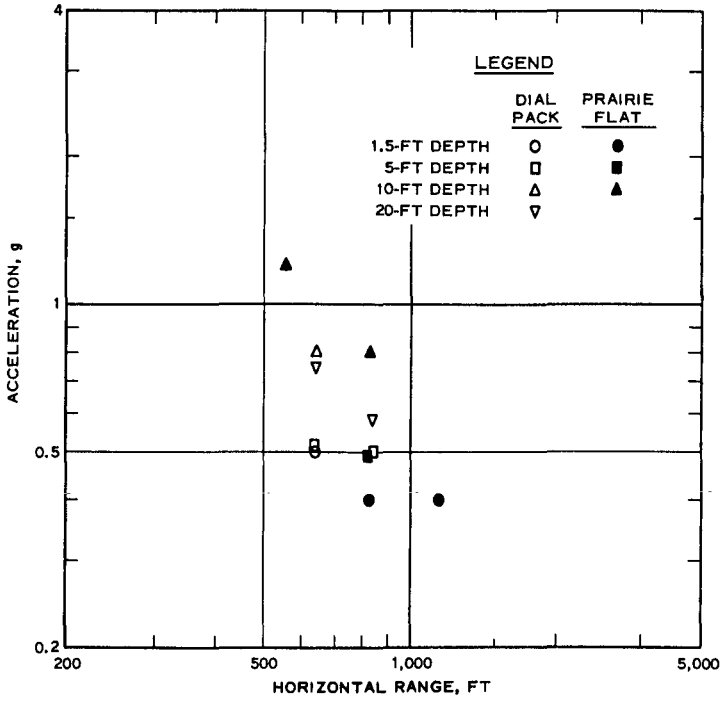

Figure 3.6 Peak outward outrunning acceleration versus horizontal range.

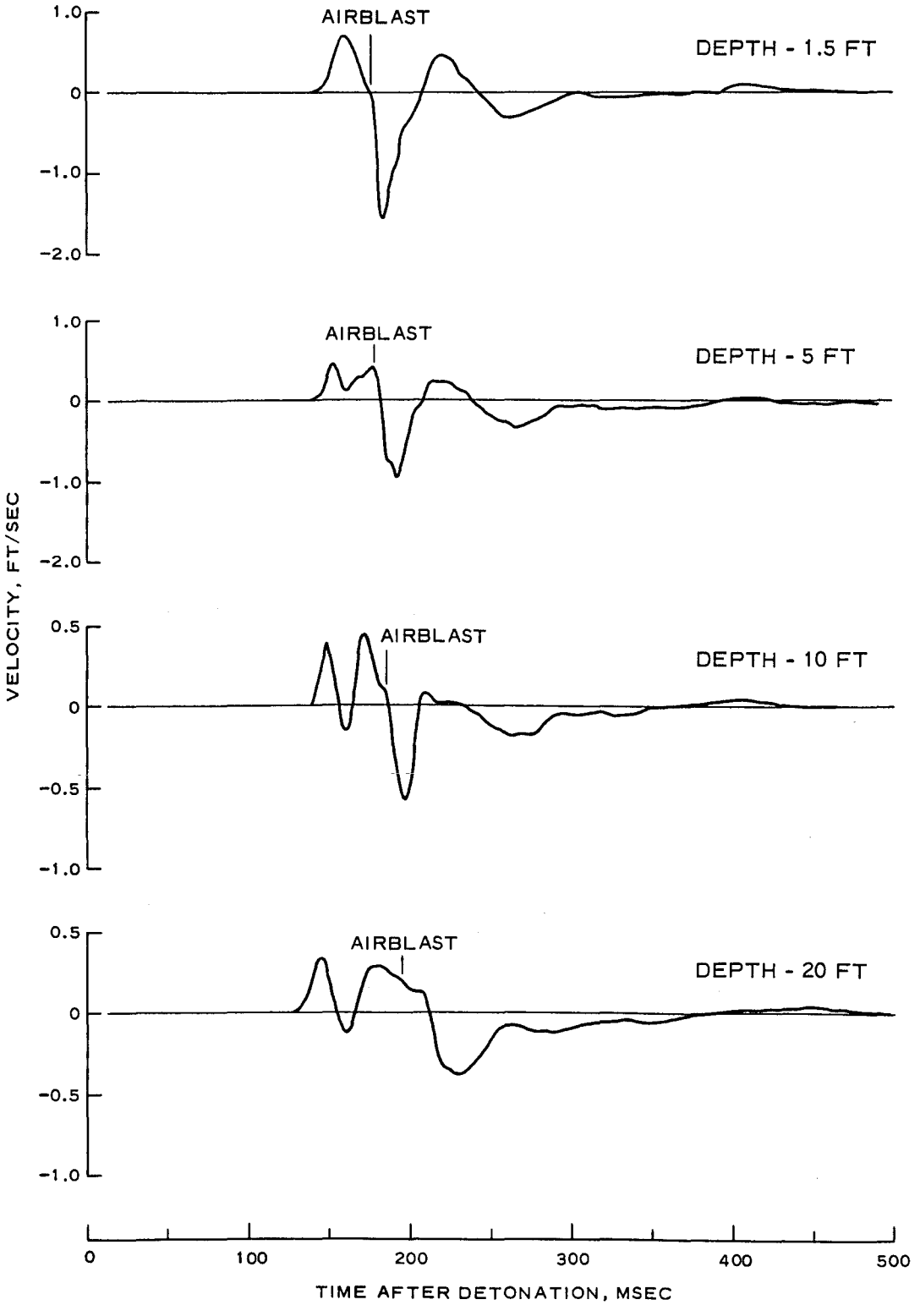

Figure 3.7 Vertical velocity-time histories for 645-foot range.

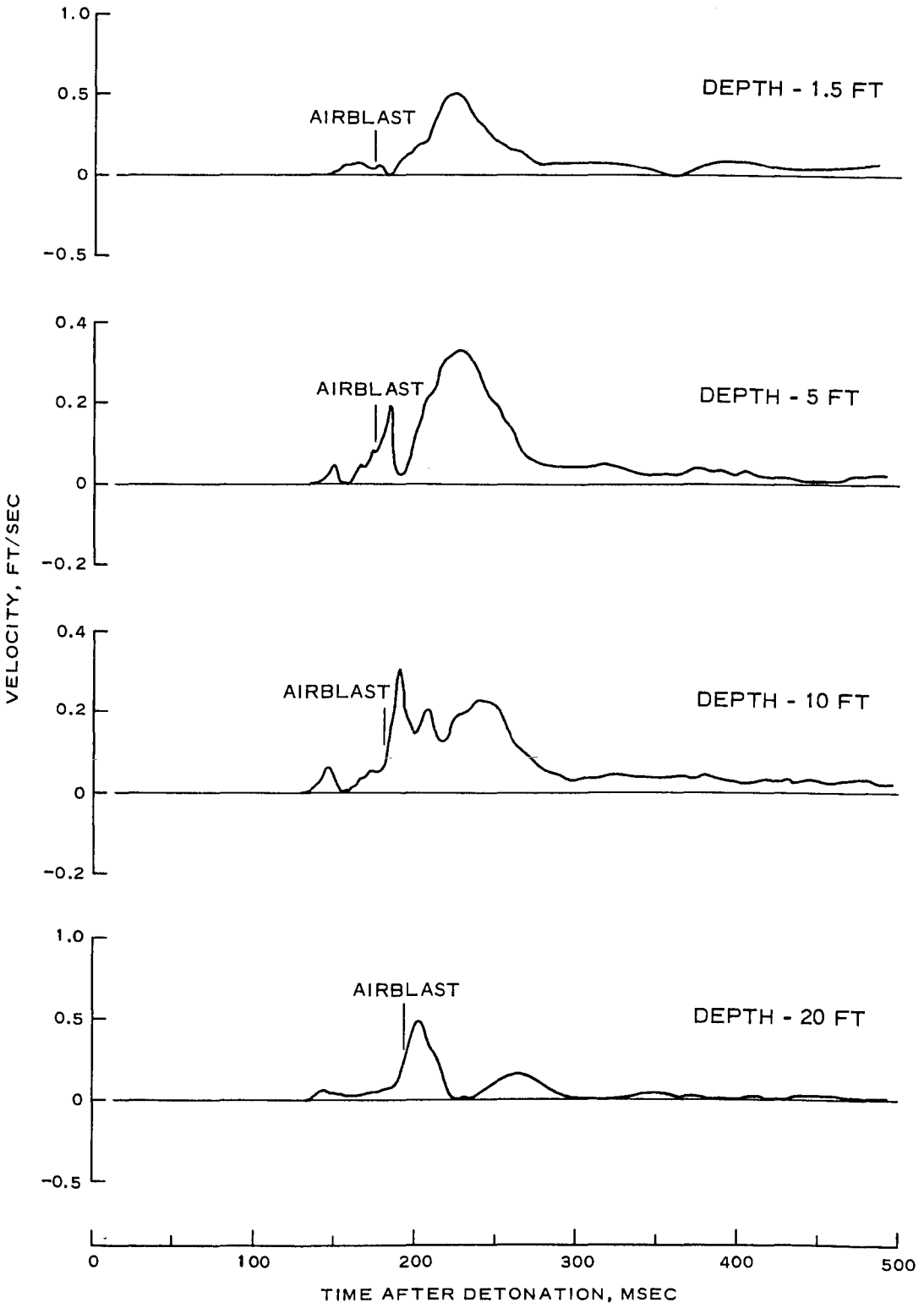

Figure 3.8 Horizontal velocity-time histories for 645-foot range.

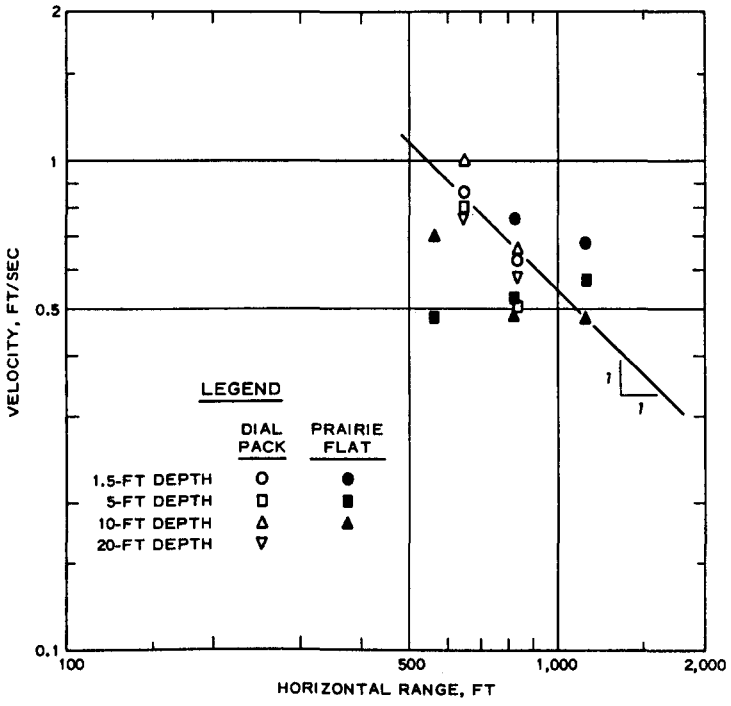

Figure 3.9 Peak upward outrunning particle velocity versus horizontal range.

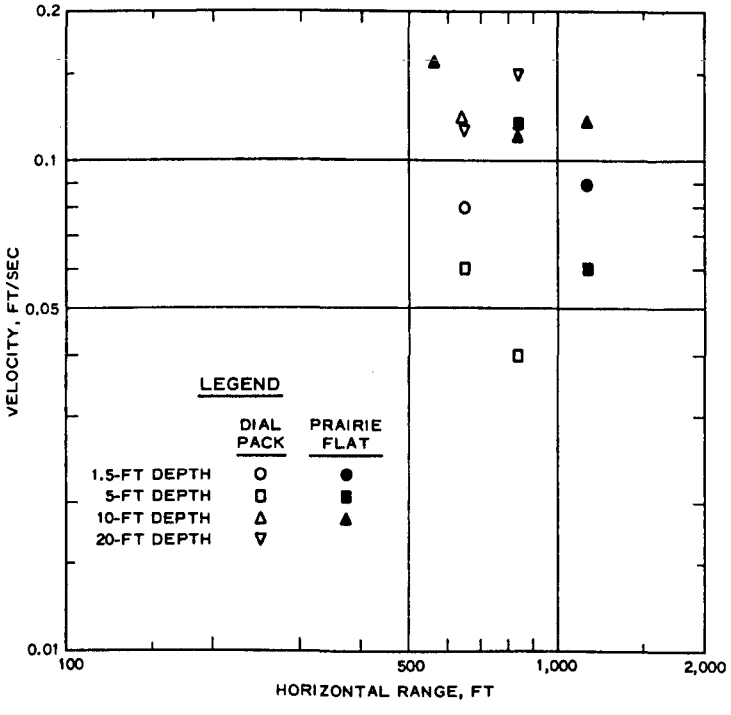

Figure 3.10 Peak outward outrunning velocity versus horizontal range.

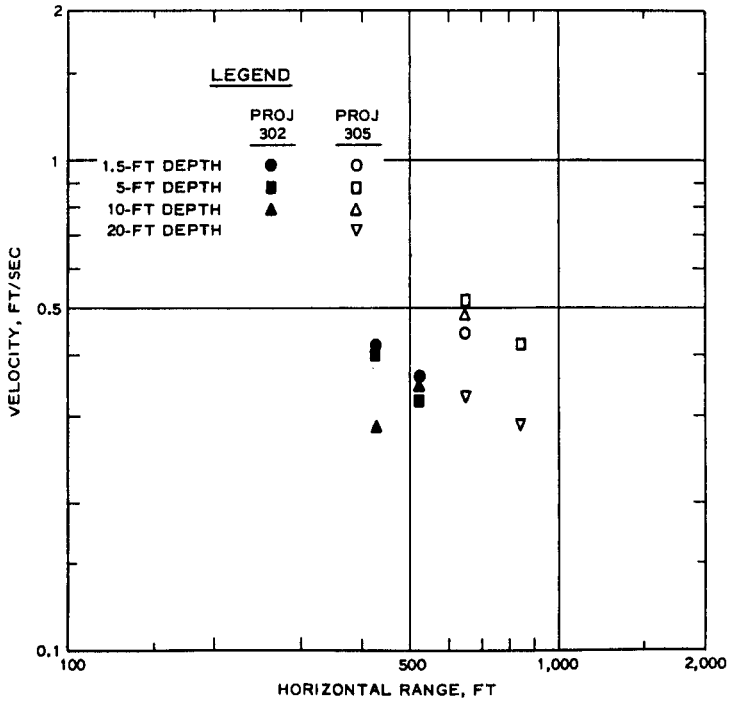

Figure 3.11 Late-time horizontal velocity versus horizontal range.

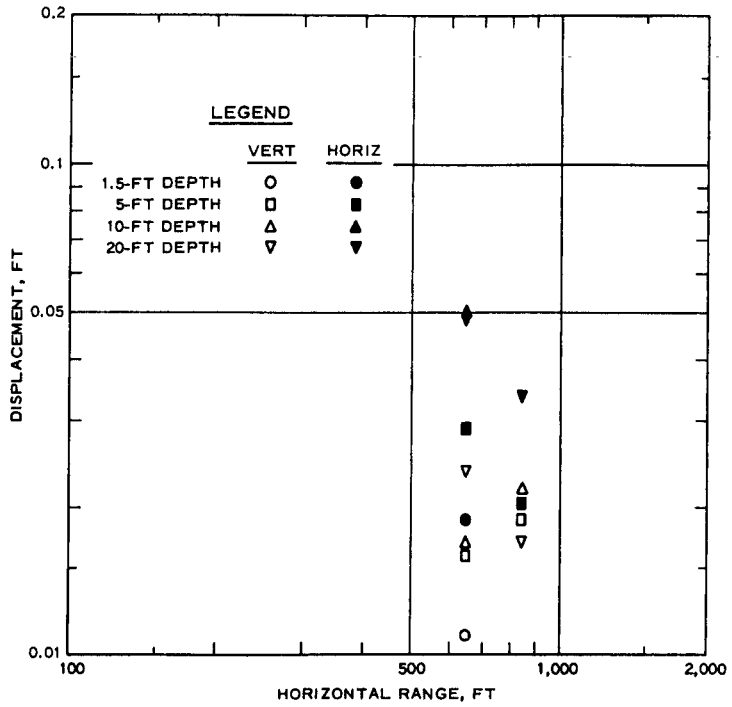

Figure 3.12 Peak initial horizontal and vertical displacements versus horizontal range.

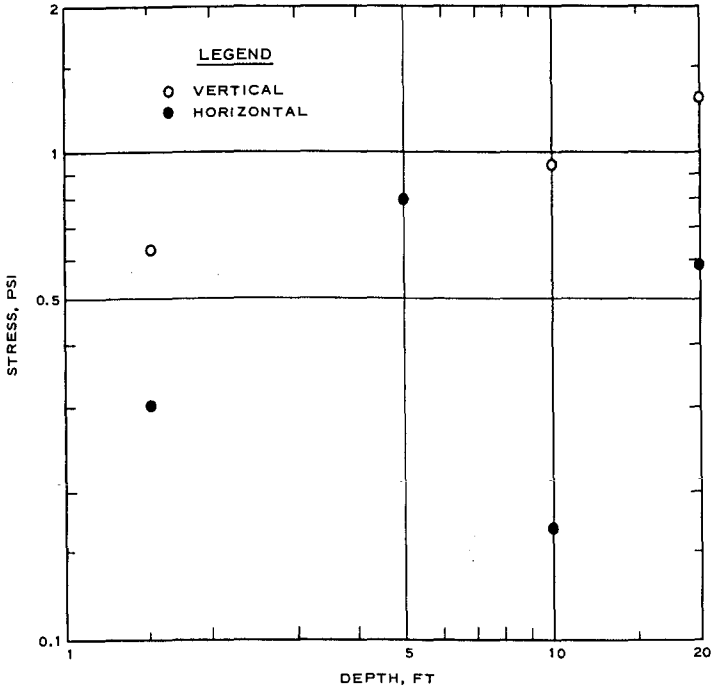

Figure 3.13 Peak horizontal and vertical outrunning stresses versus depth, 840-foot range.

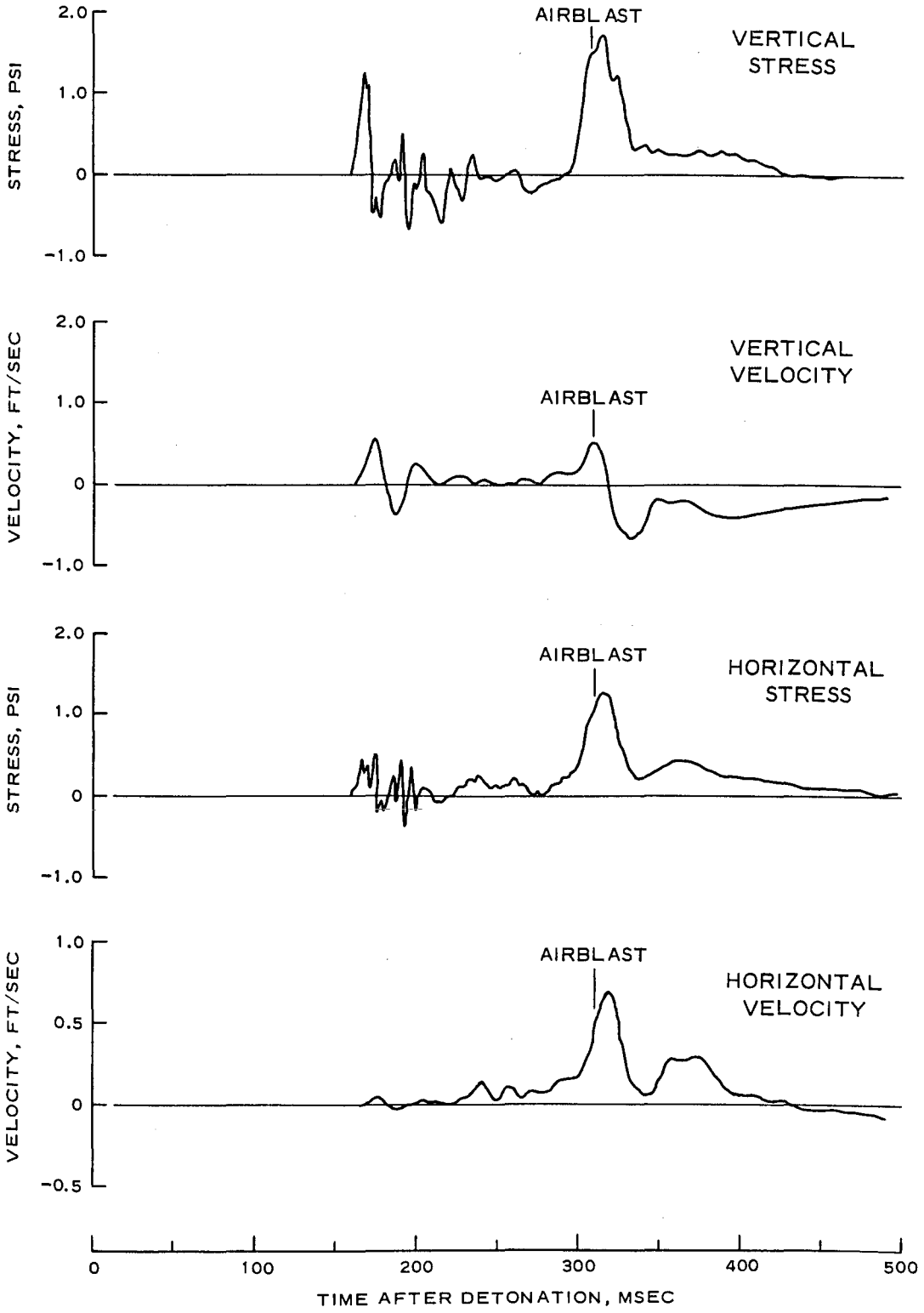

Figure 3.14 Comparison of stress and particle velocity waveforms for 840-foot horizontal range and 20-foot depth.

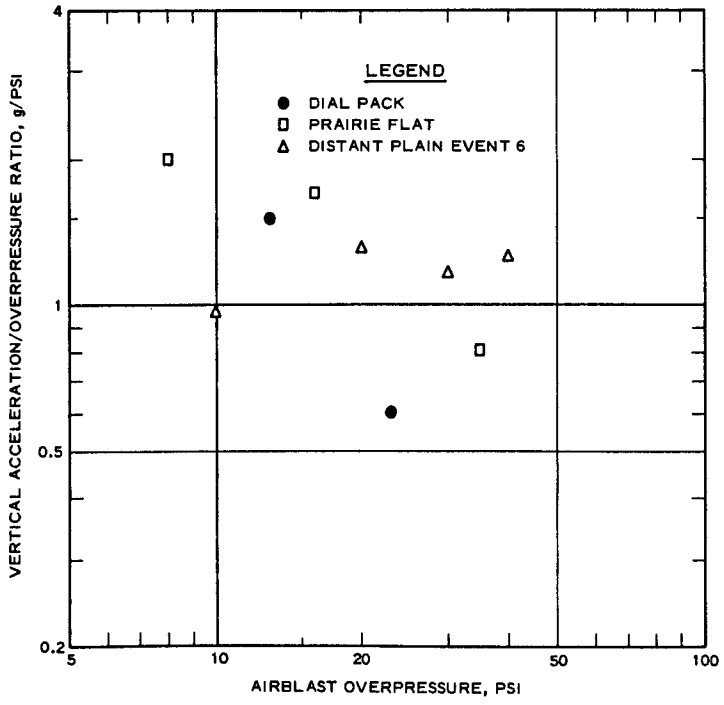

Figure 3.15 Correlation of vertical acceleration data with airblast overpressure for 1.5-foot depth.

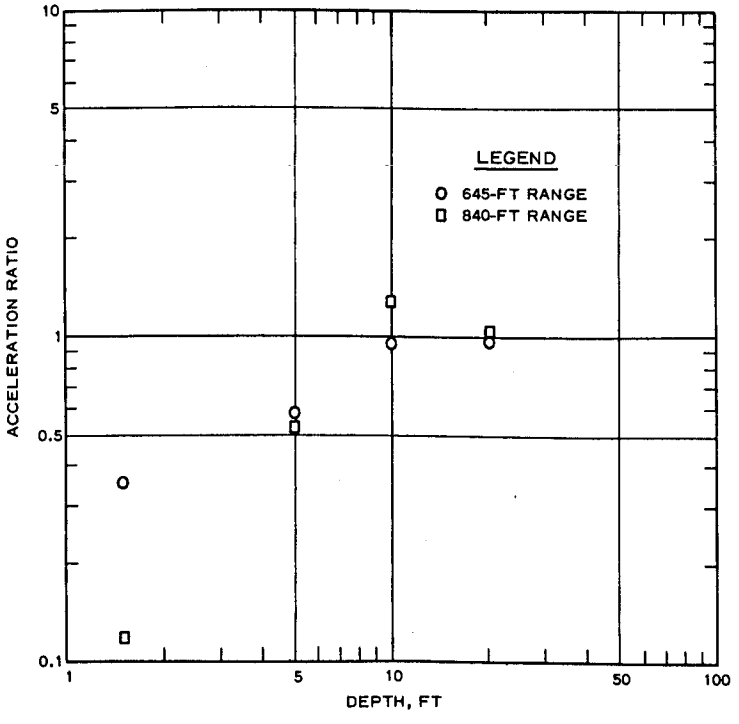

Figure 3.16 Ratio of outrunning vertical acceleration to airblast-induced vertical acceleration versus depth.

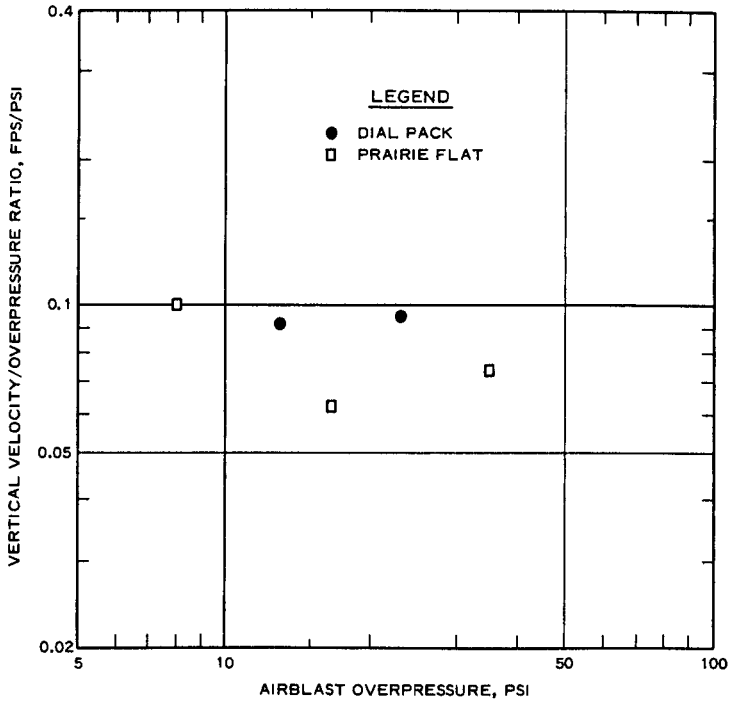

Figure 3.17 Correlation of vertical velocity data with airblast overpressure for 1.5-foot depth.

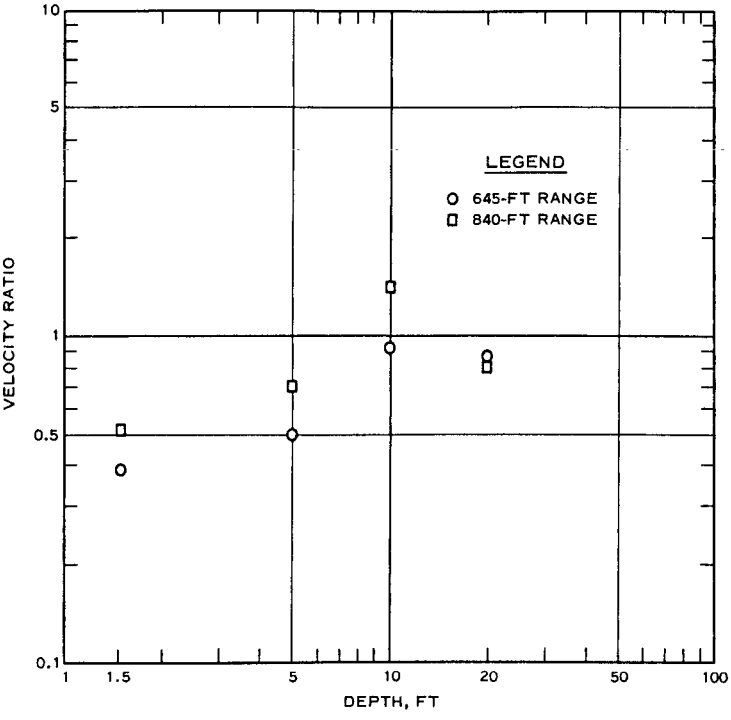

Figure 3.18 Ratio of outrunning vertical velocity to airblast-induced vertical velocity versus depth.

CHAPTER 4

CONCLUSIONS

4.1 INSTRUMENT PERFORMANCE

Overall performance of the instrumentation system for Dial Pack was excellent. Thirty-one of the thirty-two gages installed yielded high-quality data for a data recovery of 97 percent. Therefore, data presented herein are considered to reliably reflect the ground motion environment in the outrunning region for the DRES site and will provide the needed input for code calculations.

4.2 MOTION AND STRESS MEASUREMENTS

Arrival times were obtained for all operable gages and were used primarily to construct a shock front profile. From this profile, which also included data from the close-in measurements of Project LN 302 (Reference 8), it was determined that the onset of outrunning motions occurred at about the 600-foot range, which compared favorably with the onset of outrunning motions at the 560-foot range for the Prairie Flat experiment. The small difference can be attributed in part to the large-grid gage layout, which makes precise determination of the onset of outrunning difficult.

Peak outrunning accelerations attenuated only slightly, if at all, with increasing distance over the short range instrumented. Vertical outrunning accelerations were unaffected by depth (to 20 feet), but horizontal peaks tended to increase with depth. Vertical outrunning accelerations were greater than the horizontal accelerations by a factor of about 4, which is a departure from data in Reference 1 which predict roughly equal horizontal and vertical motions in the outrunning region.

Vertical accelerations were compared with those obtained in granite on a scaled-range basis, and were found greater for the DRES events by a factor of 5. This difference is supported by the greater seismic velocity in granite and the predicted inverse proportionality of acceleration and seismic velocity. Both horizontal and vertical Dial

Pack accelerations compared closely with the Prairie Flat accelerations.

Outrunning peak particle velocities (occurring prior to airdrop) followed much the same pattern as the accelerations, with a slow decay of peak values with increasing range. Horizontal measurements again increased somewhat with depth. Vertical particle velocity peaks exceeded the horizontal peaks by an average factor of 9, a considerably greater difference than was noted for accelerations.

Peak initial positive (outward and upward) displacements varied from 0.019 to 0.951 foot for horizontal measurements and 0.012 to 0.024 foot for vertical measurements. The greater horizontal displacements are contrary to the trend established for acceleration and velocity data, and are due to inclusion of an airblast-induced component in the initial outward peak displacement. Both outward and upward displacements increased with depth, but neither were consistently affected by increasing horizontal range.

Measurements of soil stress were a part of the outrunning program for the first time and were successful. Although peak values showed some scatter, the waveforms showed characteristics that could be related to velocity waveforms.

Airblast-induced motions were correlated with overpressure, and, on this basis, were found to be in good agreement with Prairie Flat motions. A comparison of vertical airblast-induced and outrunning motions showed that, for both accelerations and velocities, the airblast-induced portion was dominant at the 1.5- and 5-foot depths. At the 10- and 20-foot depths, however, the two signals were nearly equal.

REFERENCES

1. F. M. Sauer, G. B. Clark, and D. C. Anderson; "Nuclear Geoplosics; Part Four, Empirical Analysis of Ground Motion and Cratering"; DASA 1285(IV), May 1964; Stanford Research Institute, Menlo Park, California; Unclassified.

2. D. W. Murrell; "Operation Snowball, Project 3.6--Earth Motion Measurements"; Technical Report No. 1-759, March 1967; U. S. Army Engineer Waterways Experiment Station, CE, Vicksburg, Mississippi; Unclassified.

3. D. W. Murrell; "Distant Plain Events 6 and 1A, Project 3.02A, Earth Motion and Stress Measurements"; Technical Report N-70-14, September 1970; U. S. Army Engineer Waterways Experiment Station, CE, Vicksburg, Mississippi; Unclassified.

4. D. W. Murrell; "Operation Prairie Flat; Project LN 302: Earth Motion and Stress Measurements"; Technical Report N-72-2, February 1972; U. S. Army Engineer Waterways Experiment Station, CE, Vicksburg, Mississippi; Unclassified.

5. A. J. Hendron, Jr.; "Correlation of Operation Snowball Ground Motions with Dynamic Properties of Test Site Soils"; Miscellaneous Paper No. 1-745, October 1965; U. S. Army Engineer Waterways Experiment Station, CE, Vicksburg, Mississippi; Unclassified.

6. J. L. Gatz; "Soil Survey and Support Activities, Operation Distant Plain Event 6"; Miscellaneous Paper No. 3-990, April 1968; U. S. Army Engineer Waterways Experiment Station, CE, Vicksburg, Mississippi; Unclassified.

7. J. G. Jackson, Jr., and J. E. Windham; "Preliminary Report, Operation Distant Plain, Event 6, Soil Property Investigation for Project 3.10, Soil Sampling and Testing"; December 1967; prepared by U. S. Army Engineer Waterways Experiment Station, CE, Vicksburg, Mississippi, for Defense Atomic Support Agency, Washington, D. C.; Unclassified.

8. D. W. Murrell; "Earth Motion and Stress Measurements, Operation Dial Pack, Project LN 302"; (In preparation); U. S. Army Engineer Waterways Experiment Station, CE, Vicksburg, Mississippi; Unclassified.

9. J. K. Ingram; "Development of a Free-Field Soil Stress Gage for Static and Dynamic Measurements"; Technical Report No. 1-814, February 1968; U. S. Army Engineer Waterways Experiment Station, CE, Vicksburg, Mississippi; Unclassified.

10. J. H. Keefer and others; "Event Dial Pack; Preliminary Report"; DASA 2606-I, May 1971; Defense Atomic Support Agency, Information and Analysis Center; Santa Barbara, California; For Government Agencies Use Only.

APPENDIX A

STRESS- AND MOTION-TIME HISTORIES

Table A.1 presents a data processing summary, and Figures A.1 through A.31 present stress- and motion-time histories for the 31 gages that were operating at shot time. Gage locations and types are listed in the title of each figure. Gage numbers give, in order, the range from ground zero in feet, the depth of the gage in feet, and the gage type (A, U, or P) and orientation (V or H). A is acceleration, U is velocity, and P is stress; V and H are vertical and horizontal, respectively. For example, 645-1.5-AV is a vertically oriented accelerometer placed 645 feet from ground zero at a depth of 1.5 feet.

TABLE A.1 DATA PROCESSING SUMMARY

No filter.

Range	Depth	Gage	Digitizing Rate	Base-Line Shift		Response Spectra Available
				Type[a]	Amount[b]	
feet	feet		kHz			
645	1.5	AV	24	CB	-0.32	Yes
		UV	12	SB	-0.2	No
		AH	24	CB	+1.48	Yes
		UH	12	SB	+0.07	No
645	5	AV	24	CB	+1.32	No
		UV	12	SB	-0.07	No
		AH	24	CB	-5.5	No
		UH	12	SB	-0.03	No
645	10	AV	24	CB	+3.08	Yes
		UV	12	None	--	No
		AH	24	CB	-2.52	Yes
		UH	12	SB	0.025	No
645	20	AV	24	CB	-1.42	No
		UV	12	SB	-0.05	No
		AH	24	CB	+0.26	No
		UH	12	SB	-0.13	No
840	1.5	AV	24	CB	+5.1	Yes
		AH	24	CB	-4.0	Yes
		PV	12	None	--	No
		PH	12	None	--	No
840	5	AV	24	CB	-9.5	No
		AH	24	CB	-1.72	No
		PV	12	None	--	No
		PH	12	None	--	No
840	10	AV	24	CB	-0.7	No
		AH[c]	--	--	--	No
		PV	12	None	--	No
		PH	12	None	--	No
840	20	AV	24	CB	+1.16	Yes
		AH	24	CB	-0.06	Yes
		PV	12	None	--	No
		PH	12	None	--	No

[a] CB is a constant base-line shift, and SB is a sloping base-line shift.
[b] Amount of correction to velocity trace at 4-second time. A plus sign indicates that the base line shifted in a positive direction, i.e. old base line on plots lies below new base line.
[c] Gage was inoperable at shot time.

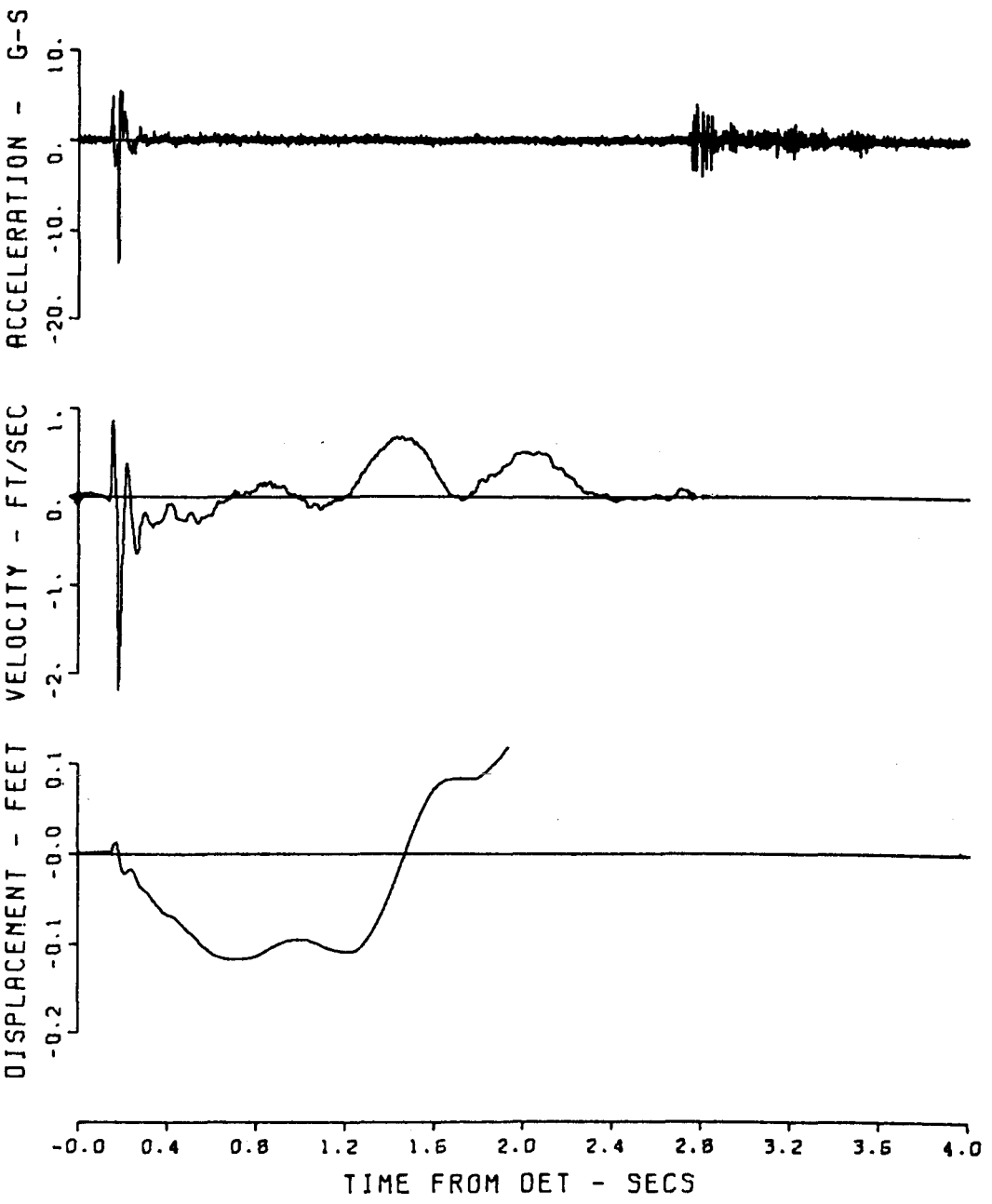

Figure A.1 Motion-time histories, Event Dial Pack, Gage 645-1.5-AV.

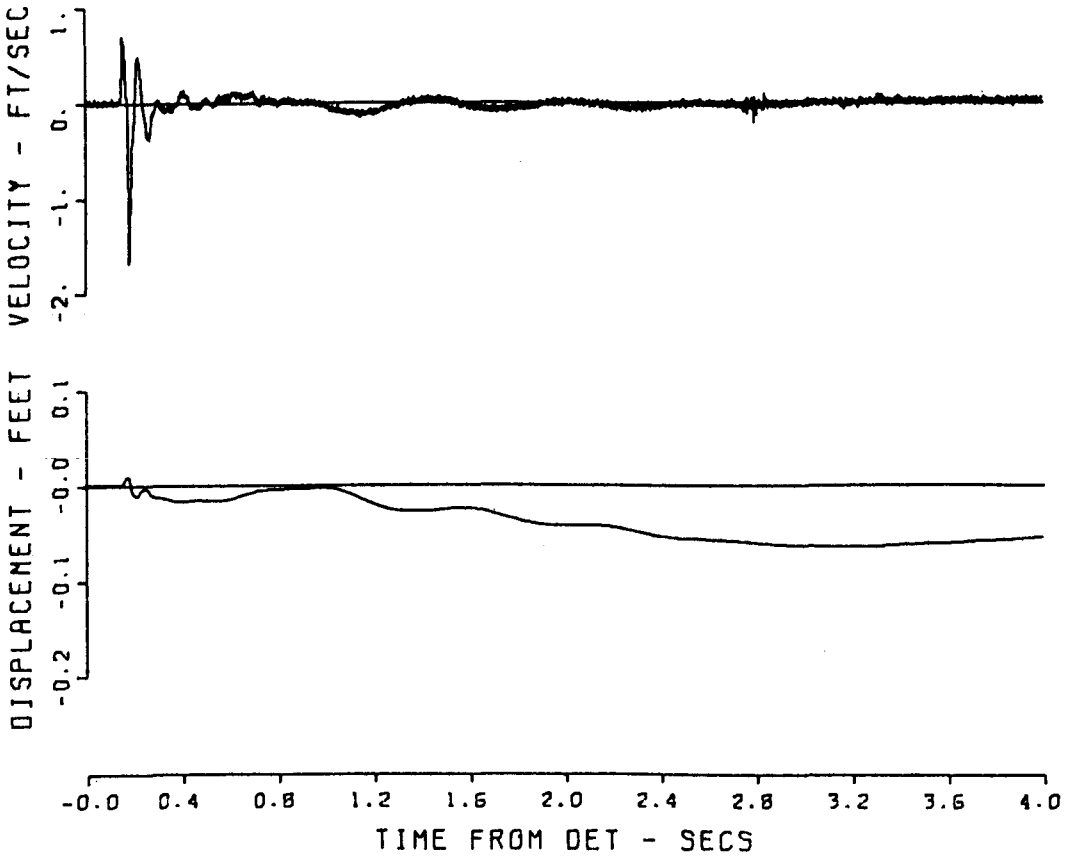

Figure A.2 Motion-time histories, Event Dial Pack, Gage 645-1.5-UV.

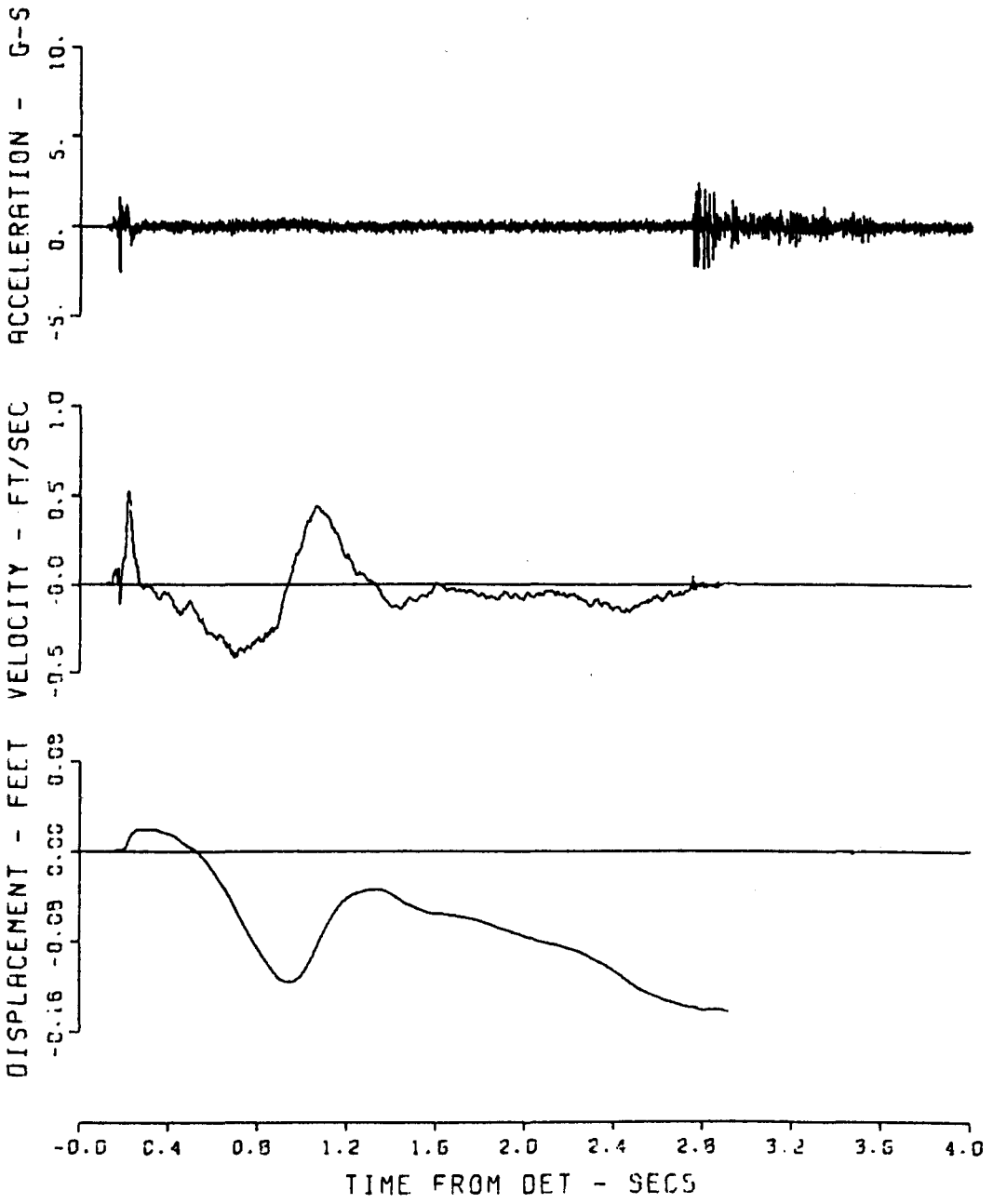

Figure A.3 Motion-time histories, Event Dial Pack, Gage 645-1.5-AH.

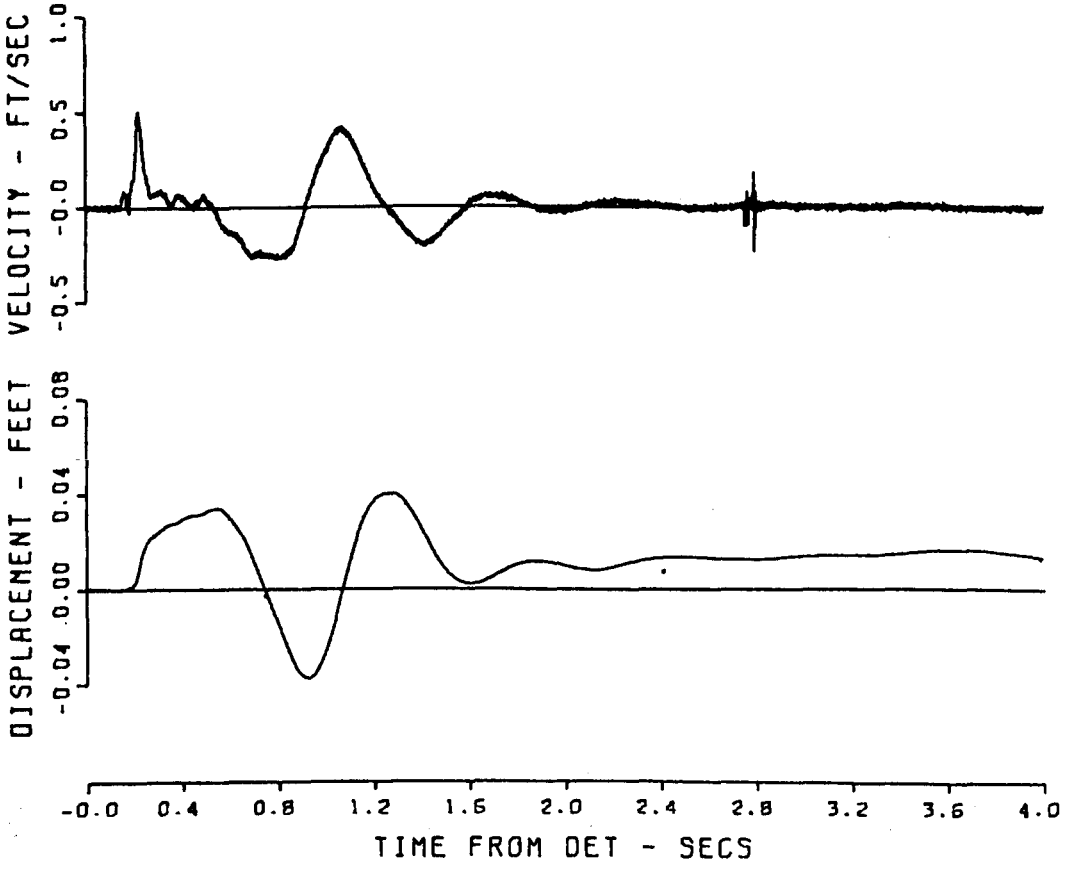

Figure A.4 Motion-time histories, Event Dial Pack, Gage 645-1.5-UH.

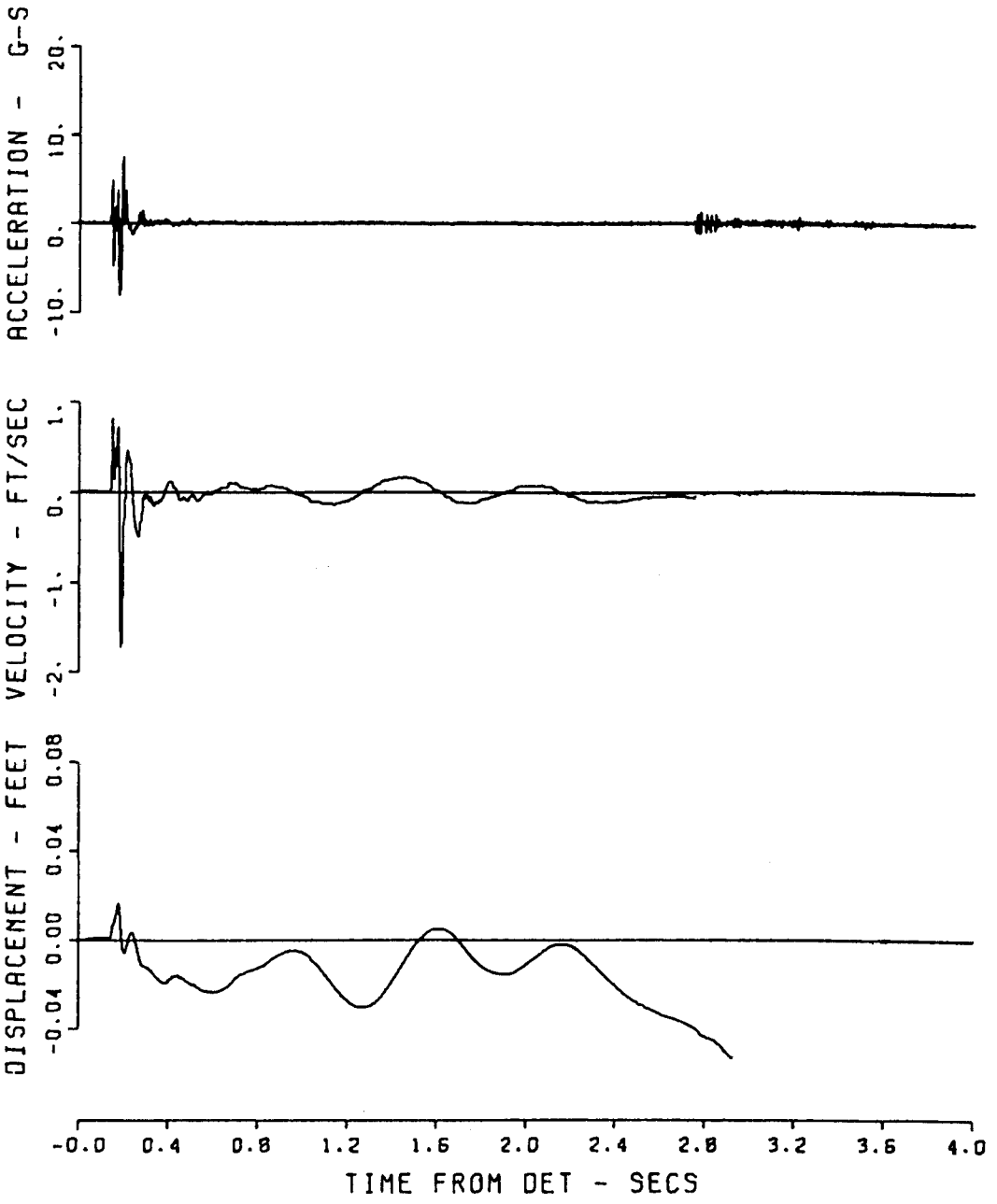

Figure A.5 Motion-time histories, Event Dial Pack, Gage 645-5-AV.

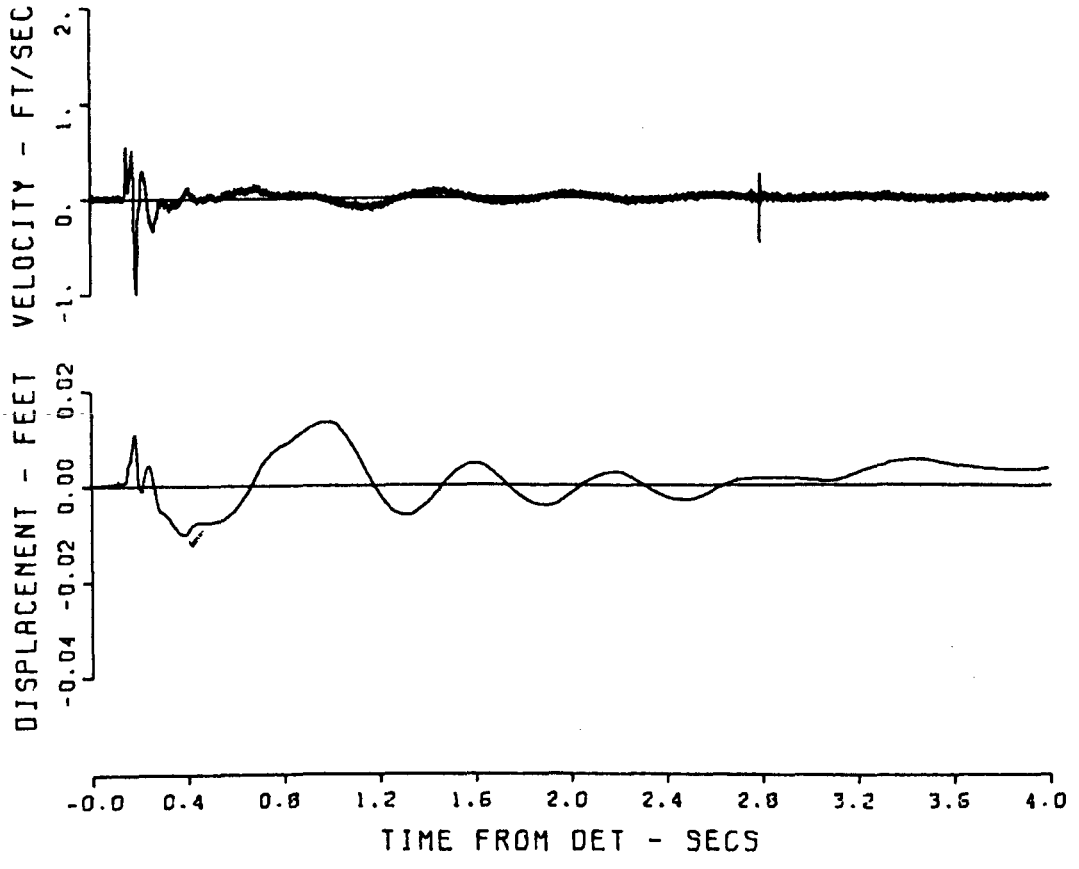

Figure A.6 Motion-time histories, Event Dial Pack, Gage 645-5-UV.

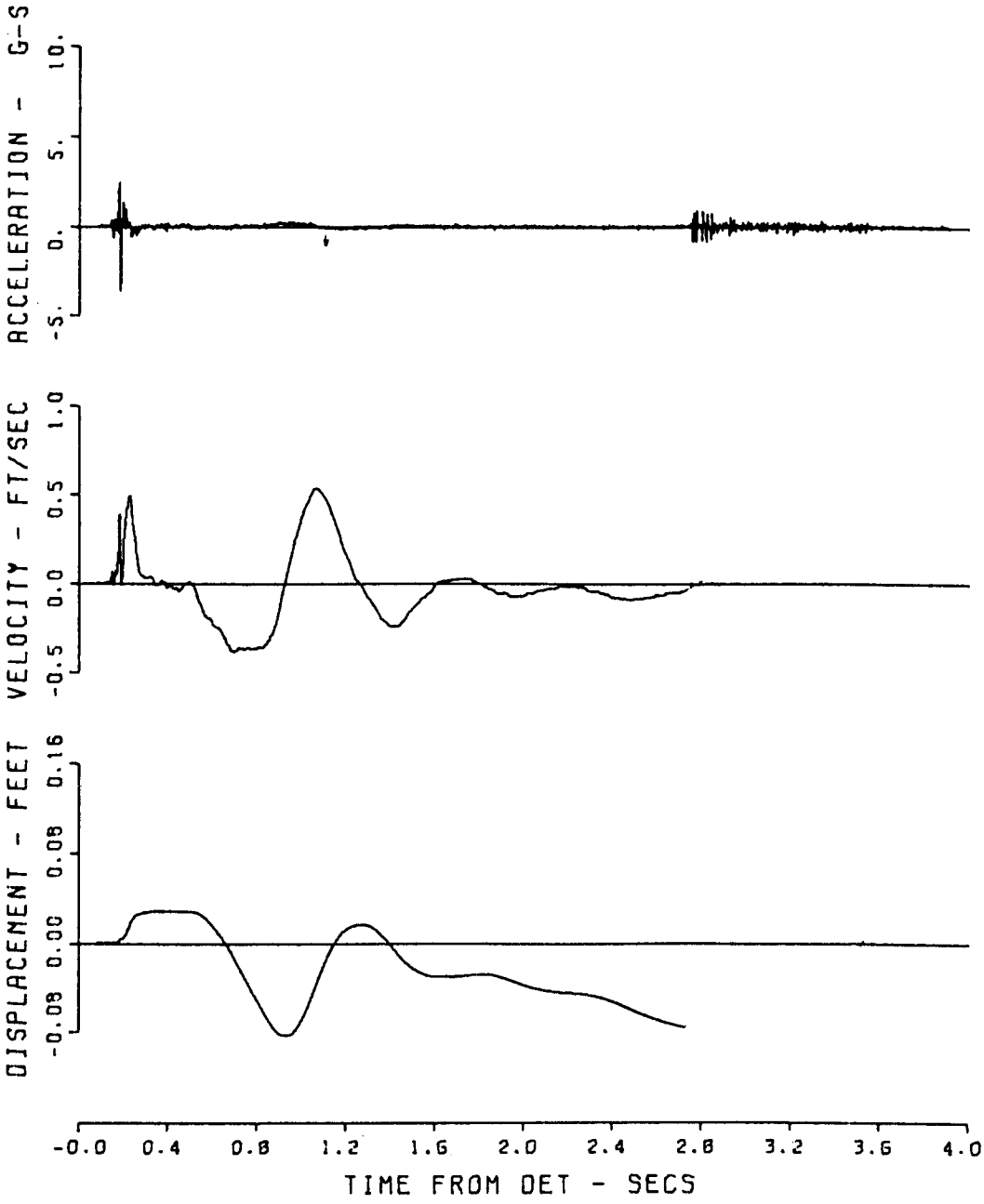

Figure A.7 Motion-time histories, Event Dial Pack, Gage 645-5-AH.

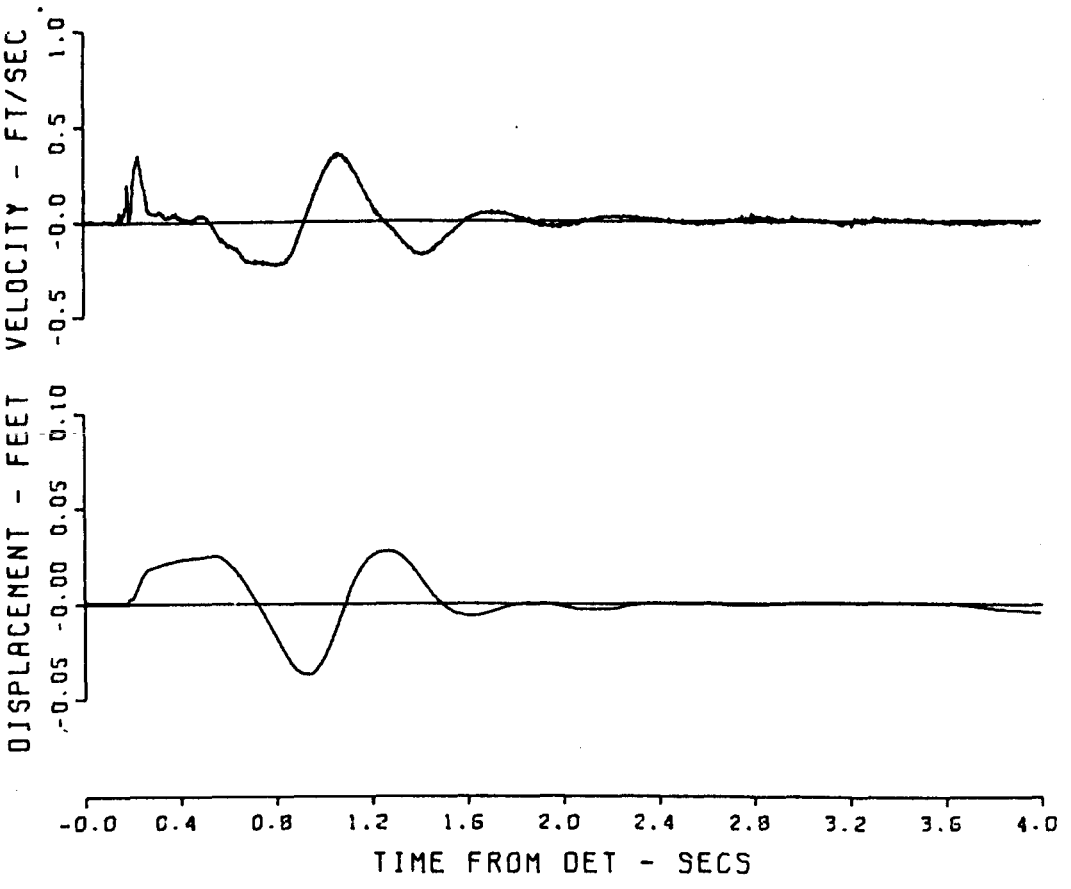

Figure A.8 Motion-time histories, Event Dial Pack, Gage 645-5-UH.

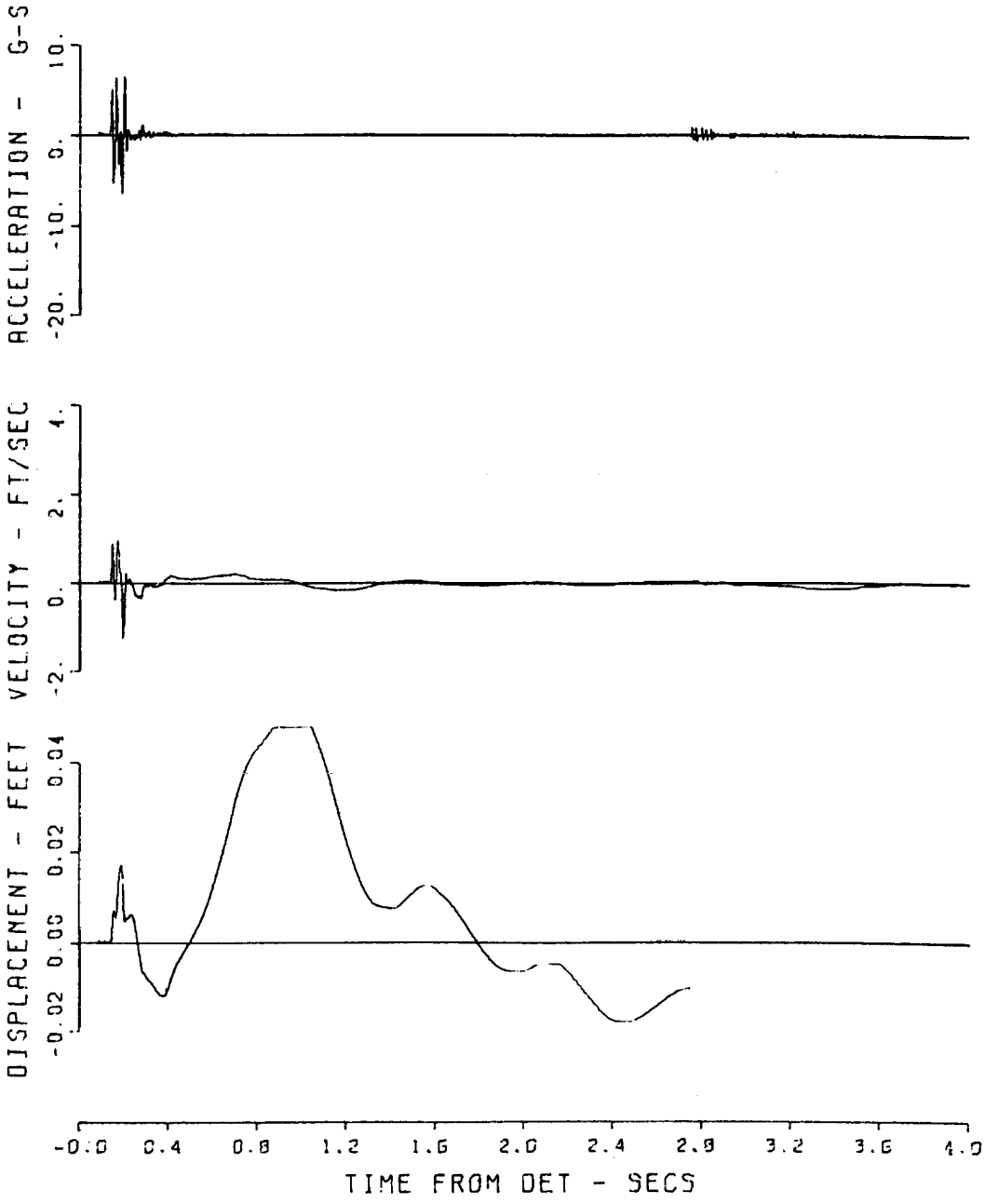

Figure A.9 Motion-time histories, Event Dial Pack, Gage 645-10-AV.

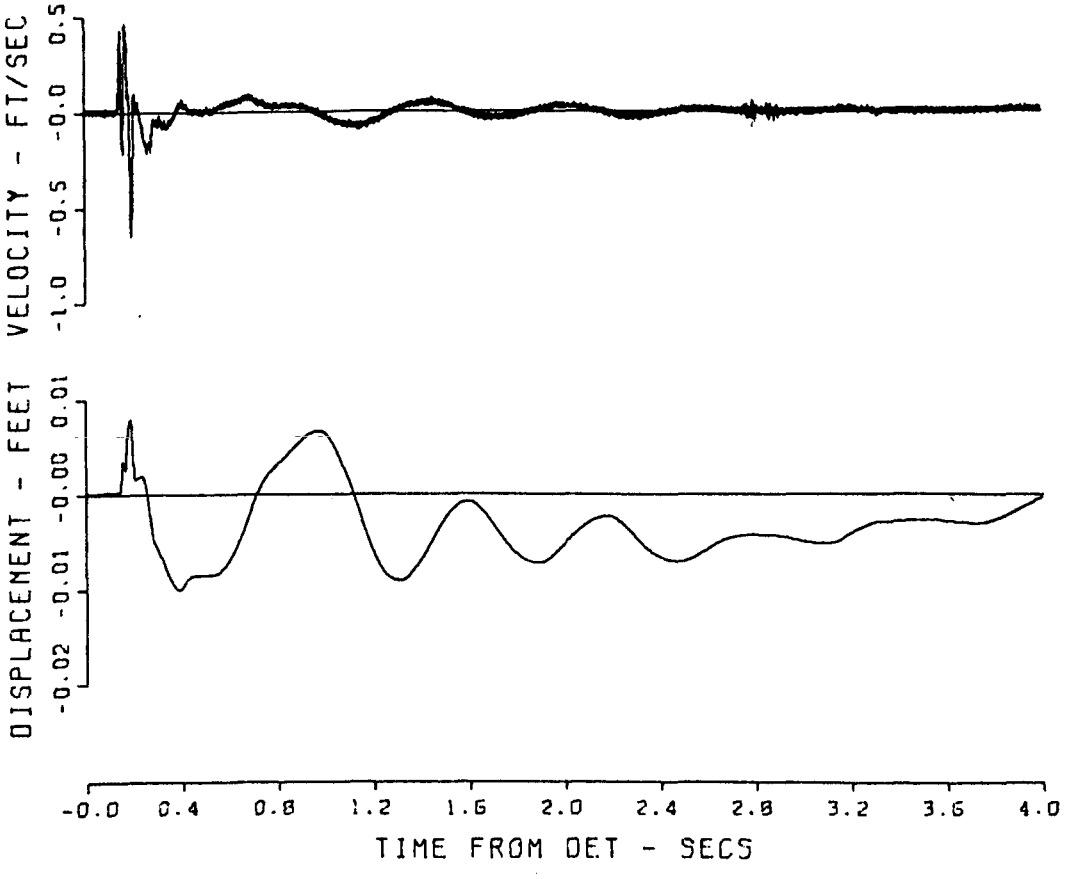

Figure A.10 Motion-time histories, Event Dial Pack, Gage 645-10-UV.

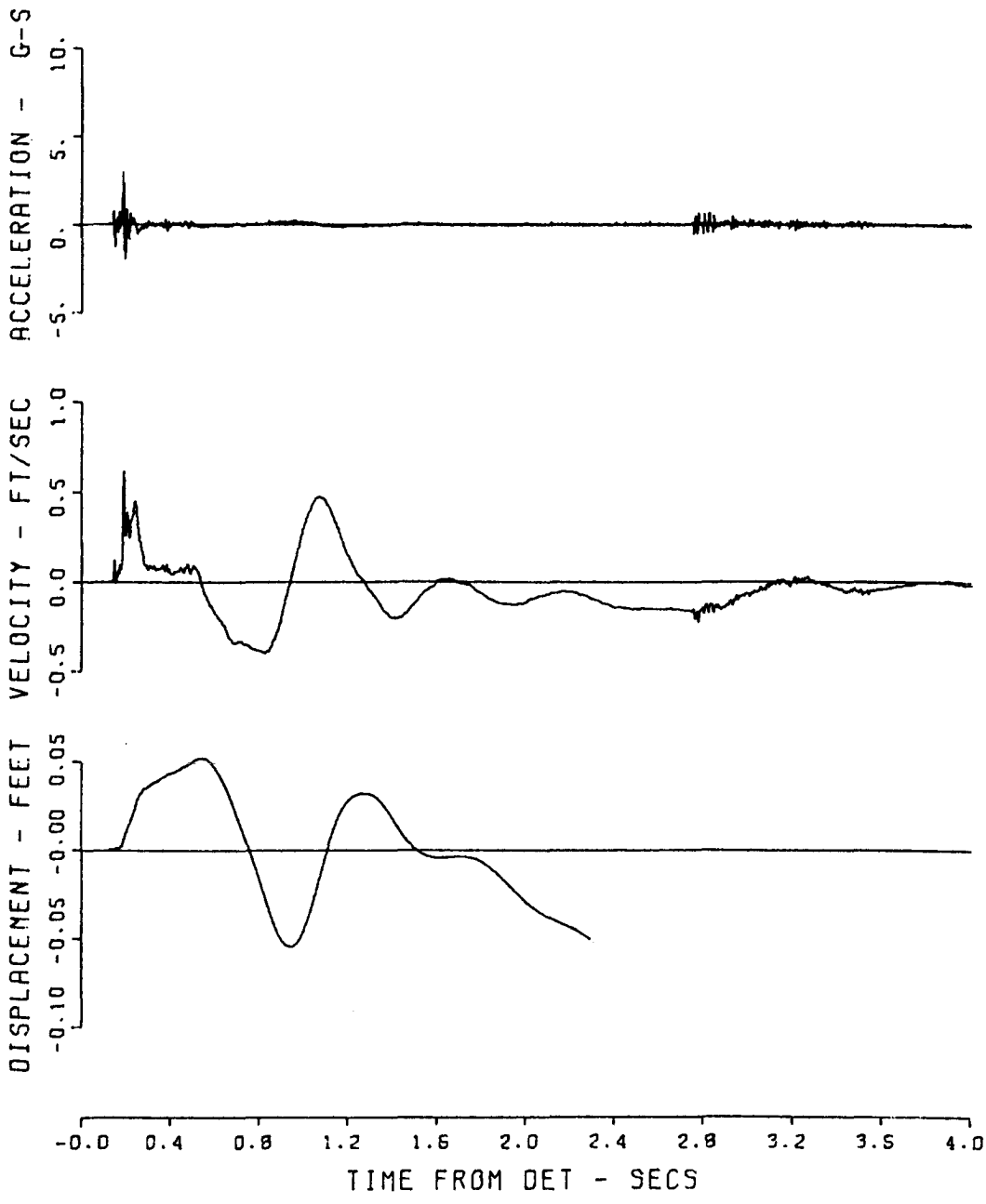

Figure A.11 Motion-time histories, Event Dial Pack, Gage 645-10-AH.

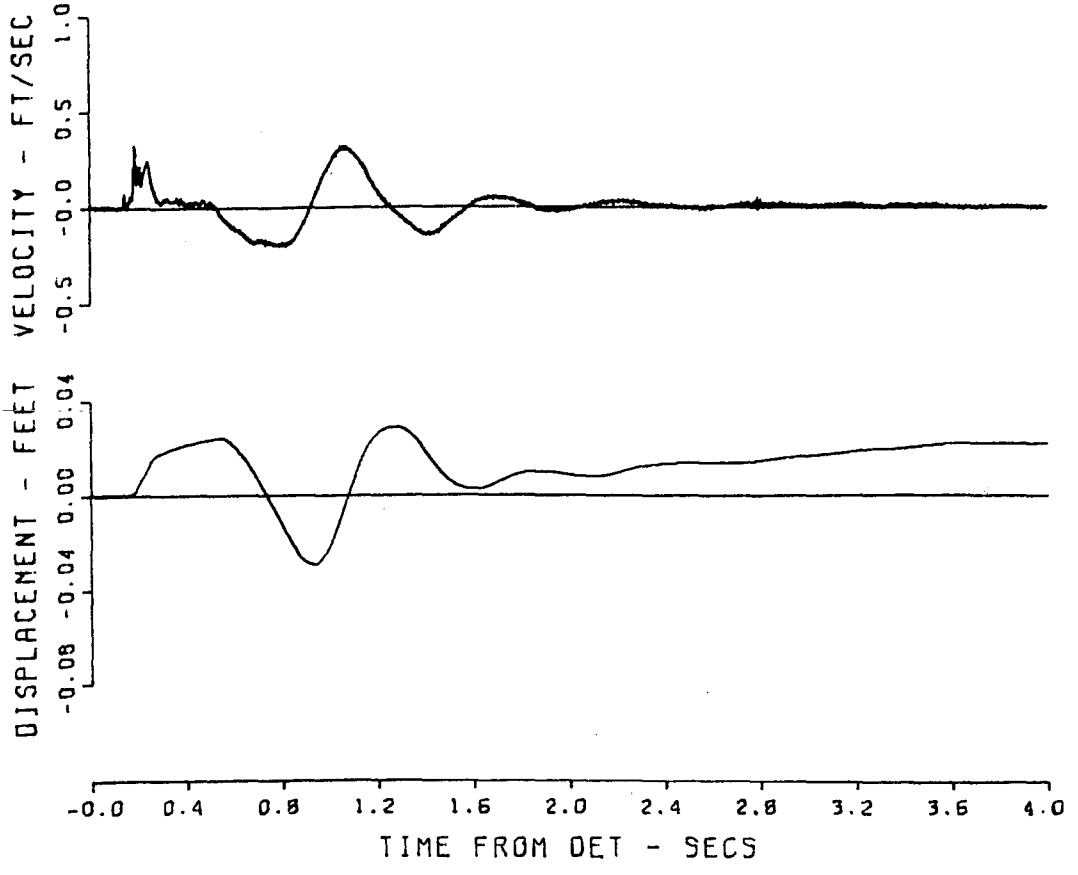

Figure A.12 Motion-time histories, Event Dial Pack, Gage 645-10-UH.

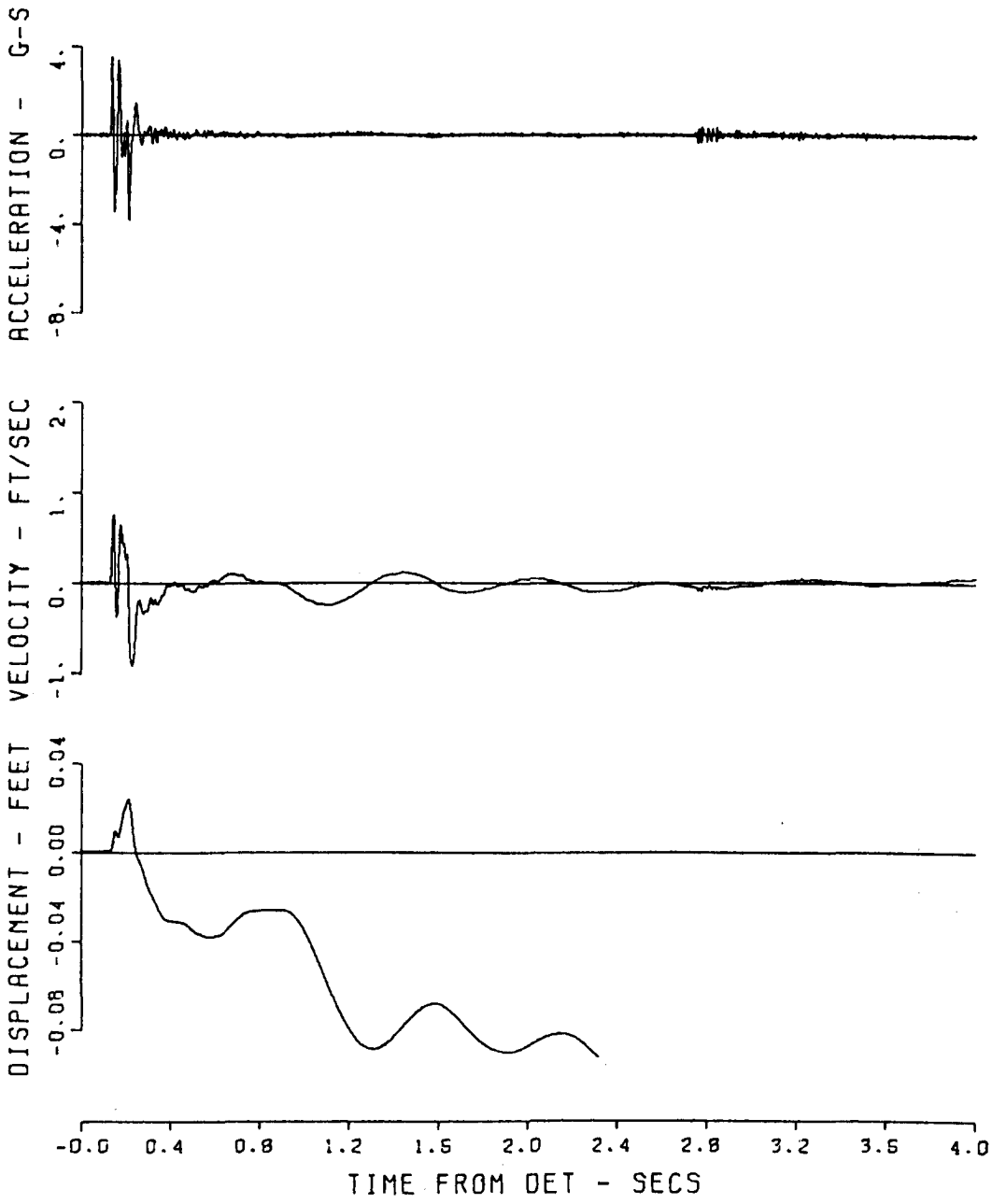

Figure A.13 Motion-time histories, Event Dial Pack, Gage 645-20-AV.

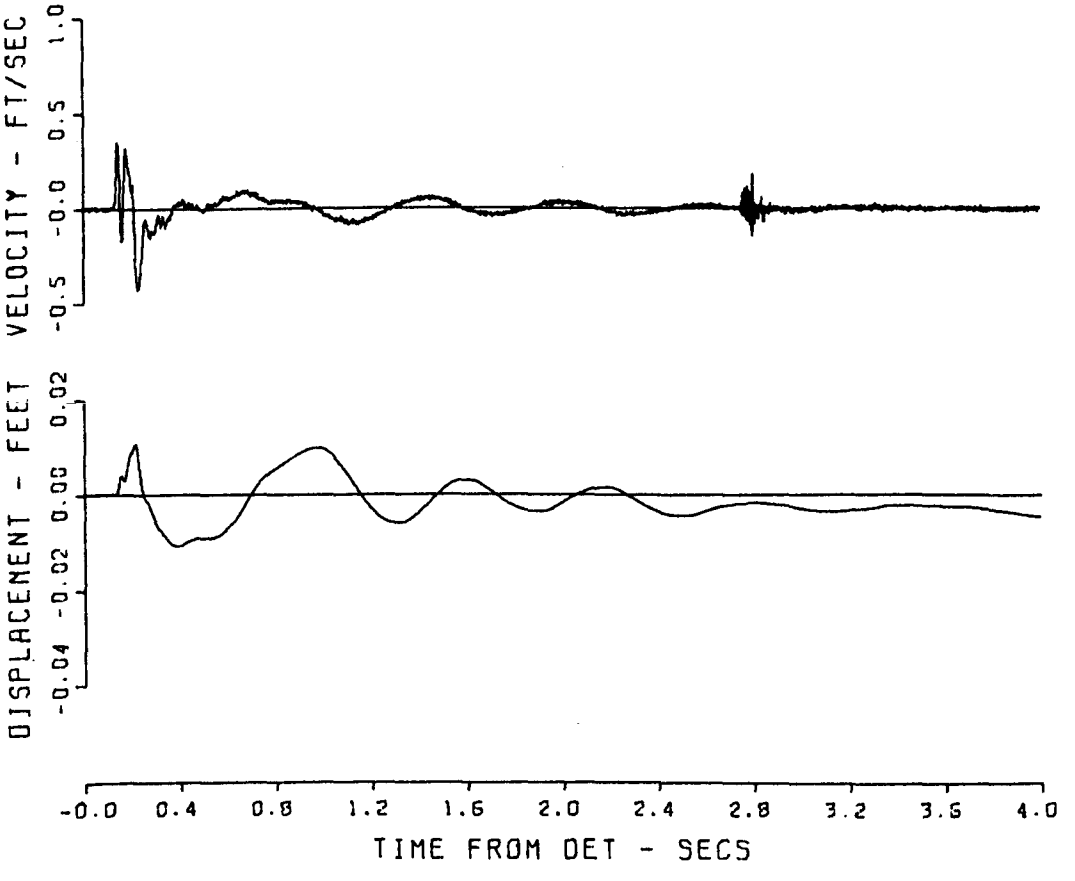

Figure A.14 Motion-time histories, Event Dial Pack, Gage 645-20-UV.

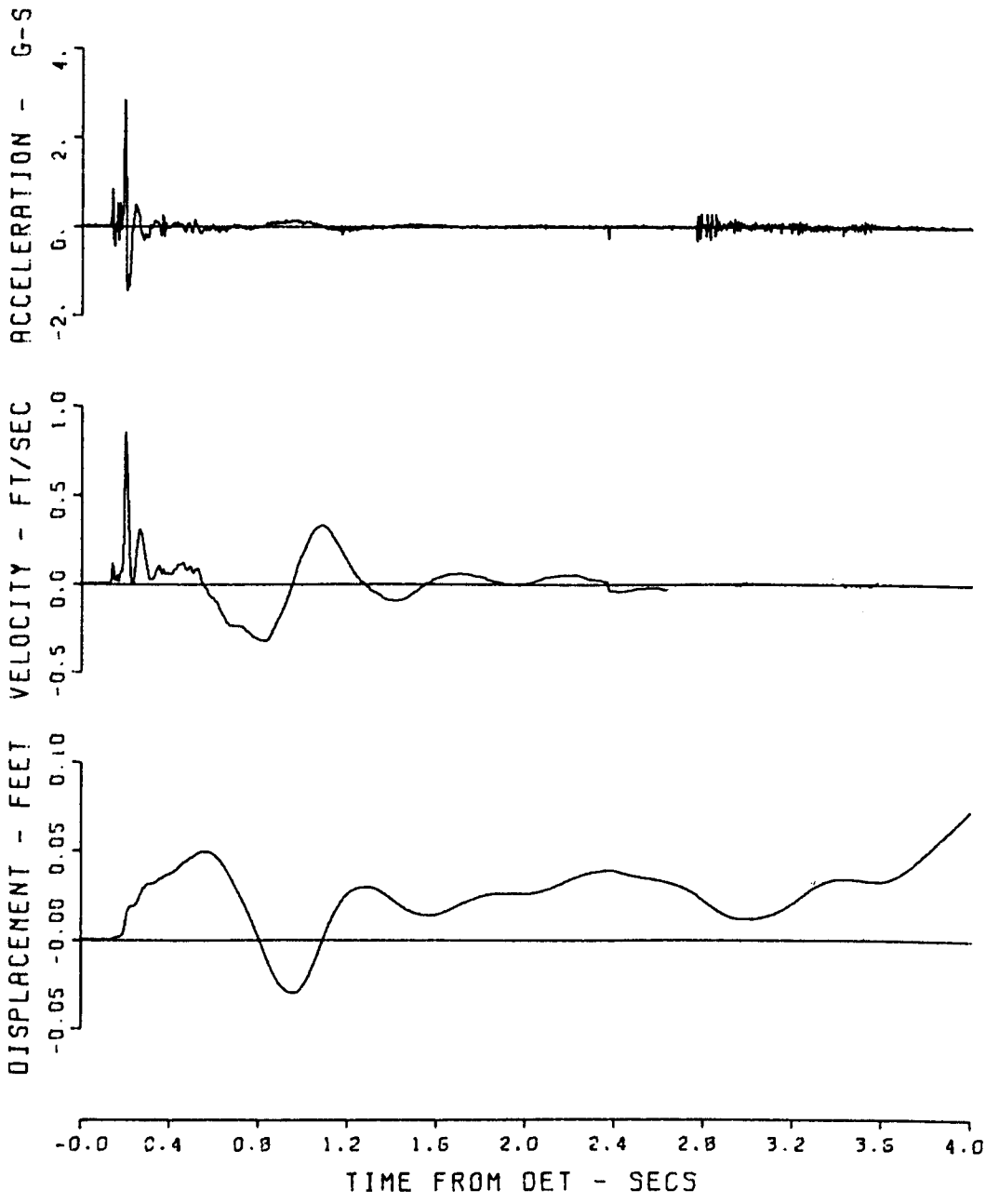

Figure A.15 Motion-time histories, Event Dial Pack, Gage 645-20-AH.

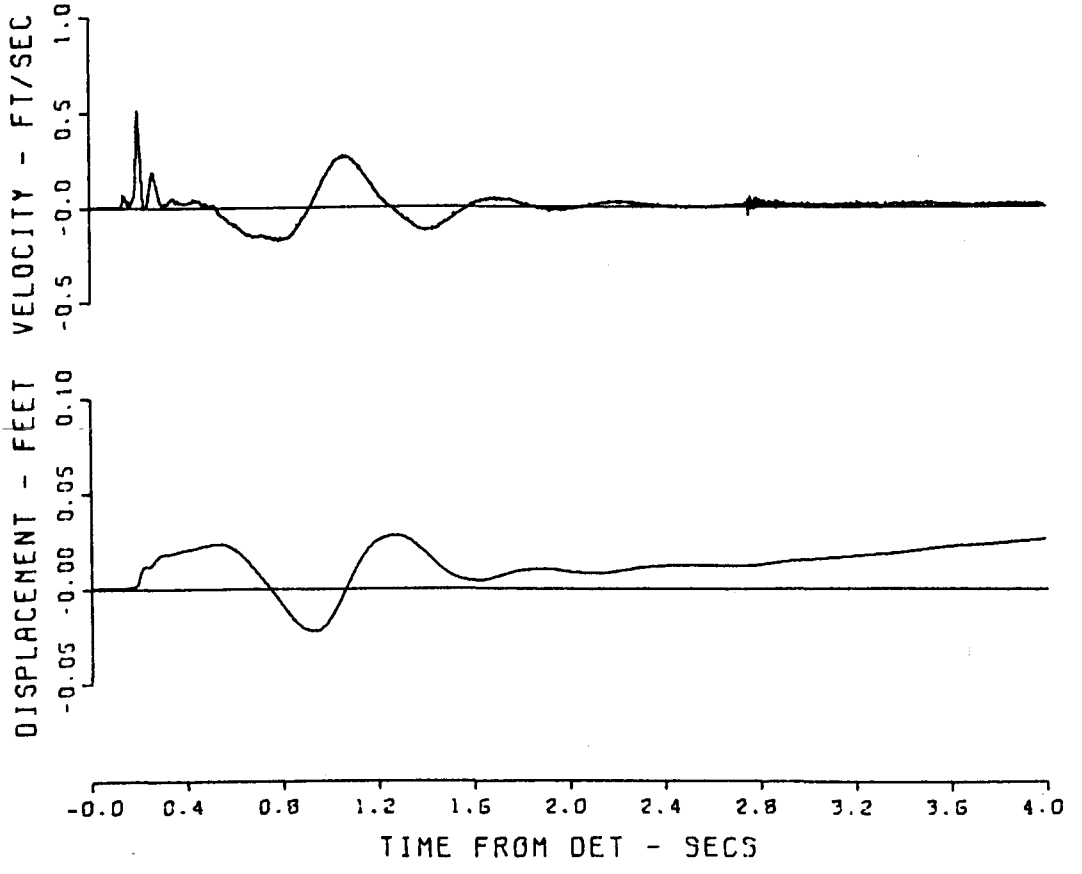

Figure A.16 Motion-time histories, Event Dial Pack, Gage 645-20-UH.

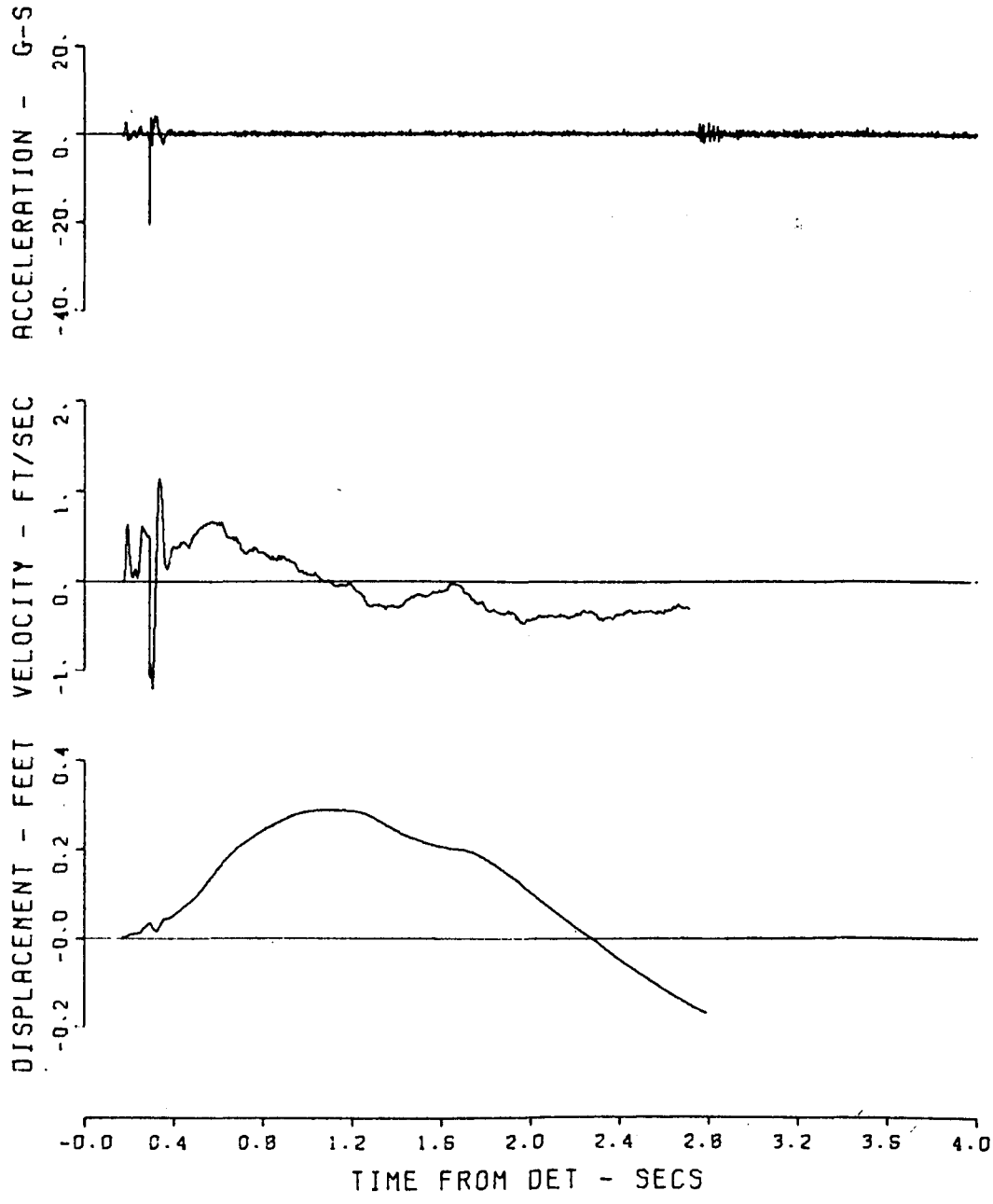

Figure A.17 Motion-time histories, Event Dial Pack, Gage 840-1.5-AV.

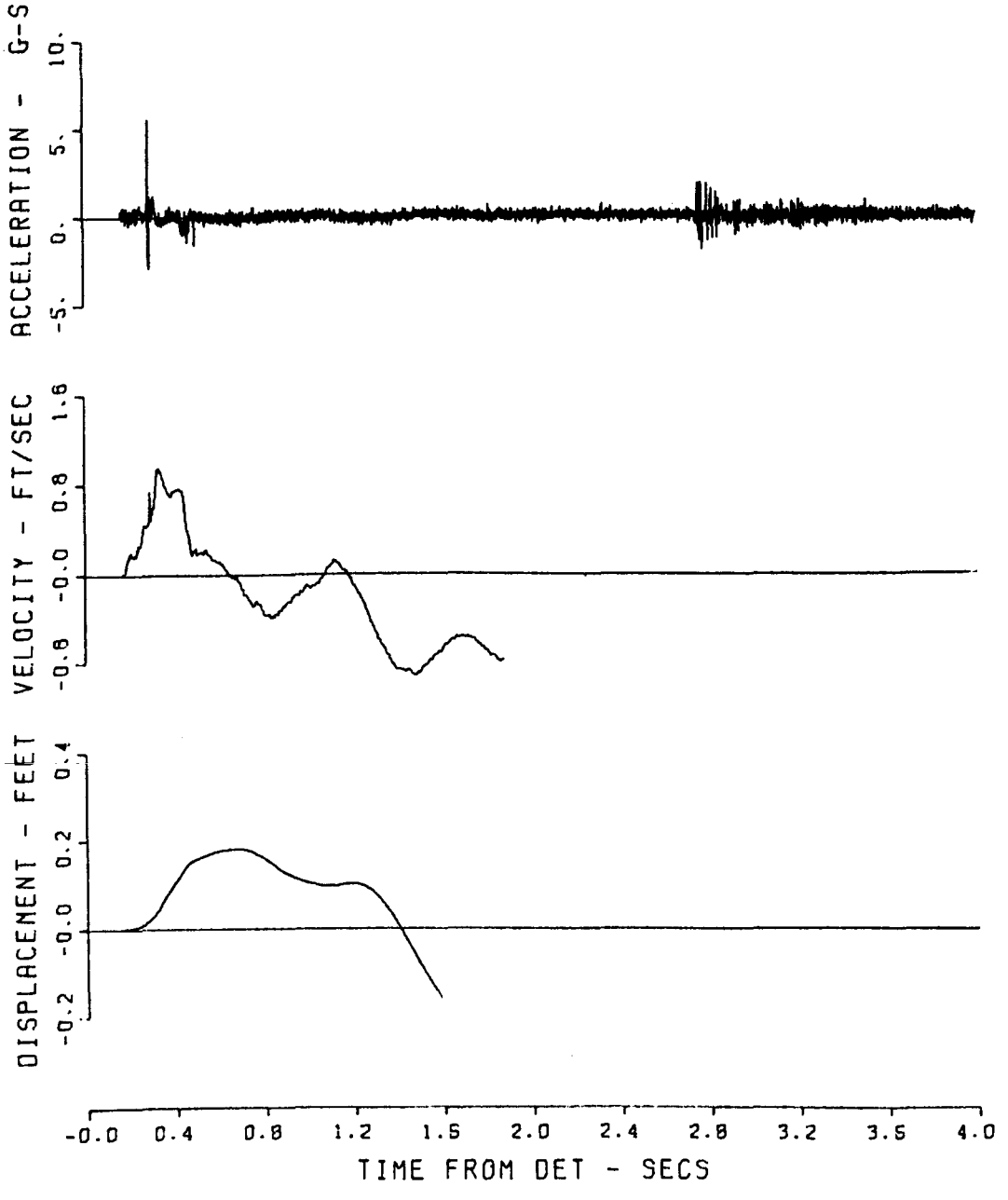

Figure A.18 Motion-time histories, Event Dial Pack, Gage 840-1.5-AH.

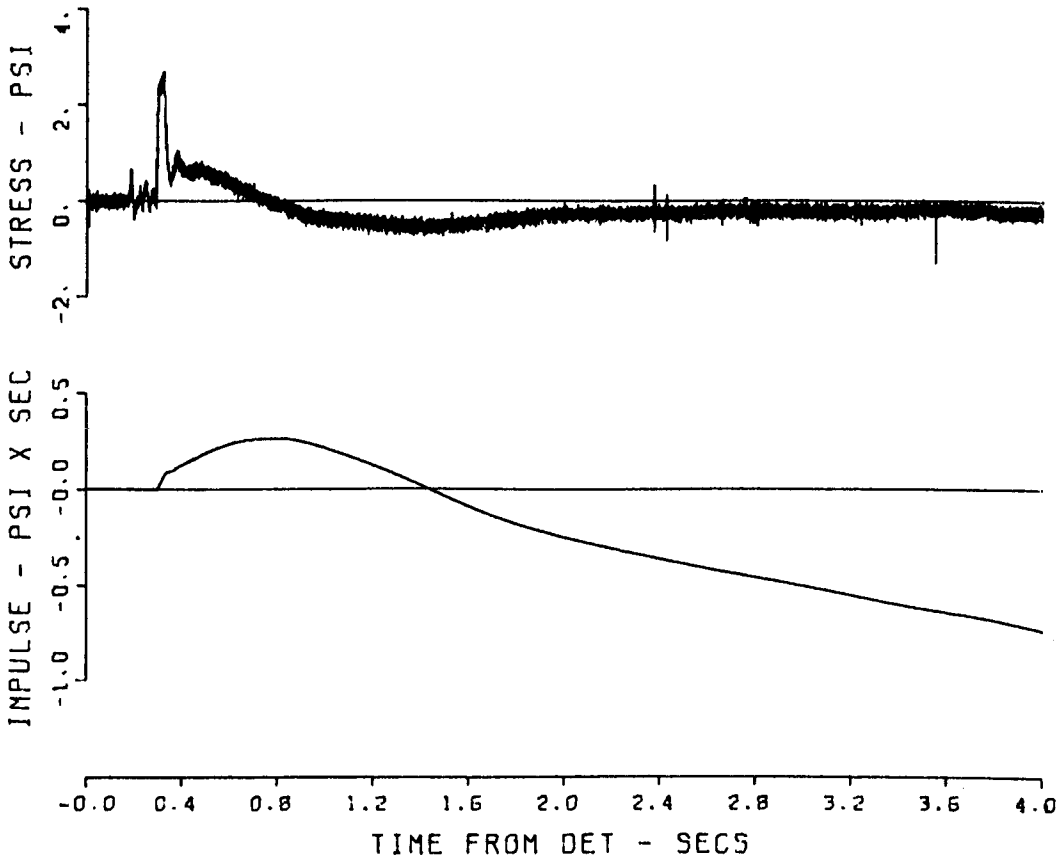

Figure A.19 Motion-time histories, Event Dial Pack, Gage 840-1.5-PV.

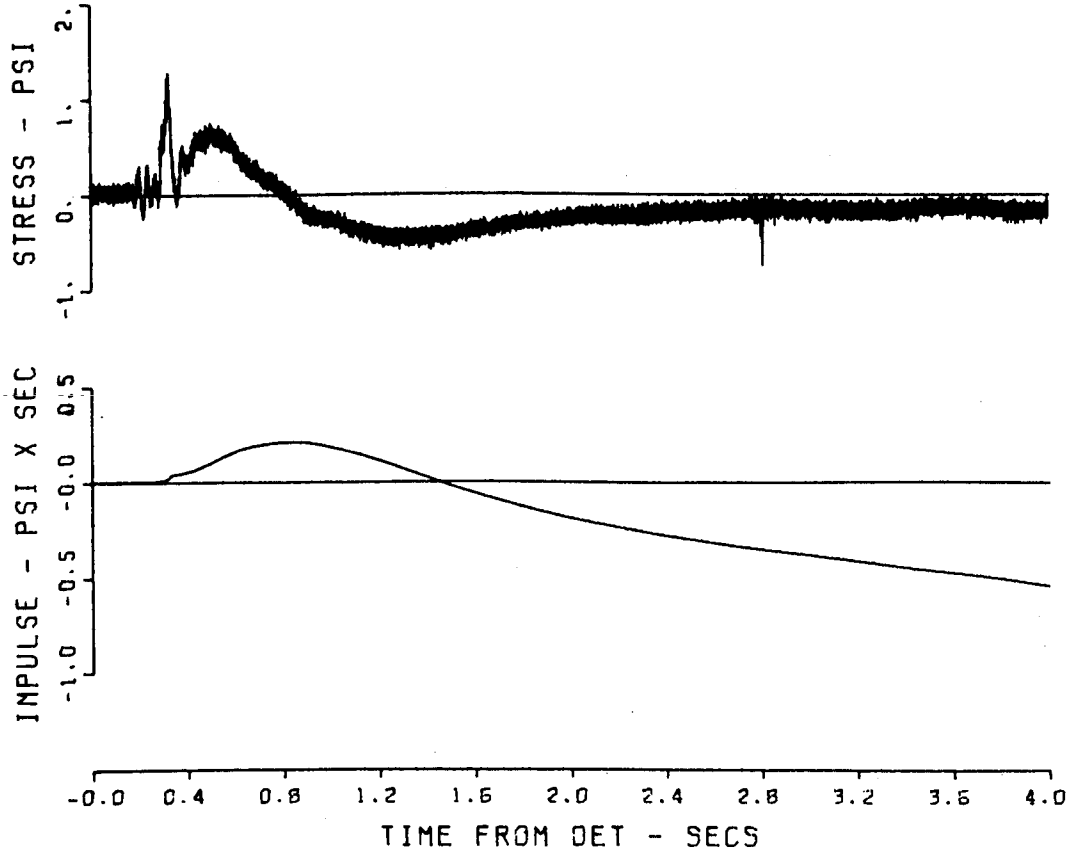

Figure A.20 Motion-time histories, Event Dial Pack, Gage 840-1.5-PH.

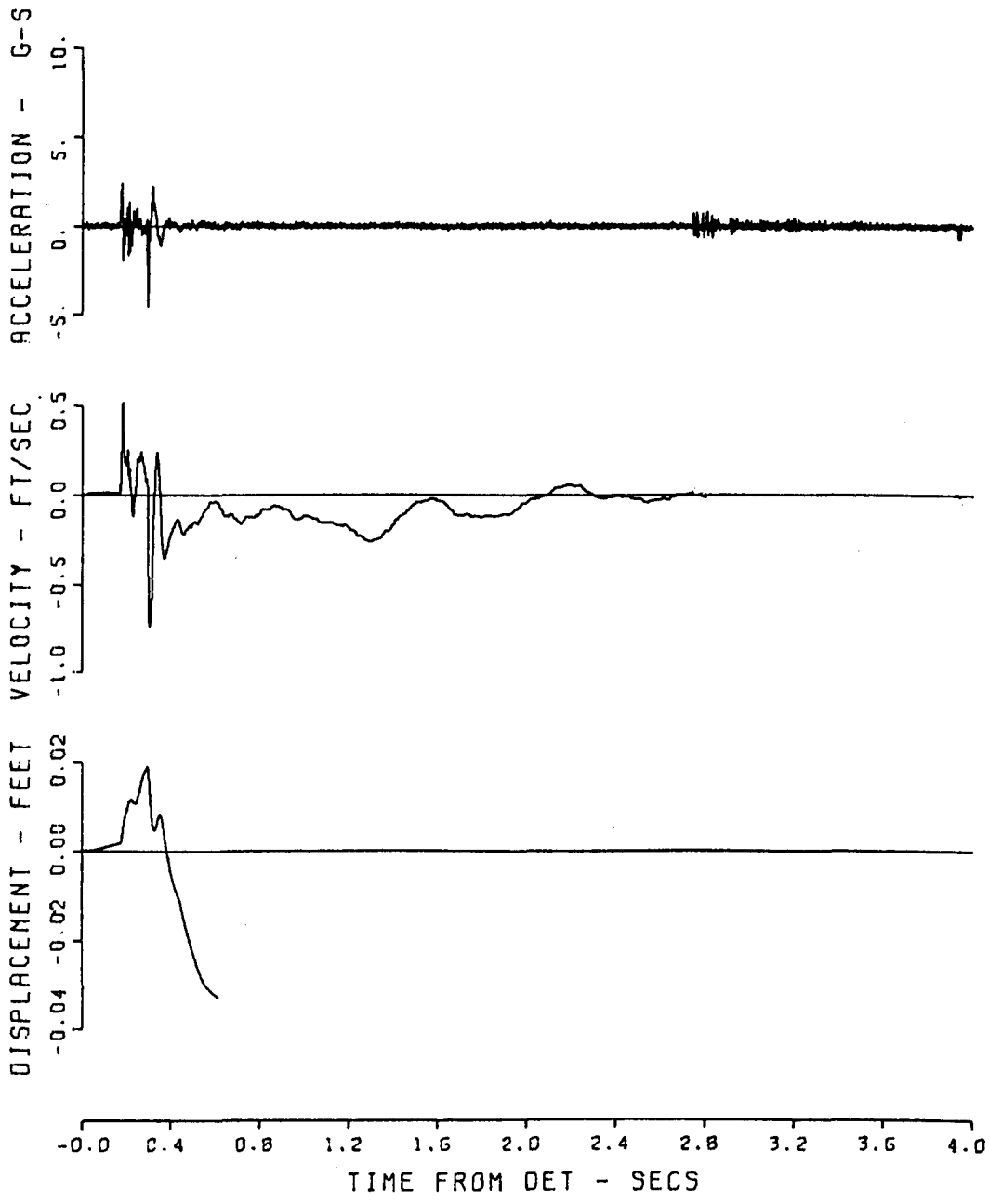

Figure A.21 Motion-time histories, Event Dial Pack, Gage 840-5-AV.

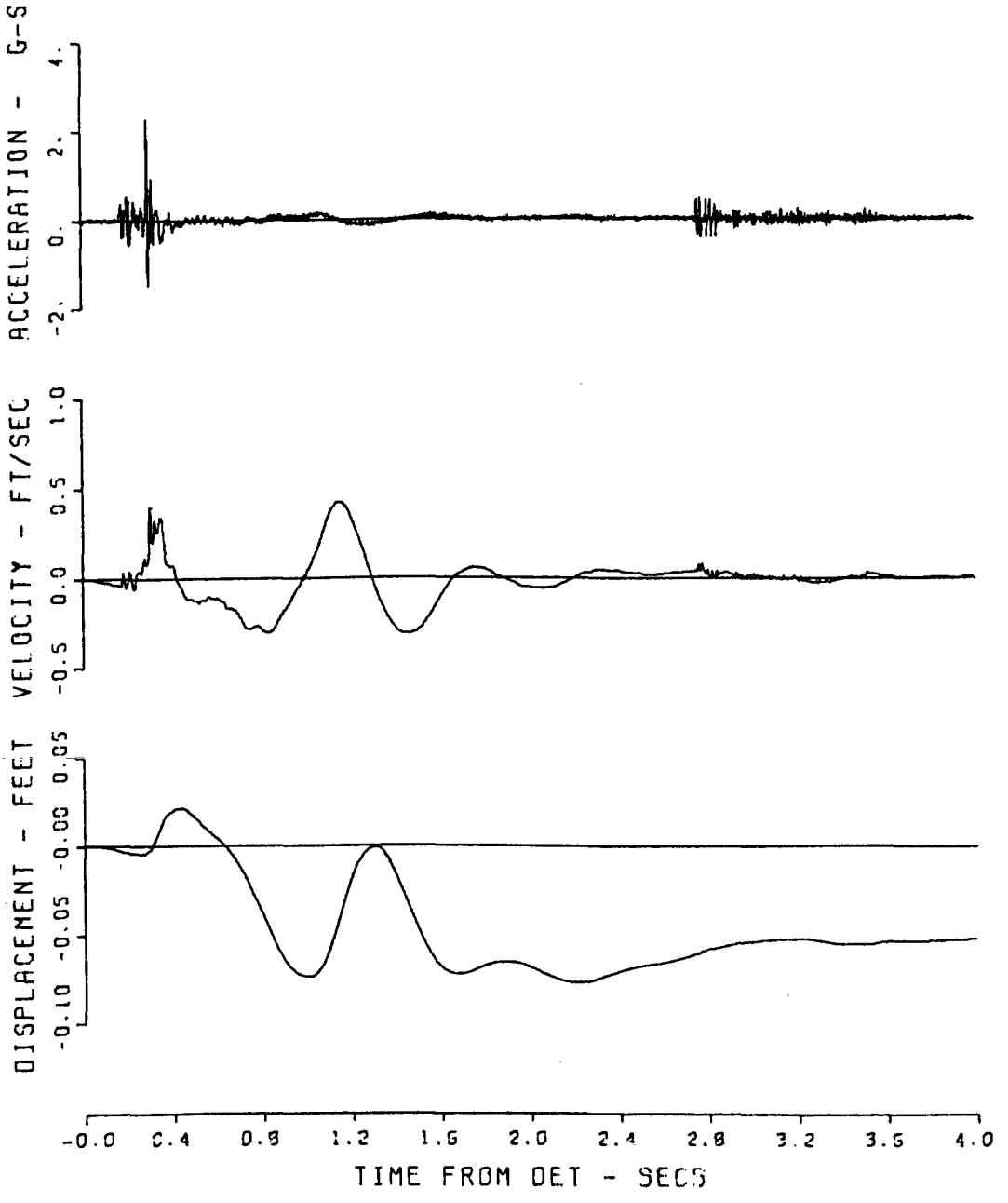

Figure A.22 Motion-time histories, Event Dial Pack, Gage 840-5-AH.

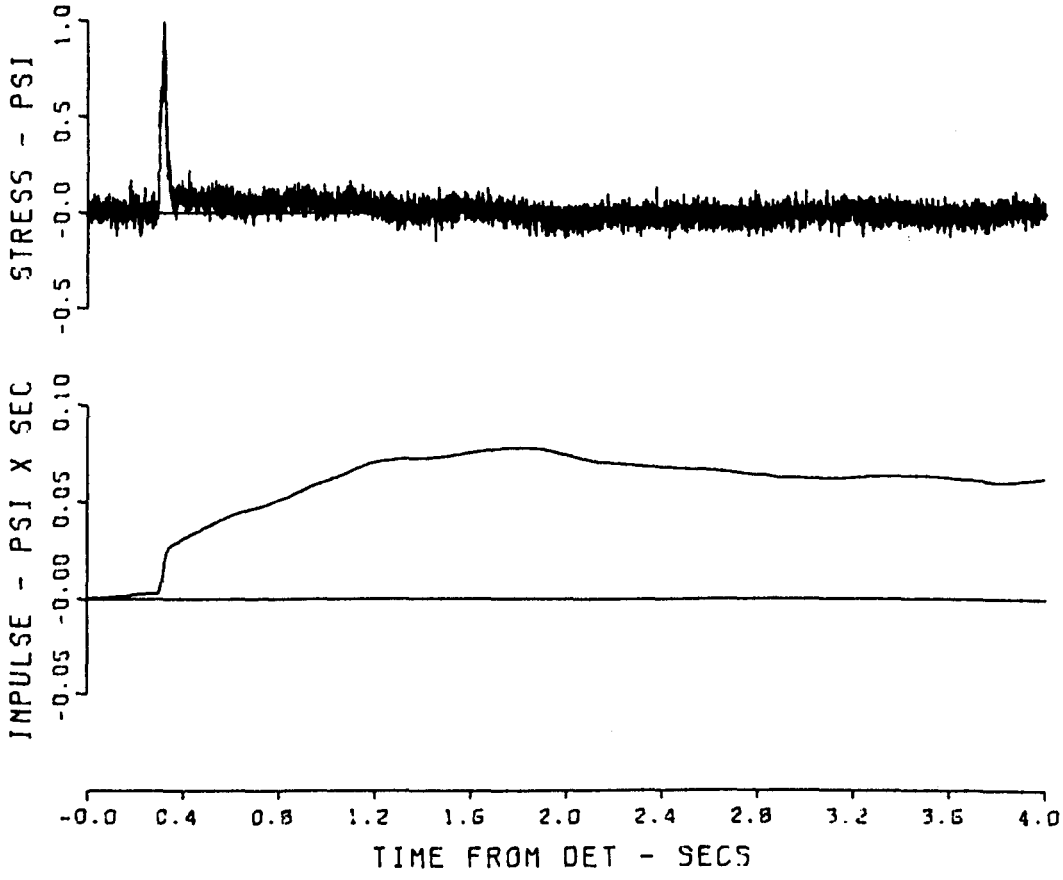

Figure A.23 Motion-time histories, Event Dial Pack, Gage 840-5-PV.

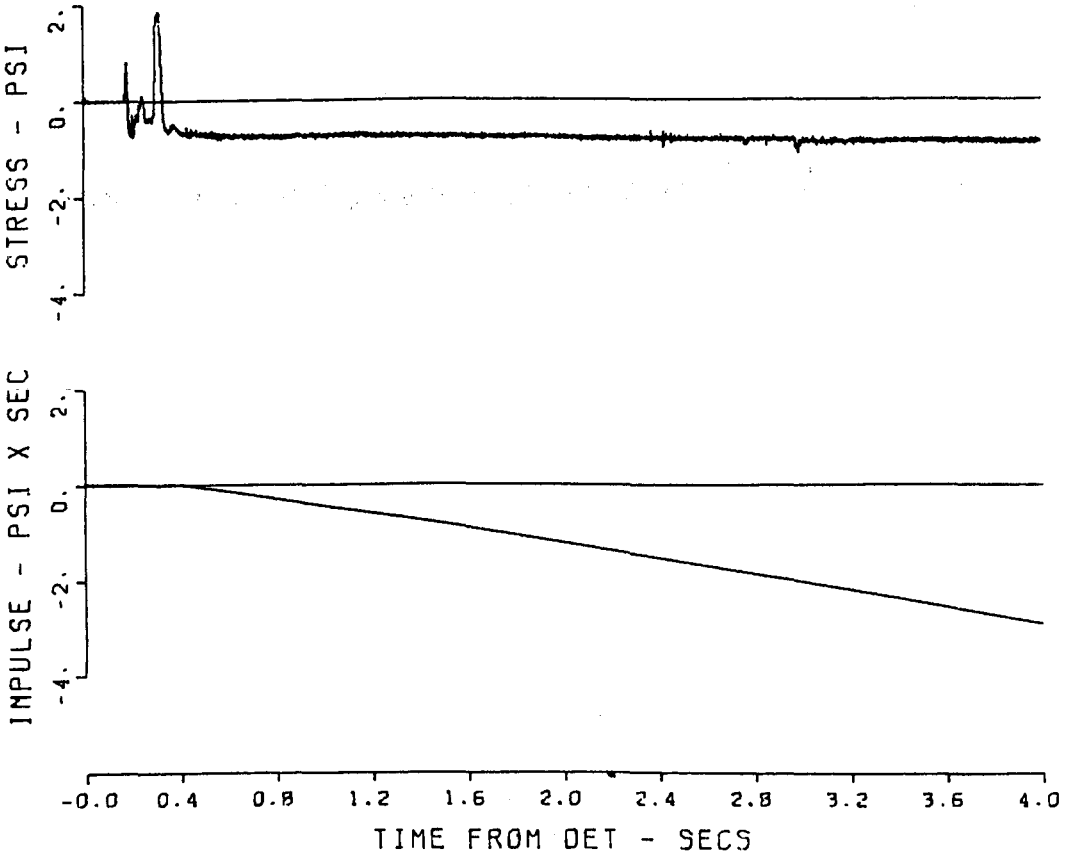

Figure A.24 Motion-time histories, Event Dial Pack, Gage 840-5-PH.

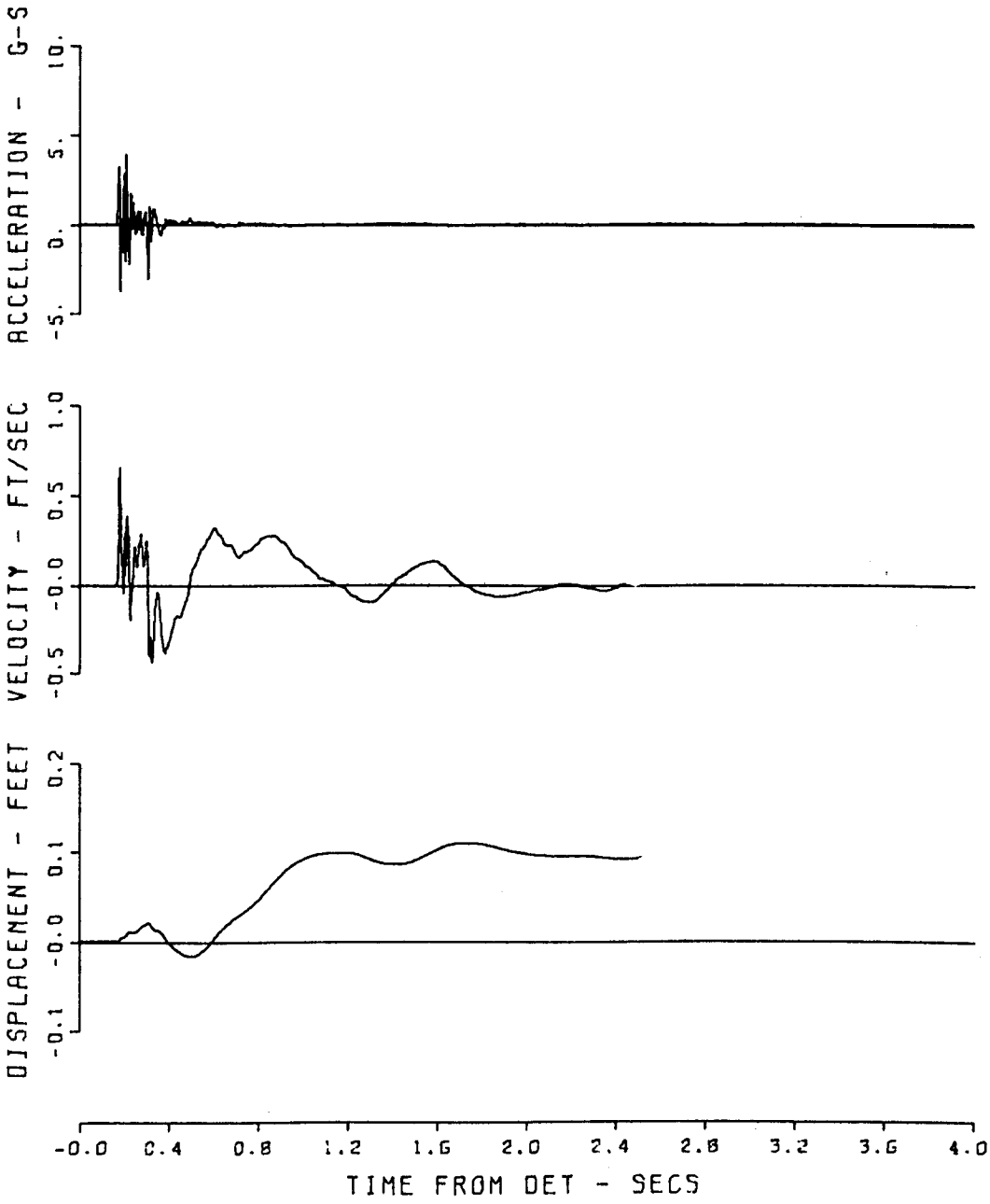

Figure A.25 Motion-time histories, Event Dial Pack, Gage 840-10-AV.

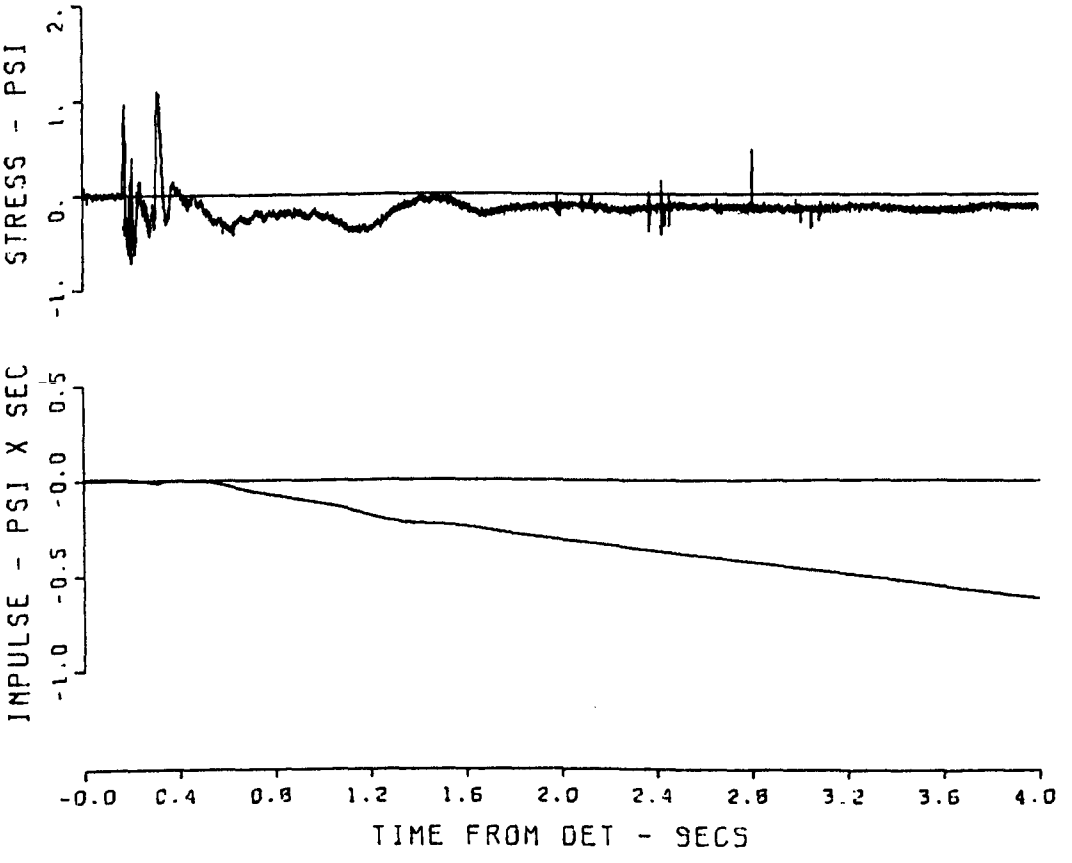

Figure A.26 Motion-time histories, Event Dial Pack, Gage 840-10-PV.

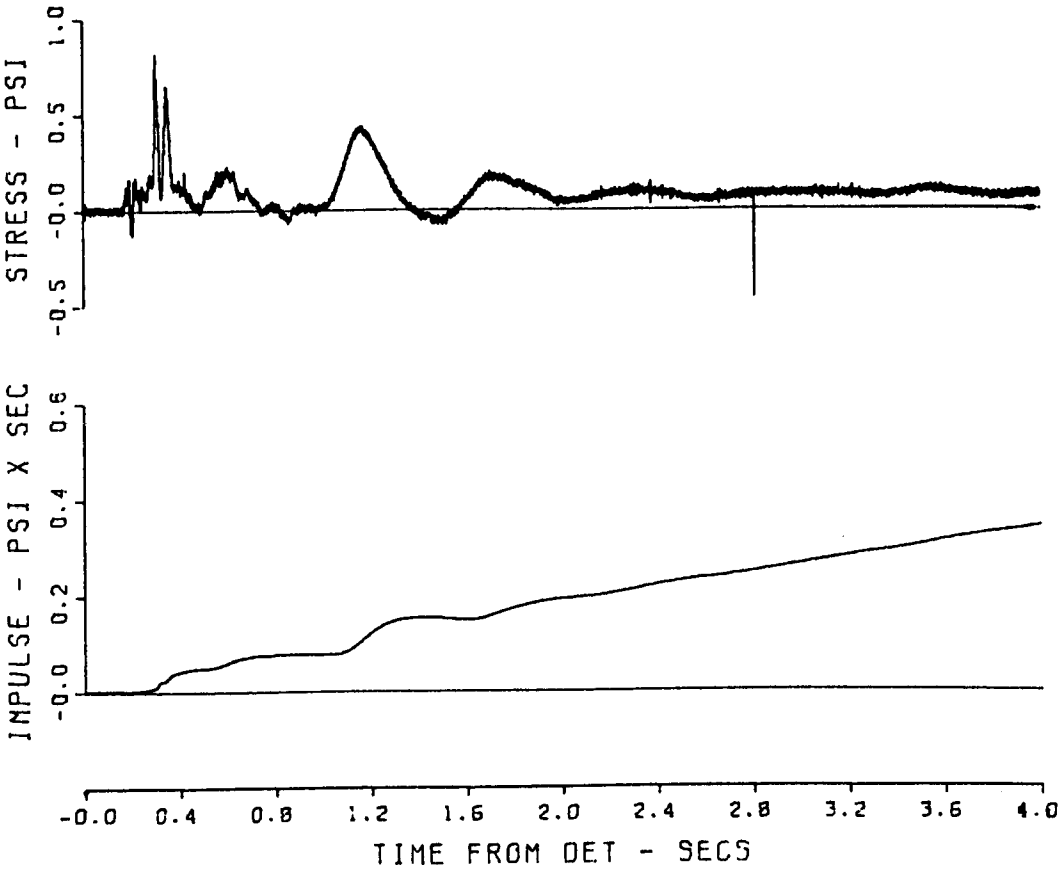

Figure A.27 Motion-time histories, Event Dial Pack, Gage 840-10-PH.

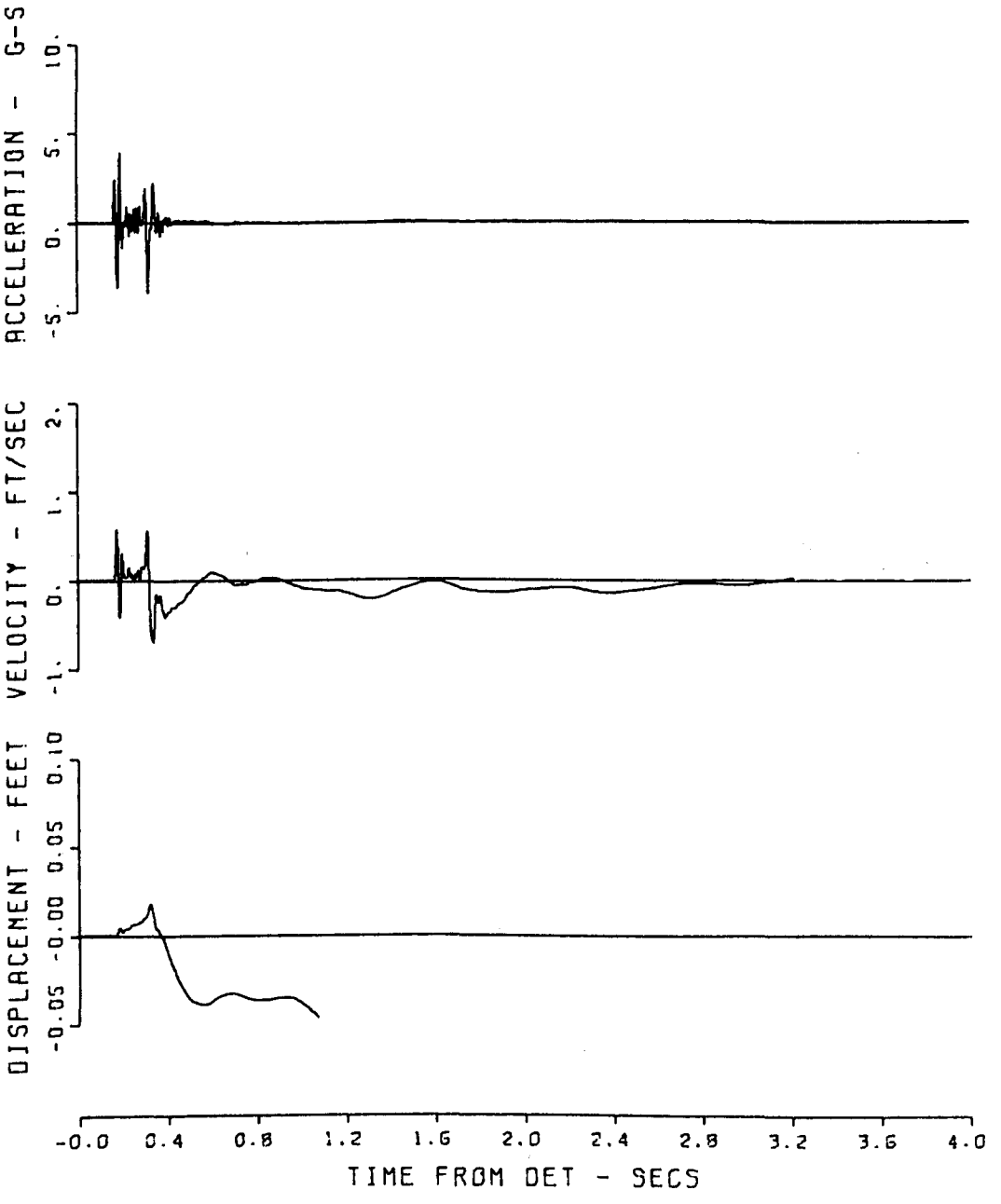

Figure A.28 Motion-time histories, Event Dial Pack, Gage 840-20-AV.

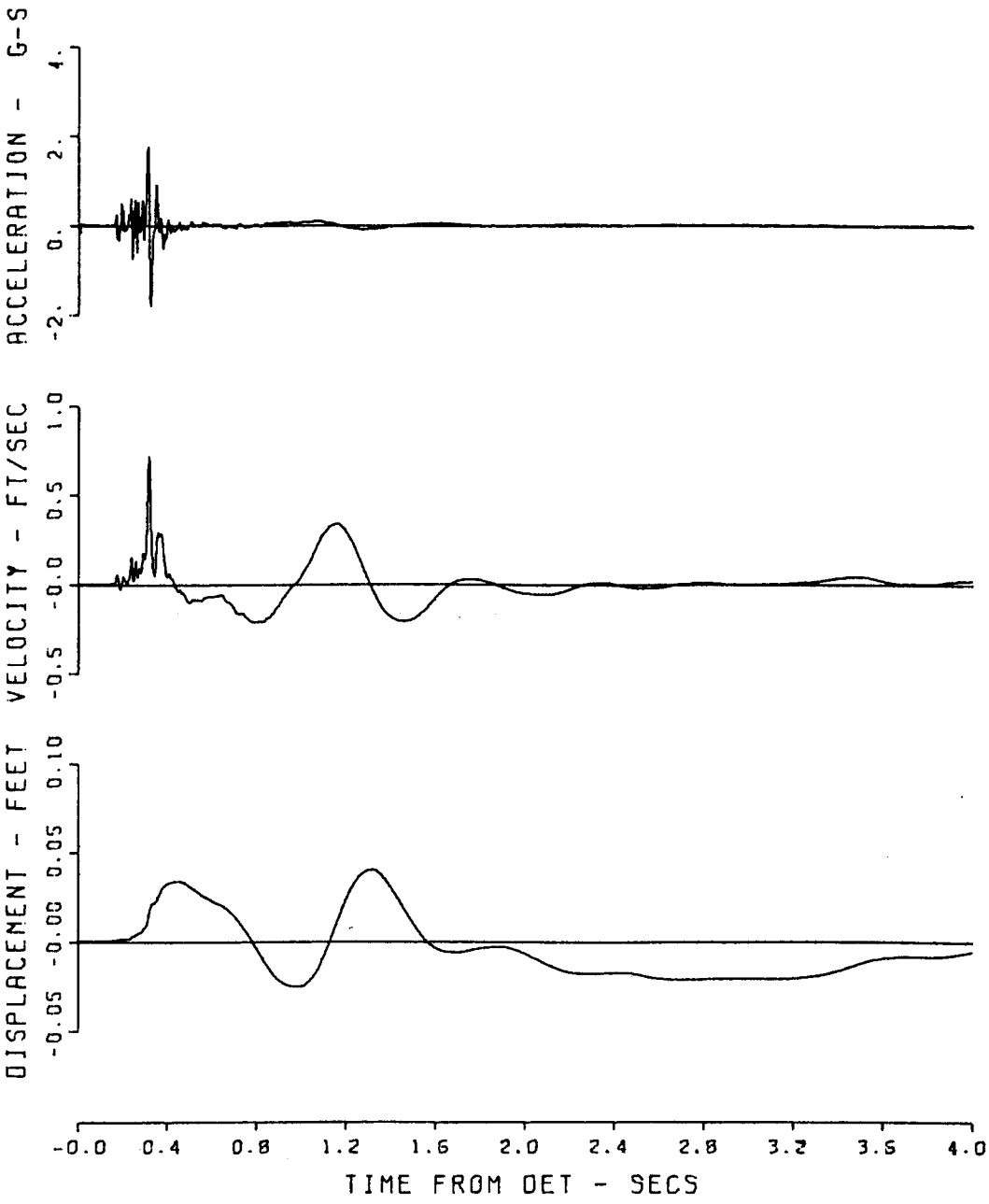

Figure A.29 Motion-time histories, Event Dial Pack, Gage 840-20-AH.

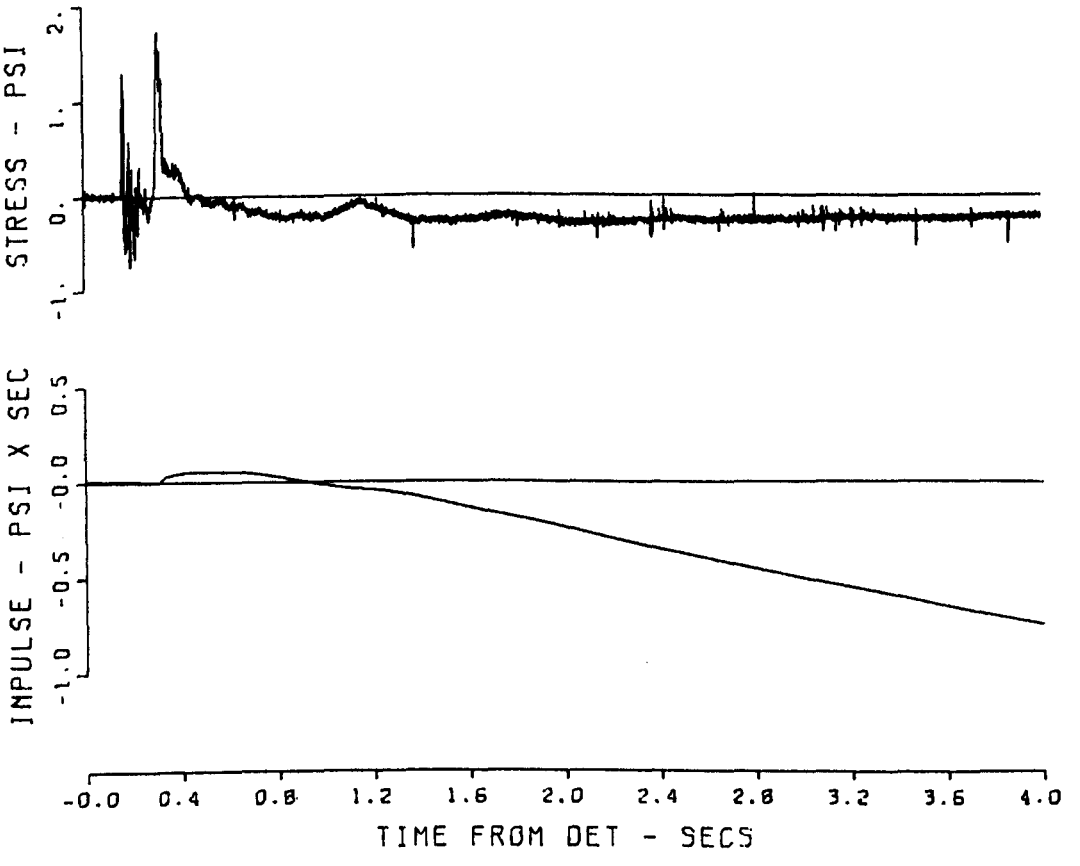

Figure A.30 Motion-time histories, Event Dial Pack, Gage 840-20-PV.

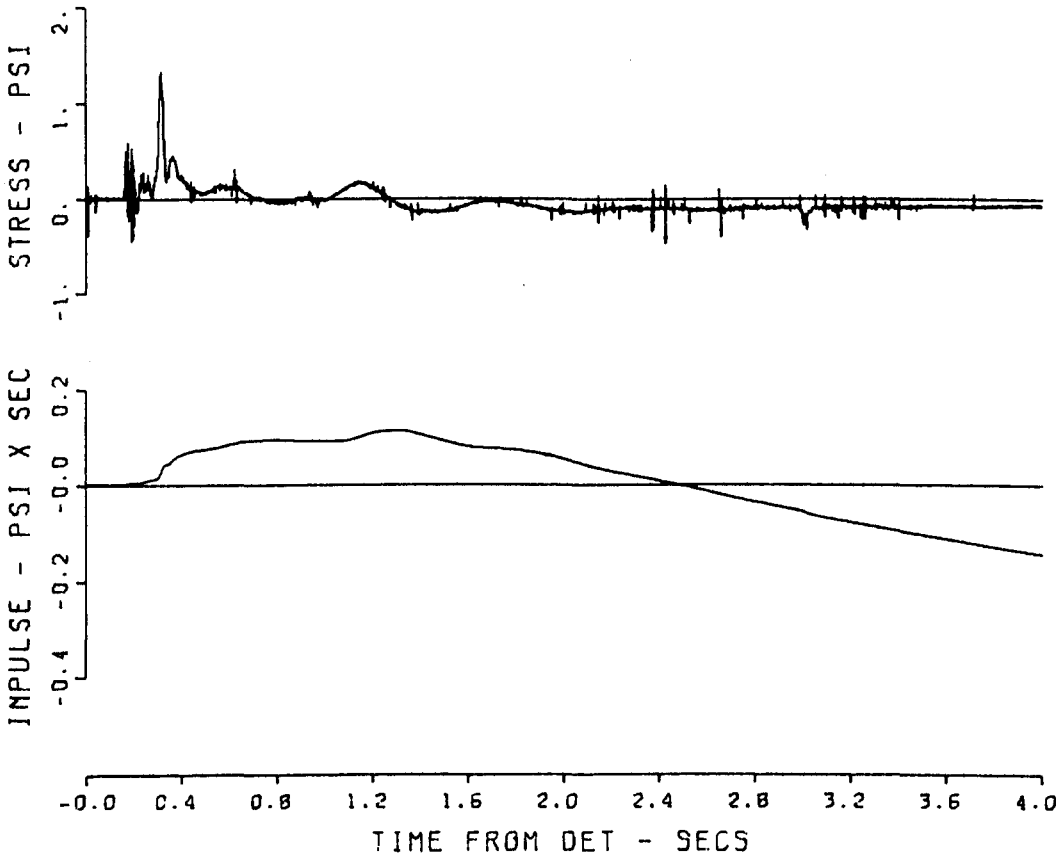

Figure A.31 Motion-time histories, Event Dial Pack, Gage 840-20-PH.

APPENDIX B

STRESS- AND MOTION-TIME HISTORIES ON EXPANDED TIME SCALE

Figures B.1 through B.31 present the same data as Figures A.1 through A.31, but on expanded time scales. Again, gage locations and types are listed in the titles, and the explanation of the gage numbers is the same as that for Appendix A.

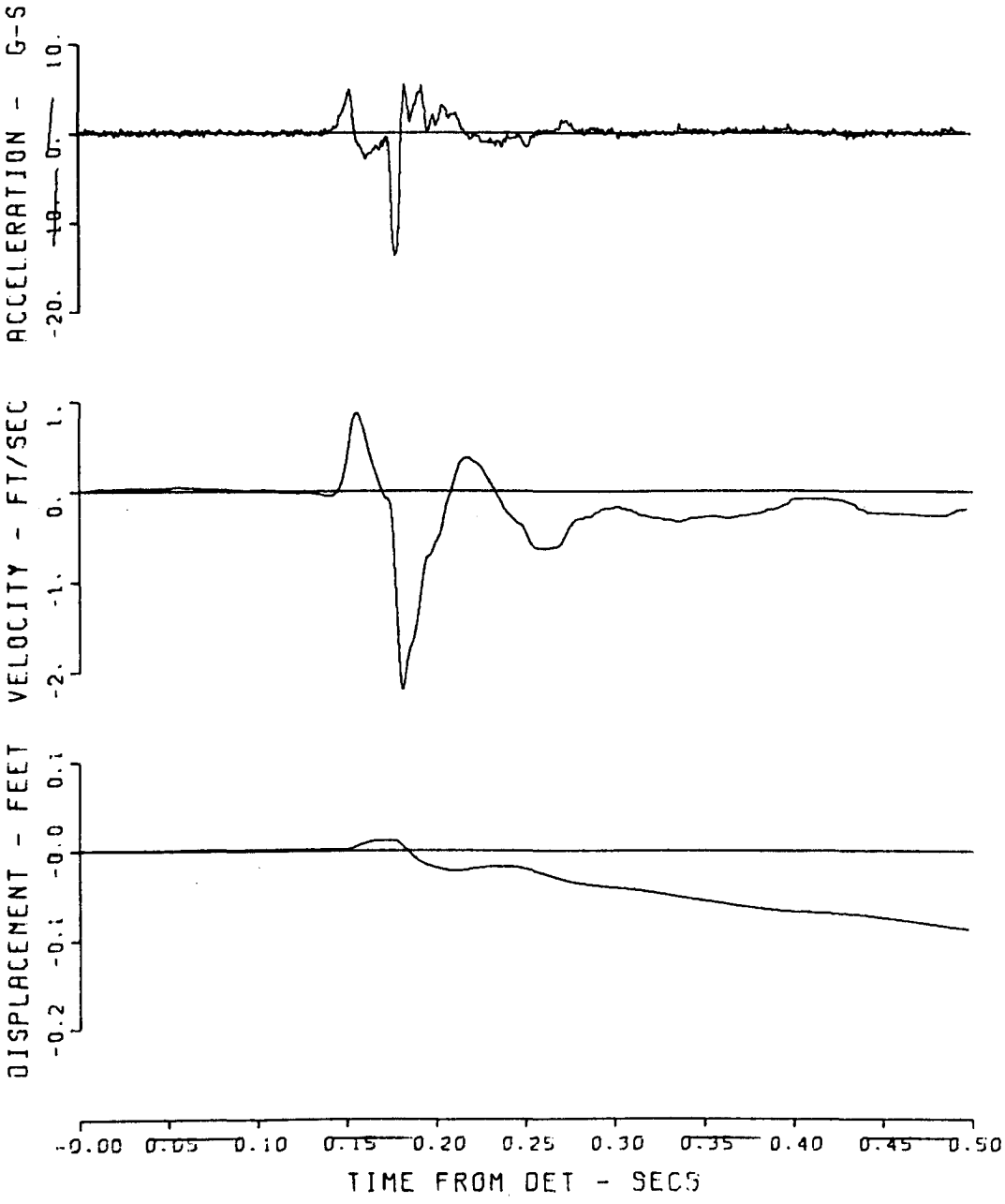

Figure B.1 Motion-time histories, Event Dial Pack (expanded time scale), Gage 645-1.5-AV.

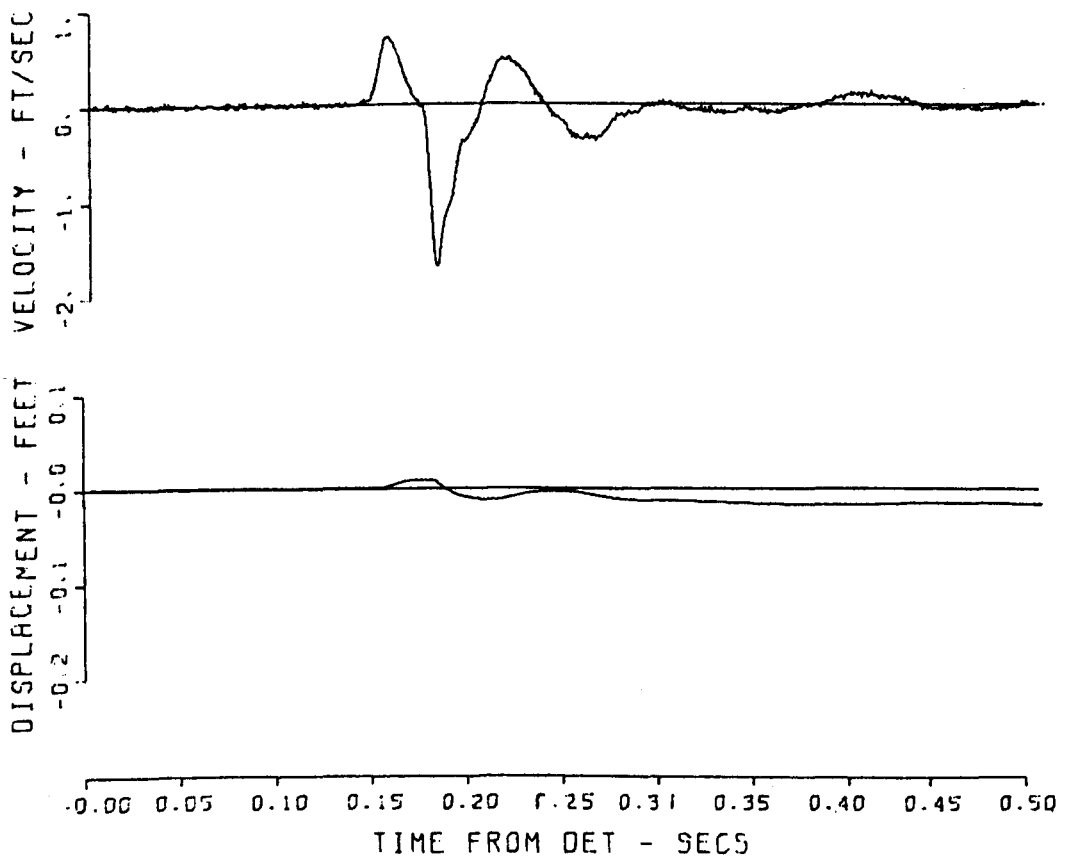

Figure B.2 Motion-time histories, Event Dial Pack (expanded time scale), Gage 645-1.5-UV.

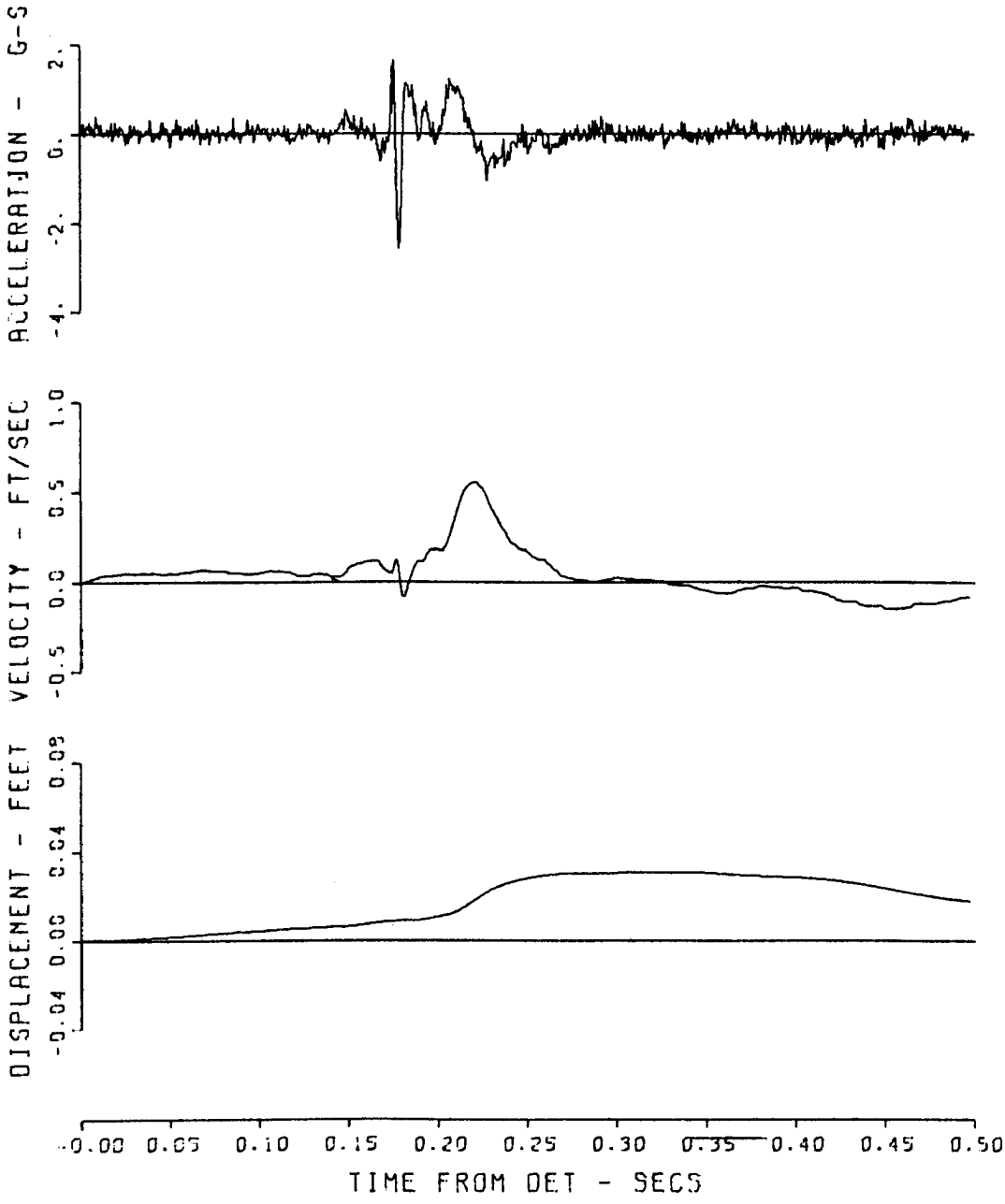

Figure B.3 Motion-time histories, Event Dial Pack (expanded time scale), Gage 645-1.5-AH.

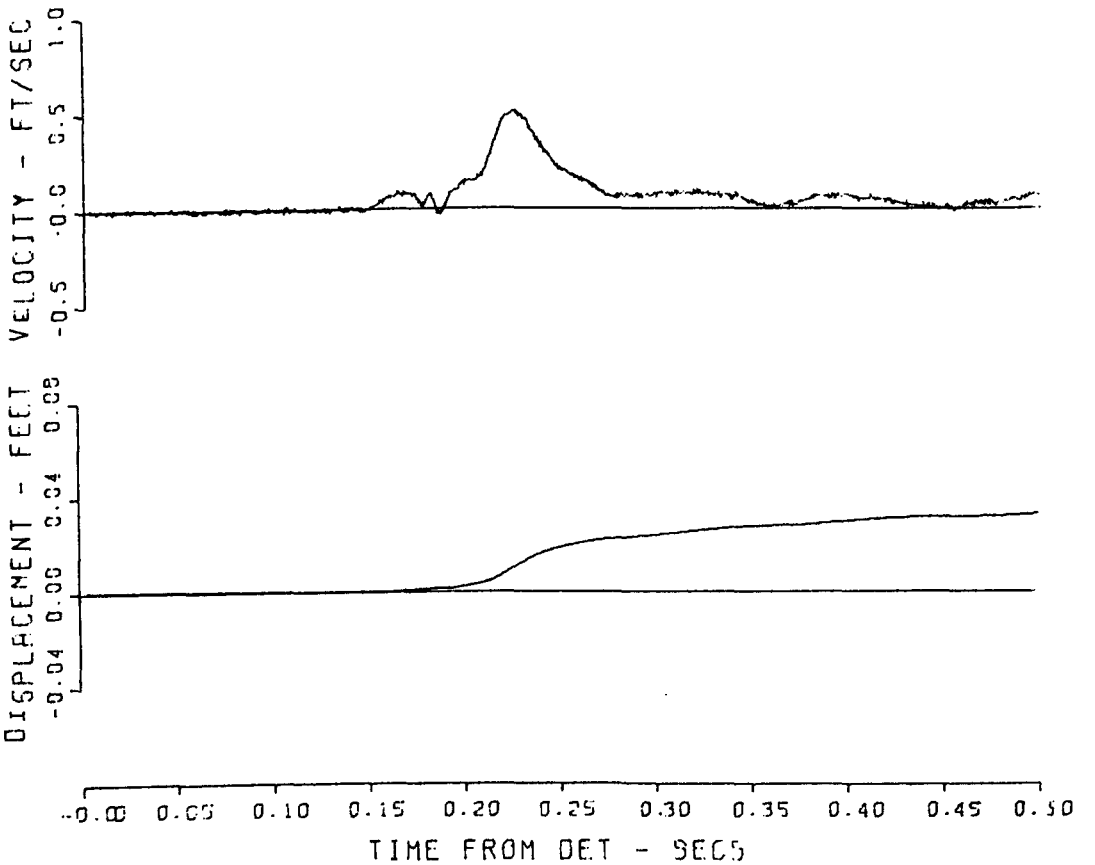

Figure B.4 Motion-time histories, Event Dial Pack (expanded time scale), Gage 645-1.5-UH.

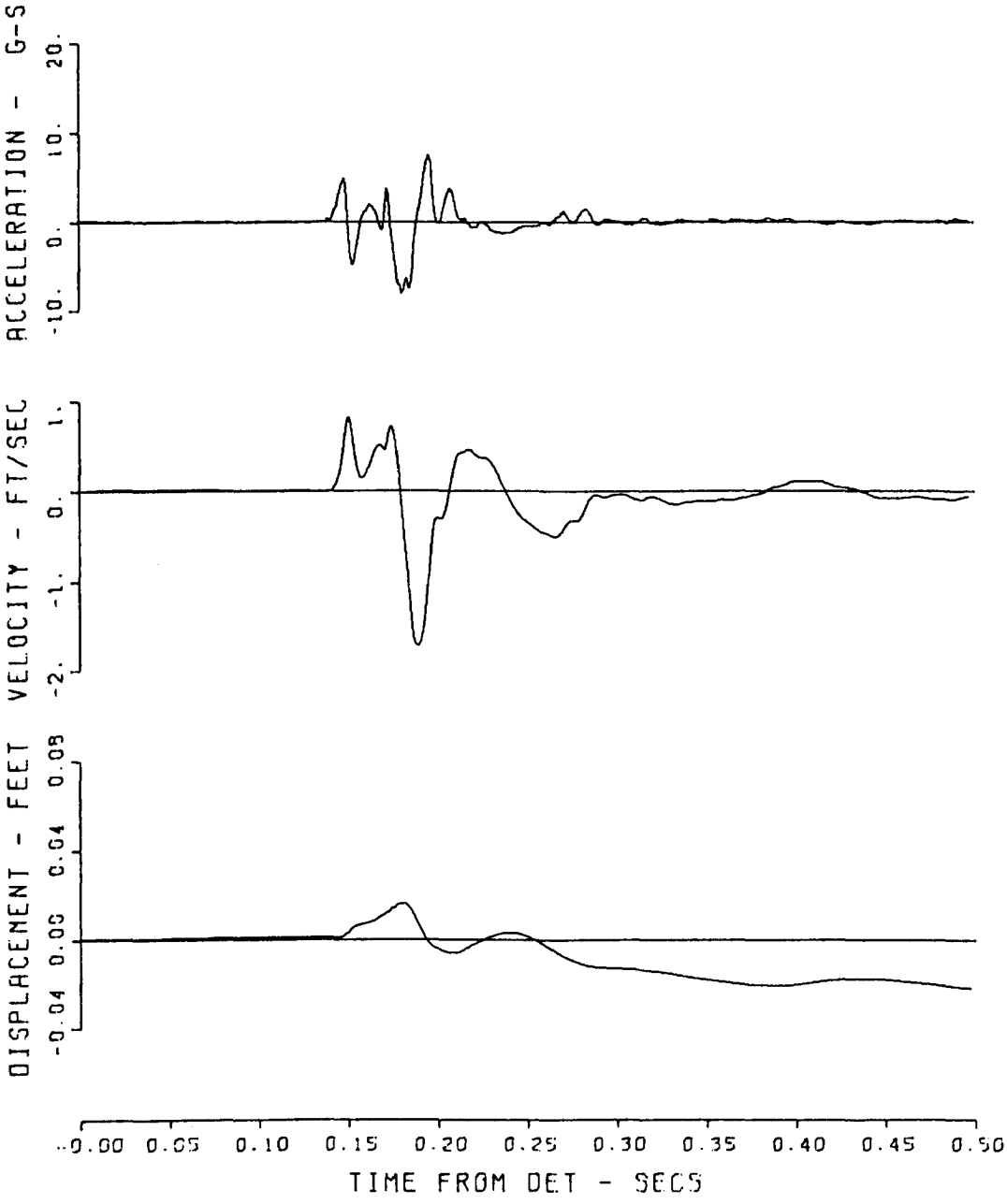

Figure B.5 Motion-time histories, Event Dial Pack (expanded time scale), Gage 645-5-AV.

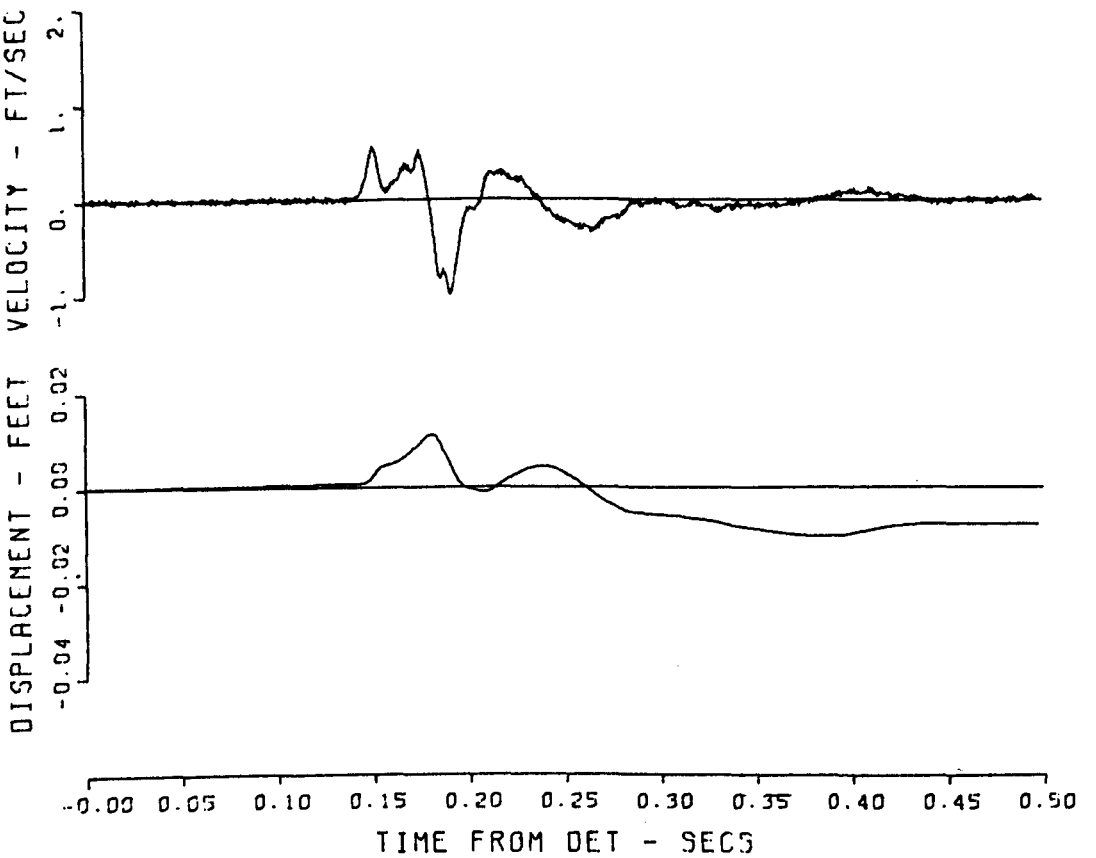

Figure B.6 Motion-time histories, Event Dial Pack (expanded time scale), Gage 645-5-UV.

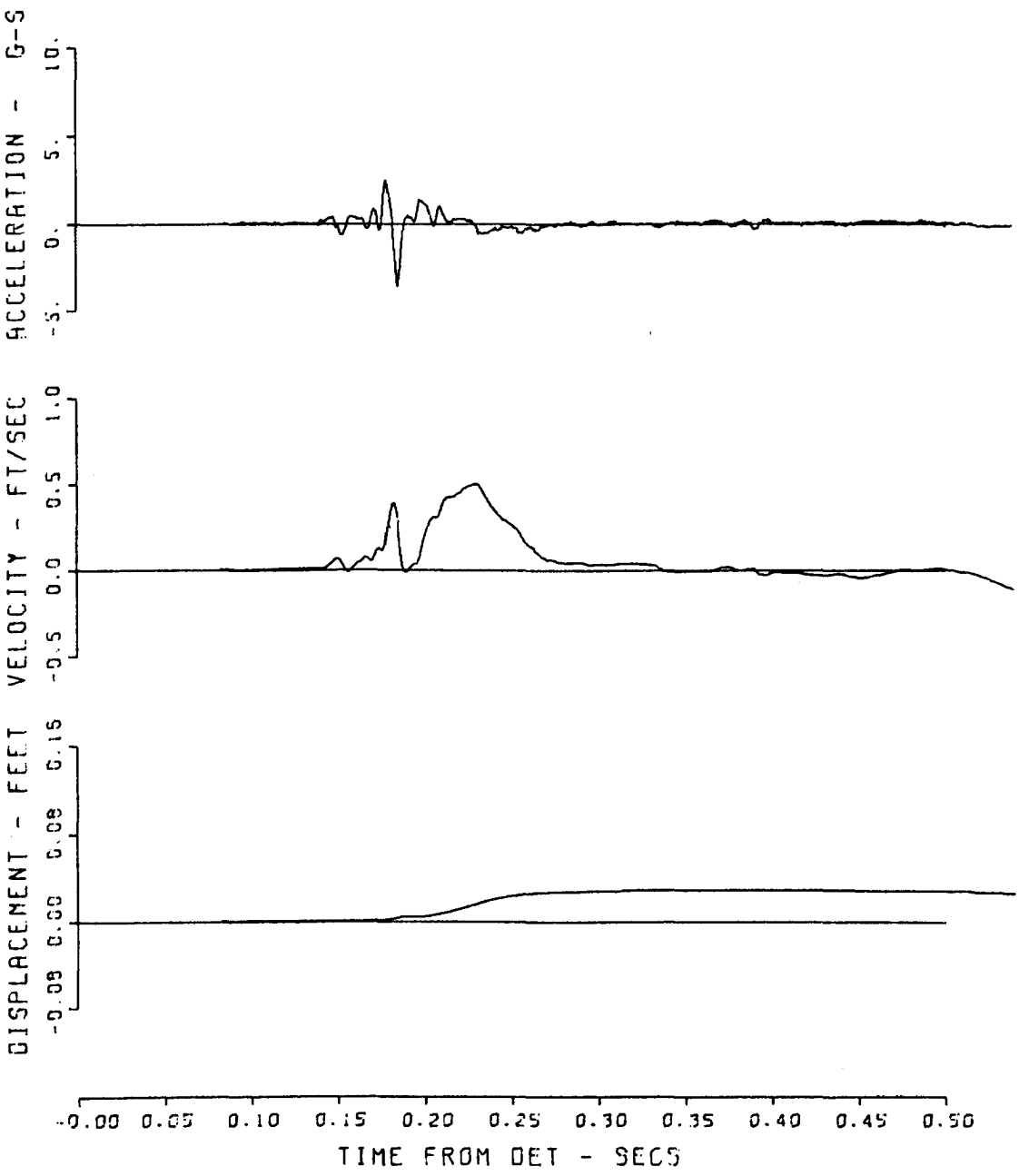

Figure B.7 Motion-time histories, Event Dial Pack (expanded time scale), Gage 645-5-AH.

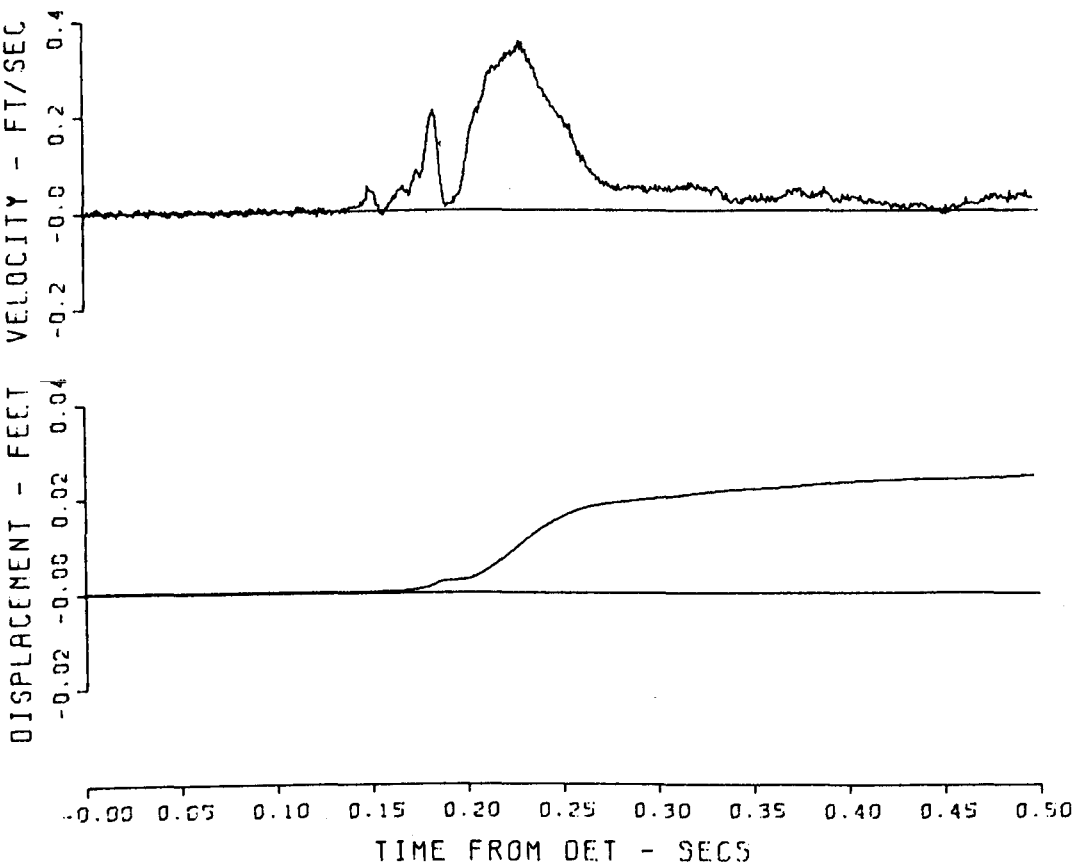

Figure B.8 Motion-time histories, Event Dial Pack (expanded time scale), Gage 645-5-UH.

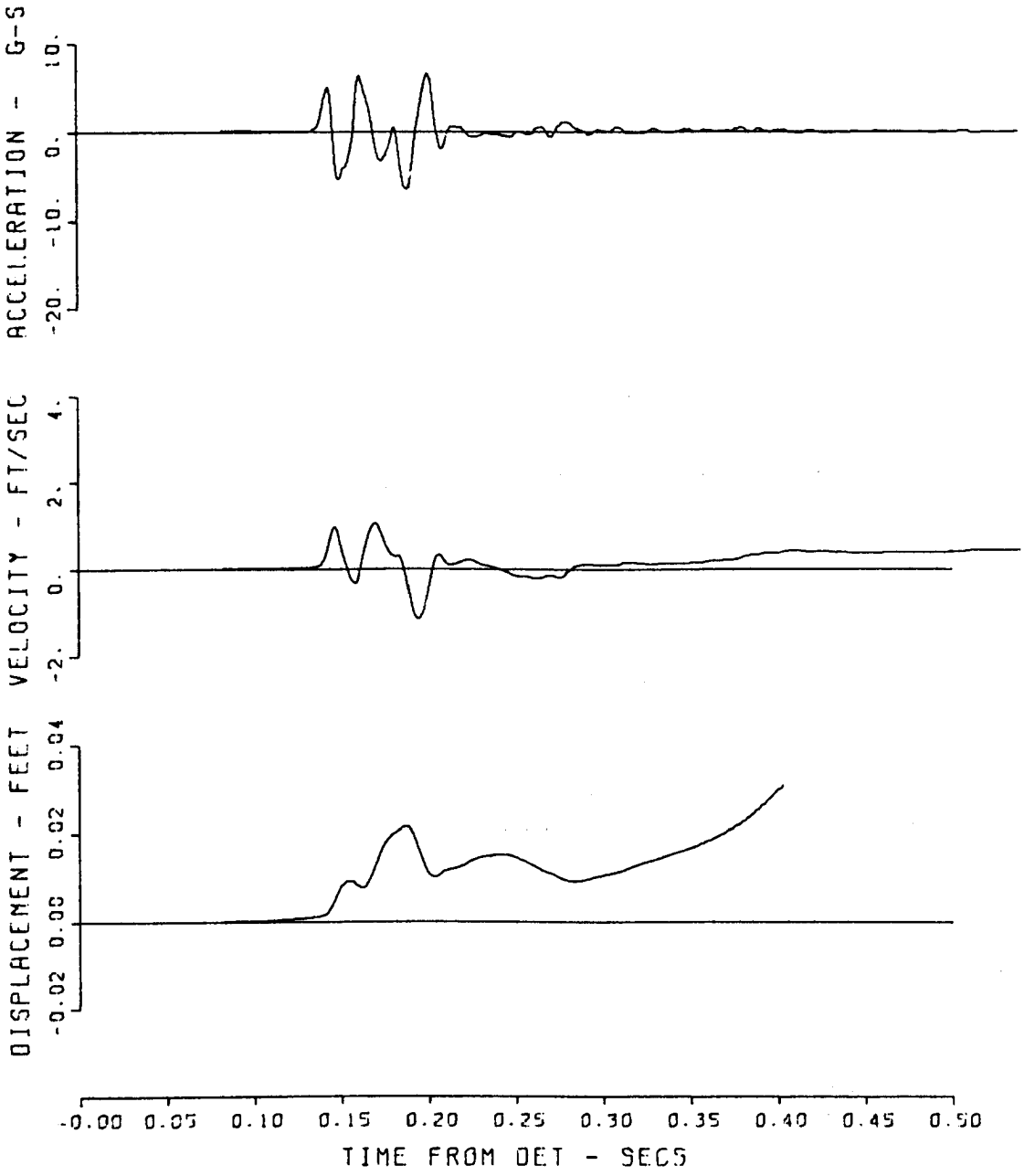

Figure B.9 Motion-time histories, Event Dial Pack (expanded time scale), Gage 645-10-AV.

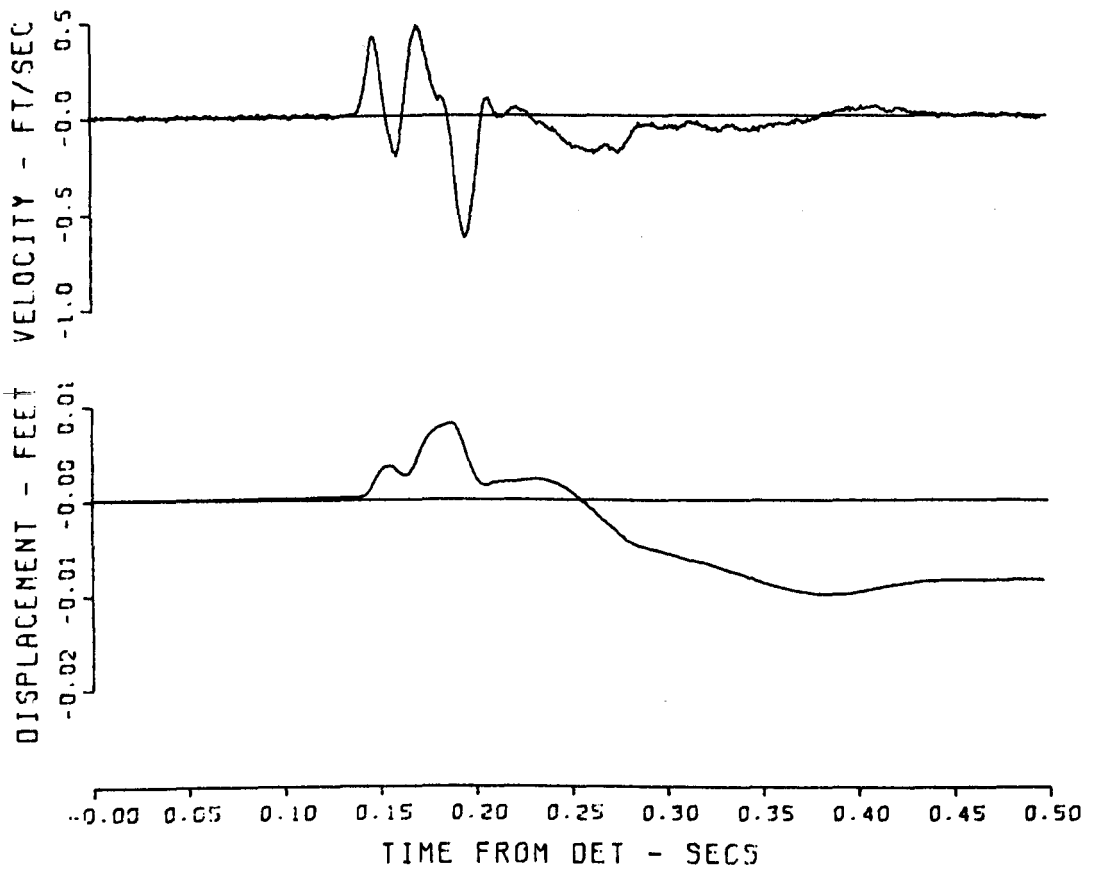

Figure B.10 Motion-time histories, Event Dial Pack (expanded time scale), Gage 645-10-UV.

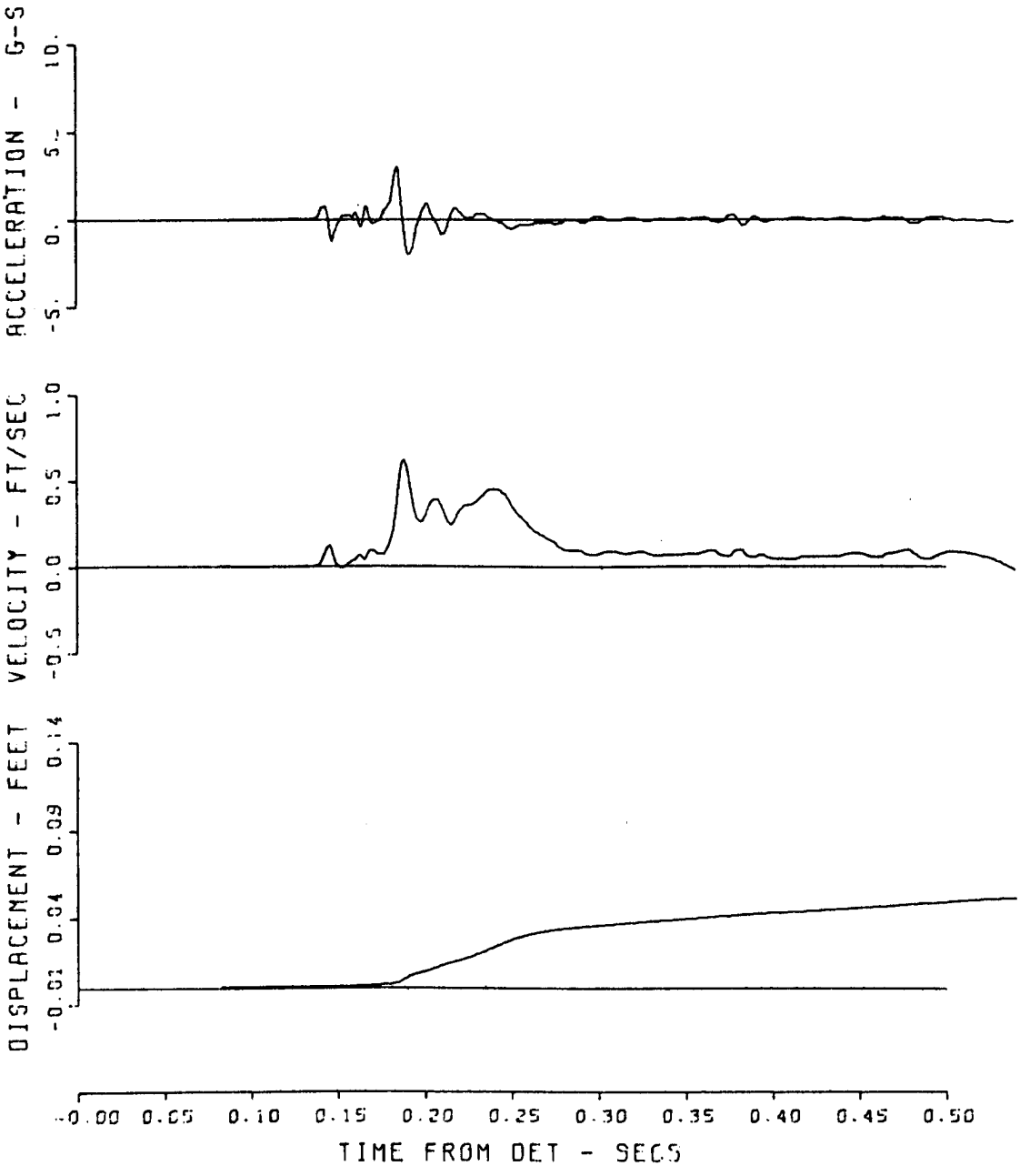

Figure B.11 Motion-time histories, Event Dial Pack (expanded time scale), Gage 645-10-AH.

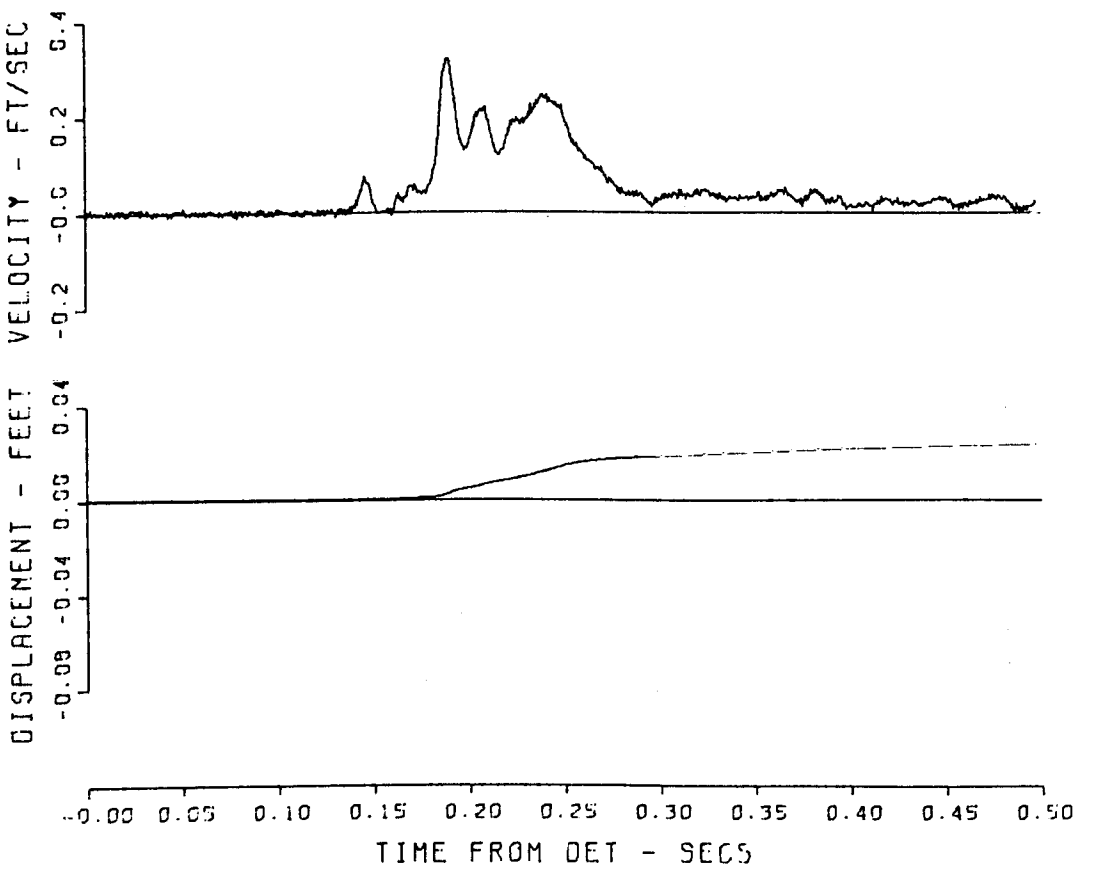

Figure B.12 Motion-time histories, Event Dial Pack (expanded time scale), Gage 645-10-UH.

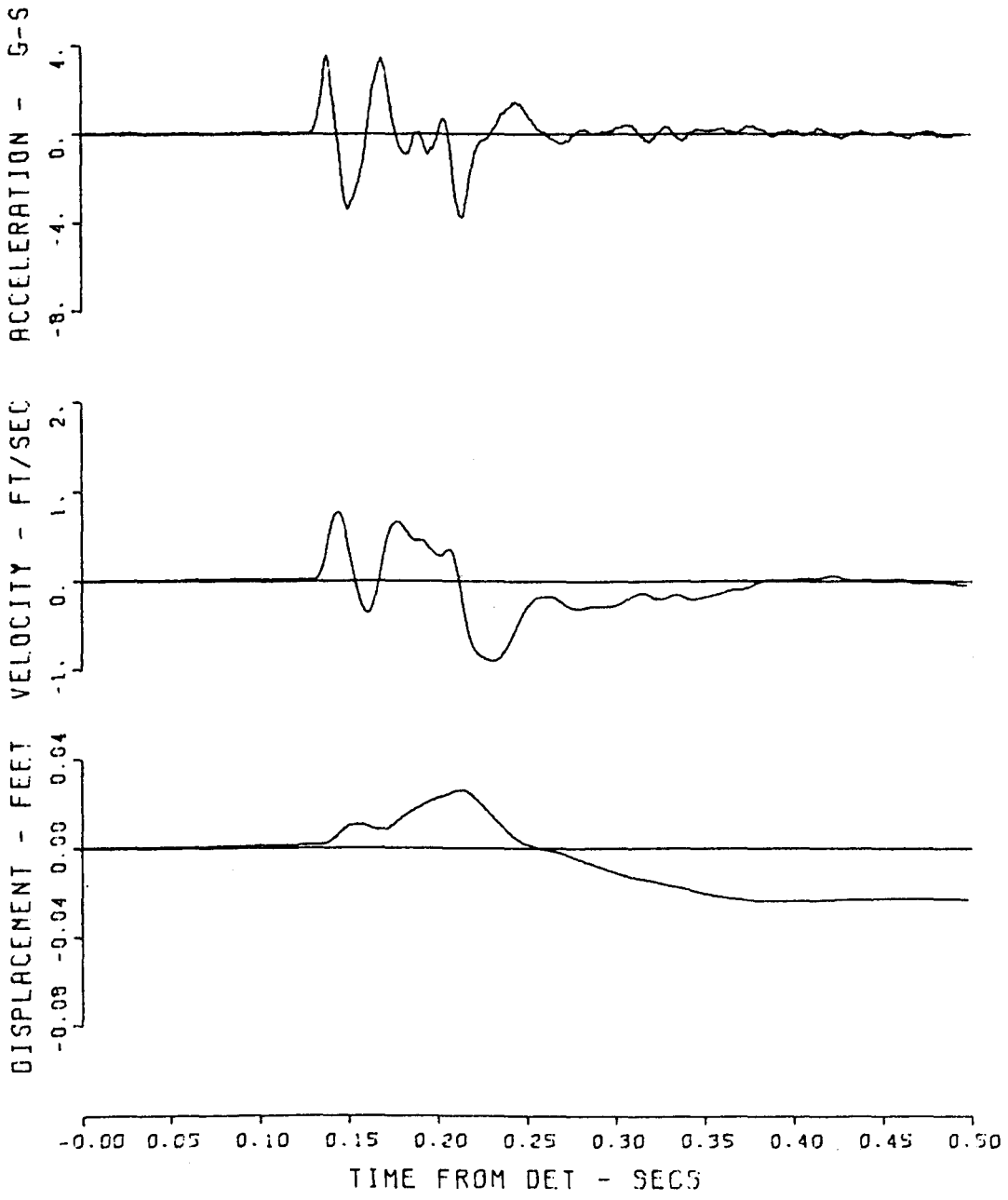

Figure B.13 Motion-time histories, Event Dial Pack (expanded time scale), Gage 645-20-AV.

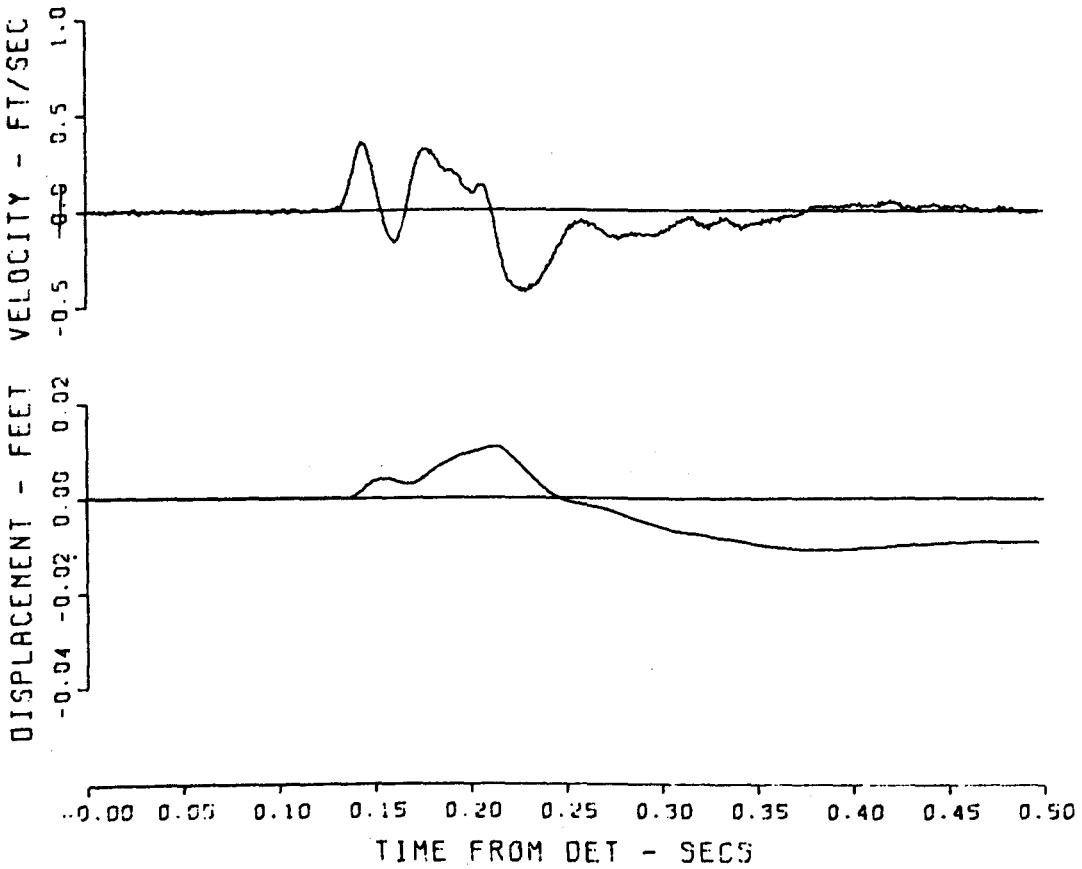

Figure B.14 Motion-time histories, Event Dial Pack (expanded time scale), Gage 645-20-UV.

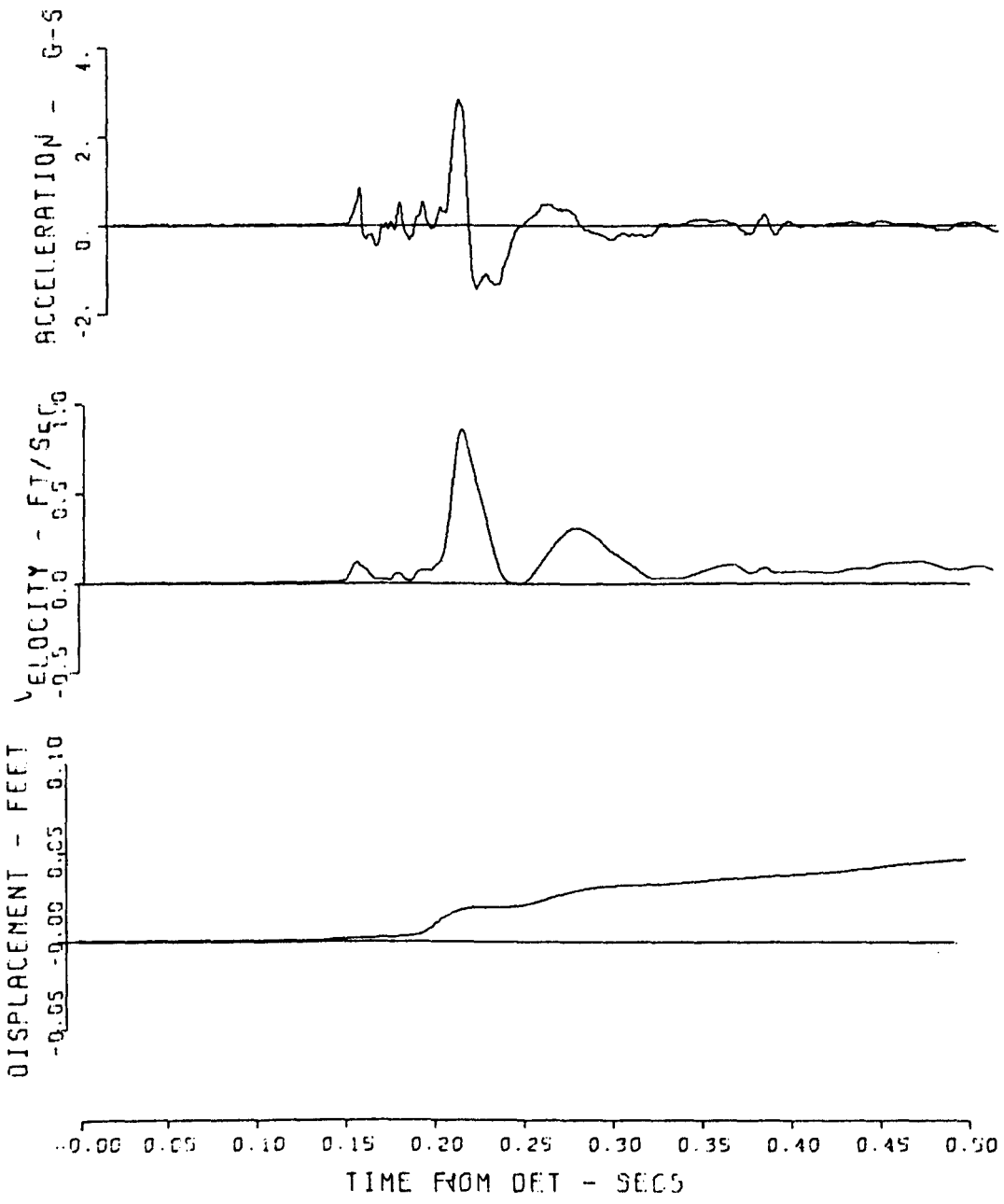

Figure B.15 Motion-time histories, Event Dial Pack (expanded time scale), Gage 645-20-AH.

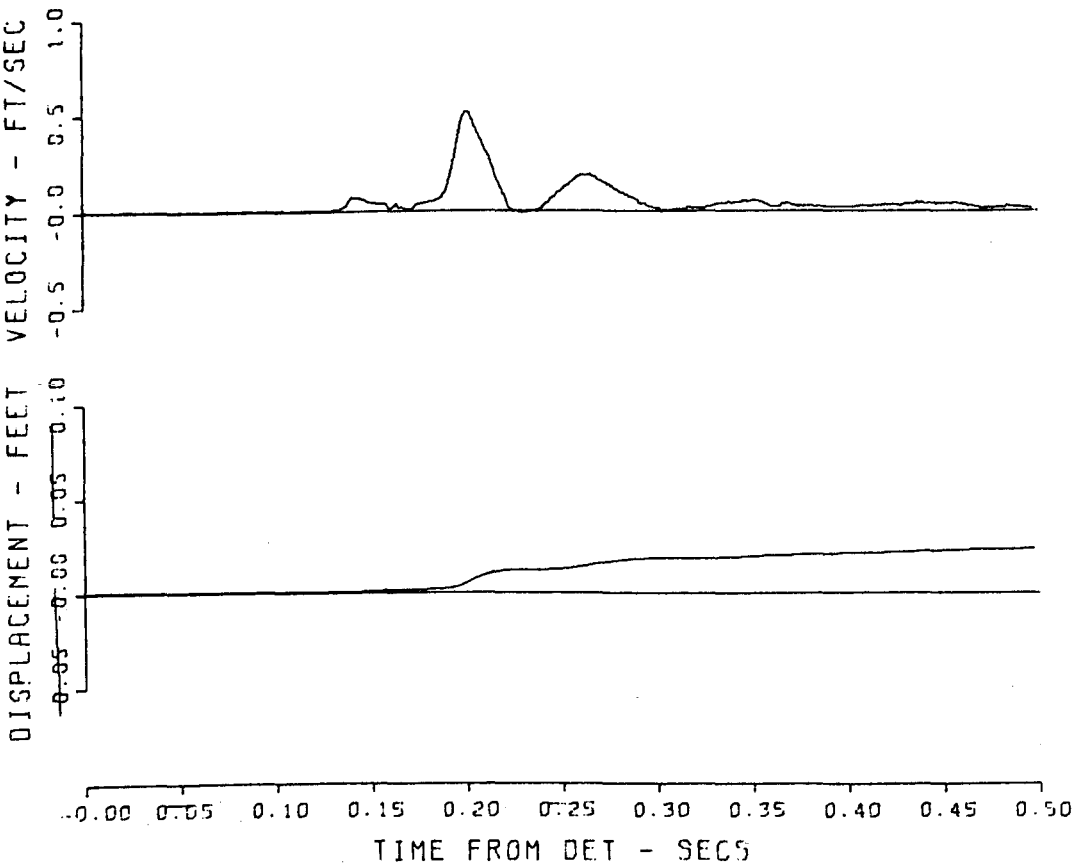

Figure B.16 Motion-time histories, Event Dial Pack (expanded time scale), Gage 645-20-UH.

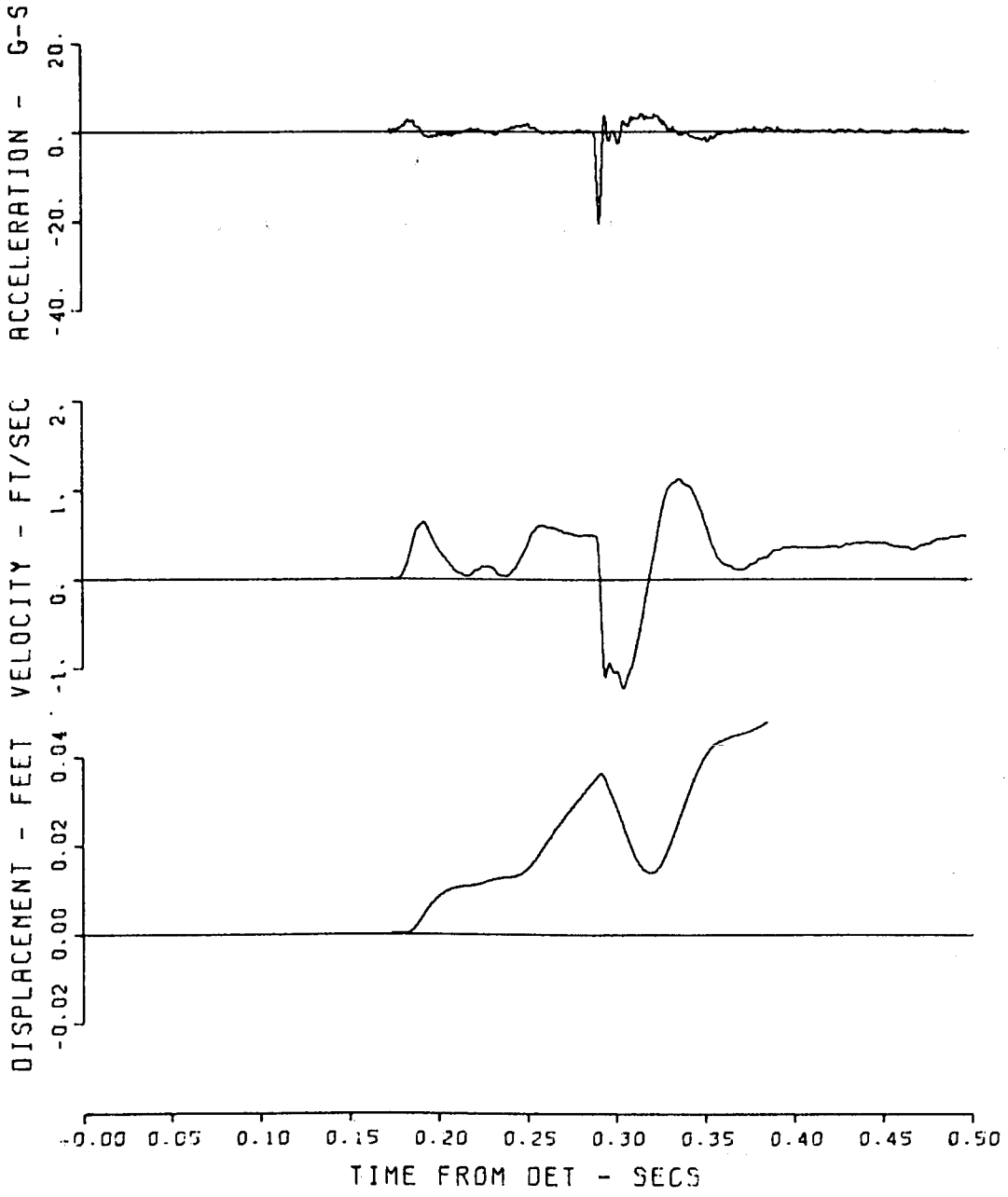

Figure B.17 Motion-time histories, Event Dial Pack (expanded time scale), Gage 840-1.5-AV.

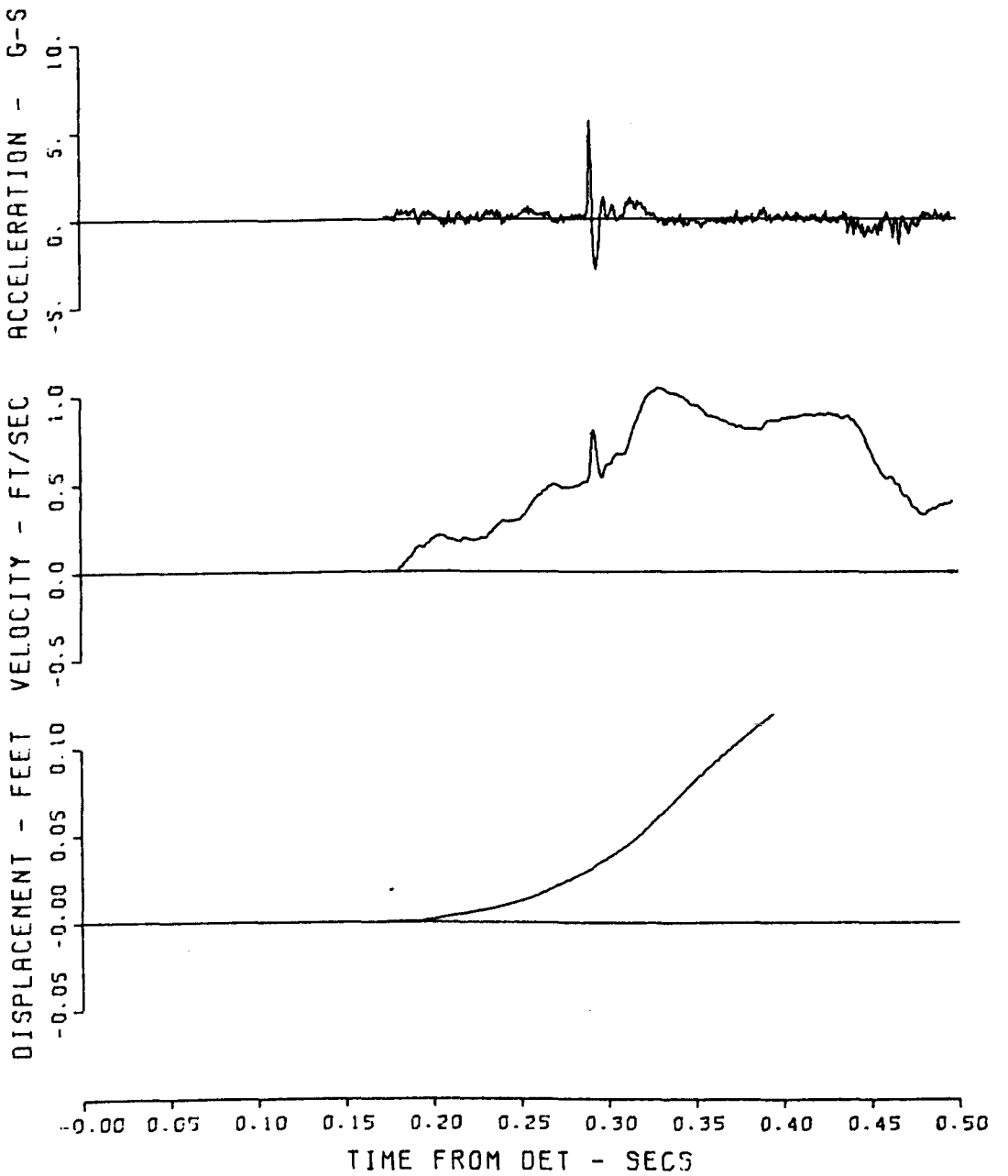

Figure B.18 Motion-time histories, Event Dial Pack (expanded time scale), Gage 840-1.5-AH.

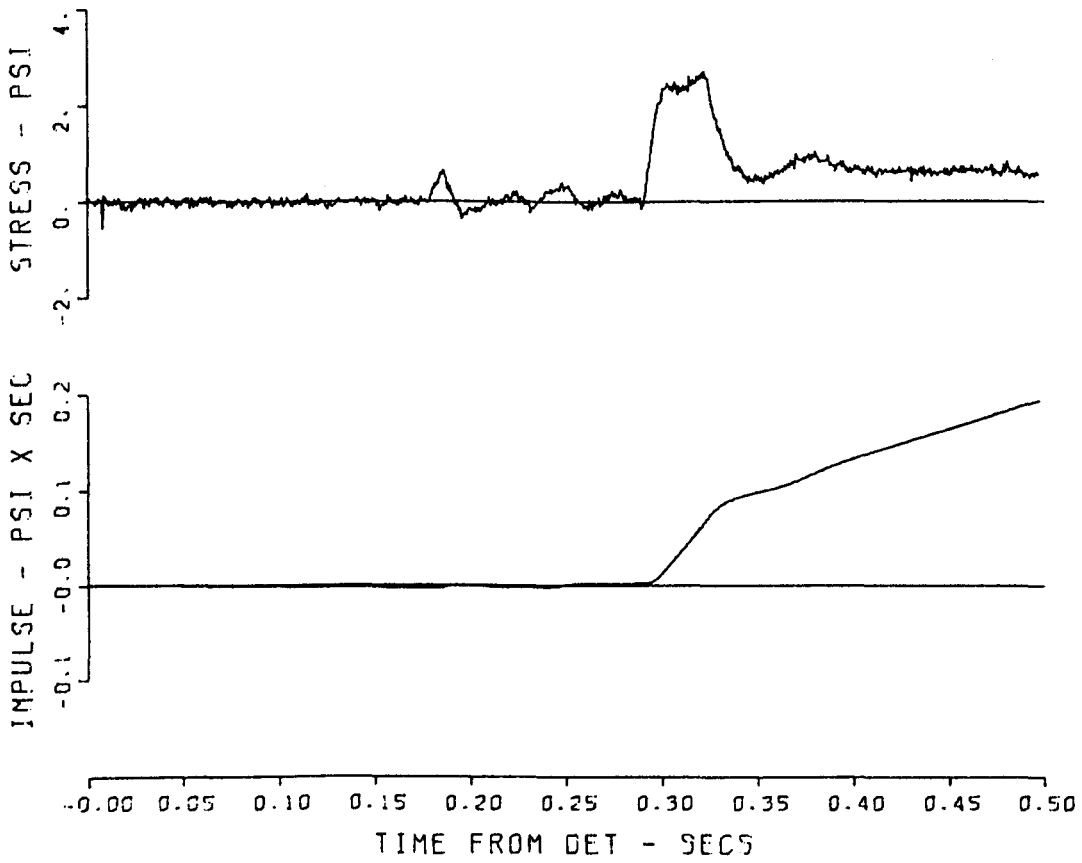

Figure B.19 Motion-time histories, Event Dial Pack (expanded time scale), Gage 840-1.5-PV.

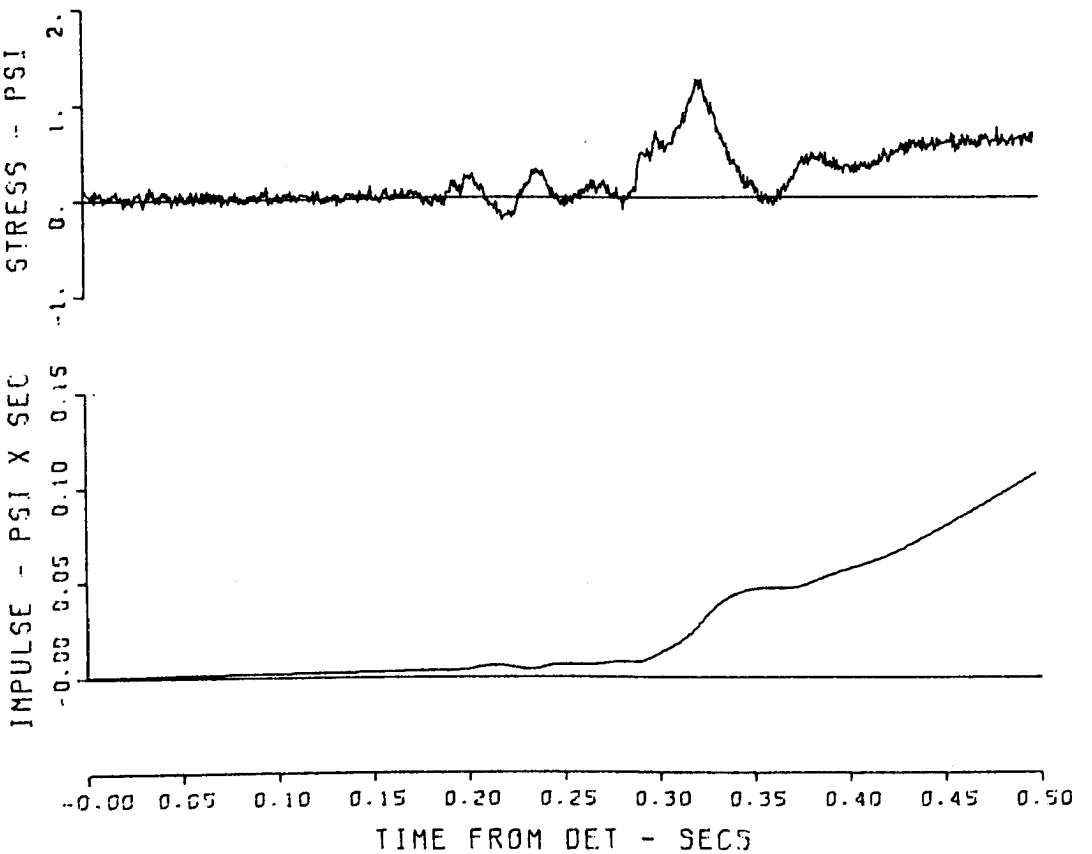

Figure B.20 Motion-time histories, Event Dial Pack (expanded time scale), Gage 840-1.5-PH.

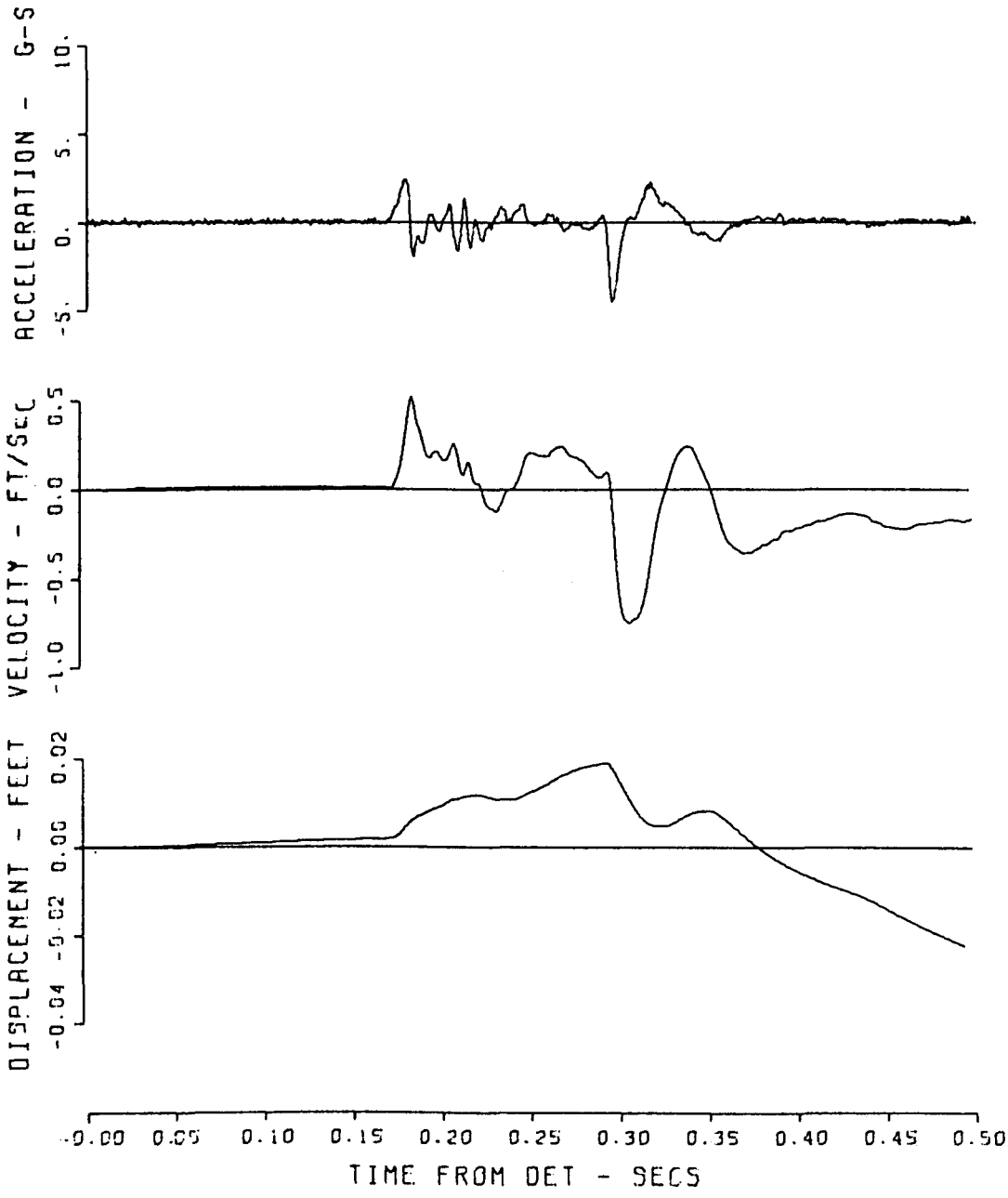

Figure B.21 Motion-time histories, Event Dial Pack (expanded time scale), Gage 840-5-AV.

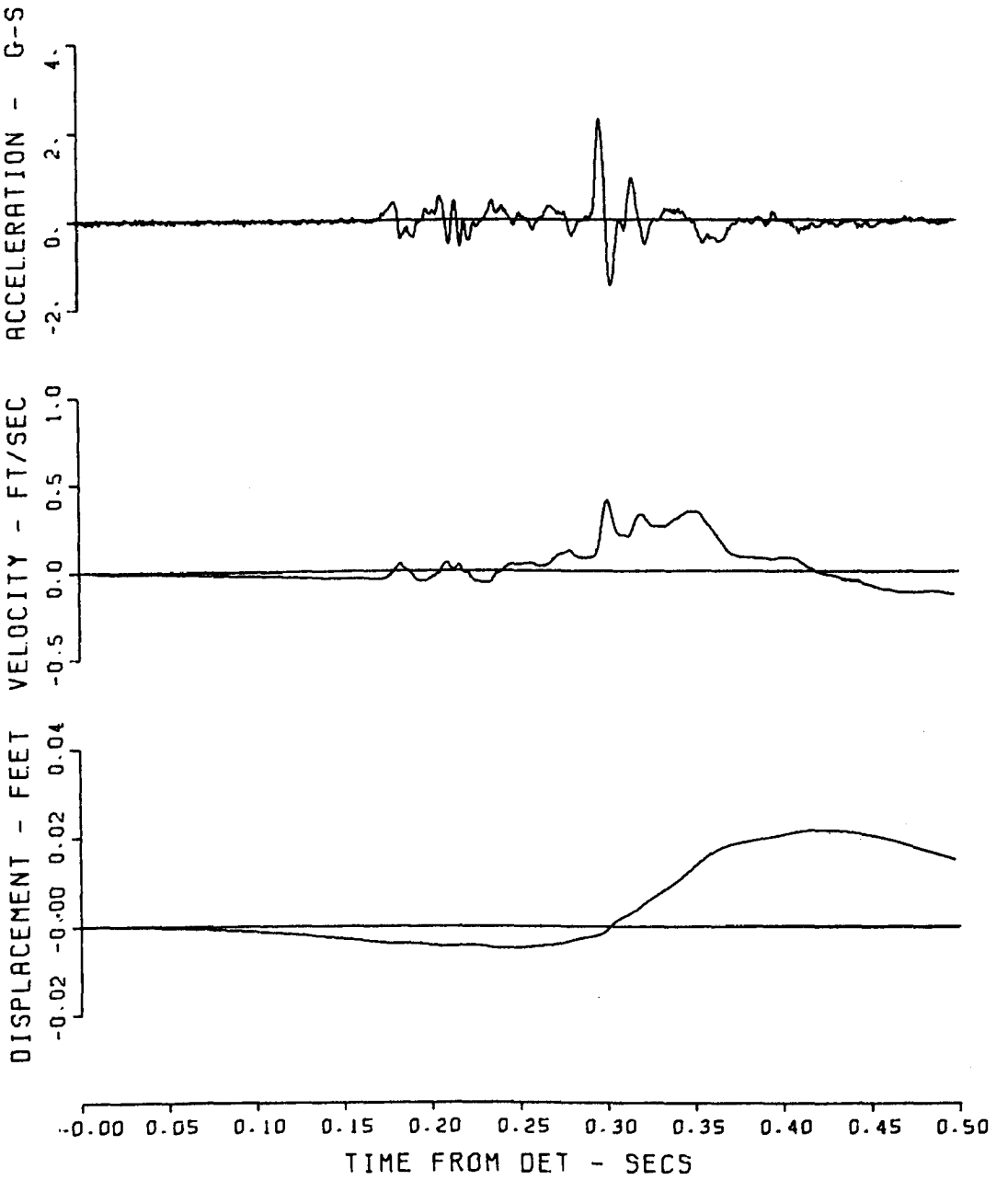

Figure B.22 Motion-time histories, Event Dial Pack (expanded time scale), Gage 840-5-AH.

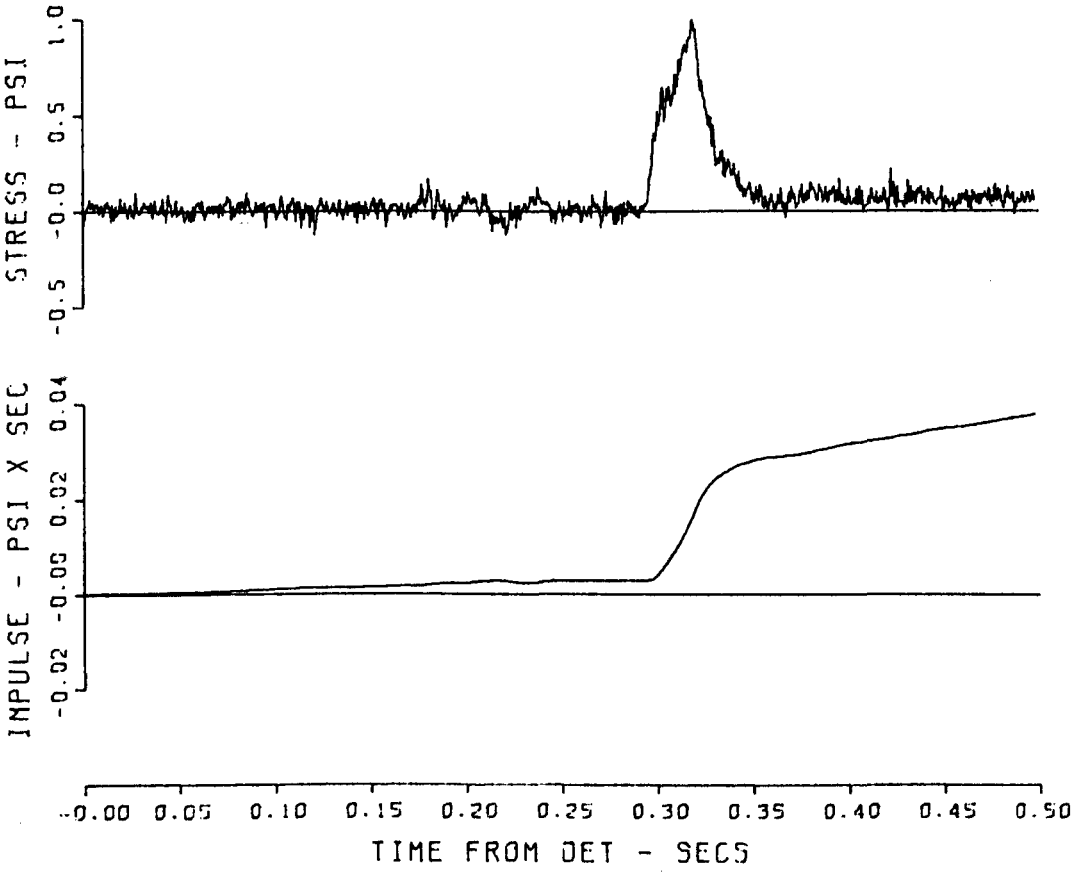

Figure B.23 Motion-time histories, Event Dial Pack (expanded time scale), Gage 840-5-PV.

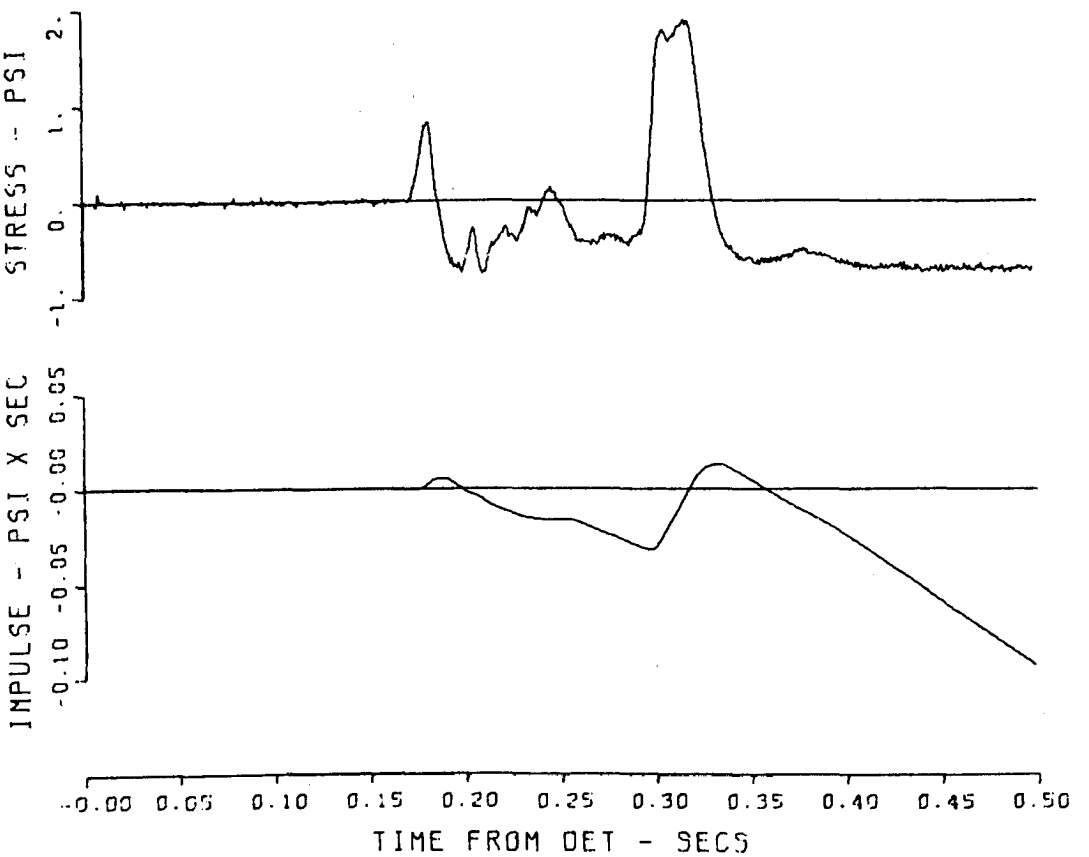

Figure B.24 Motion-time histories, Event Dial Pack (expanded time scale), Gage 840-5-PH.

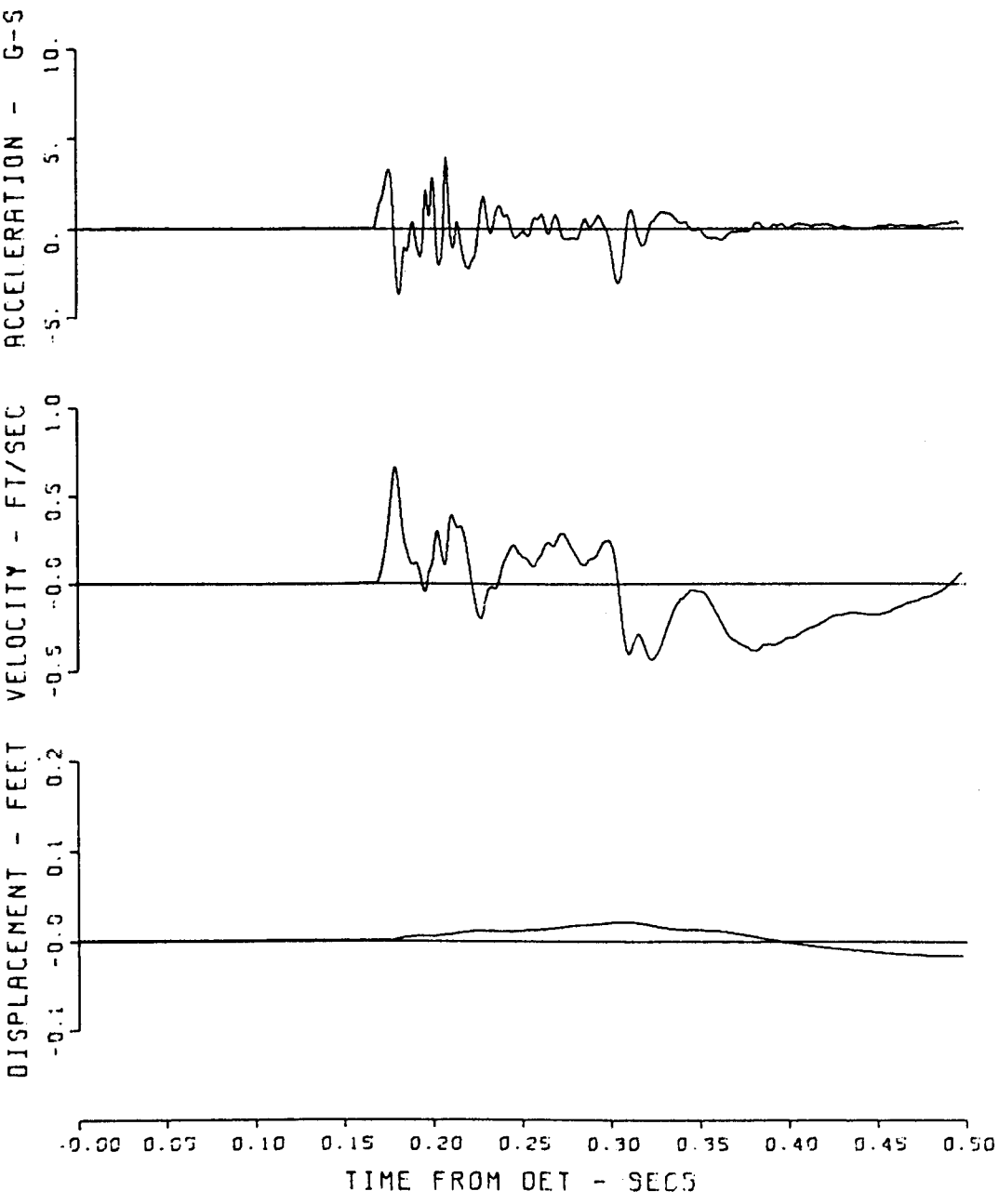

Figure B.25 Motion-time histories, Event Dial Pack (expanded time scale), Gage 840-10-AV.

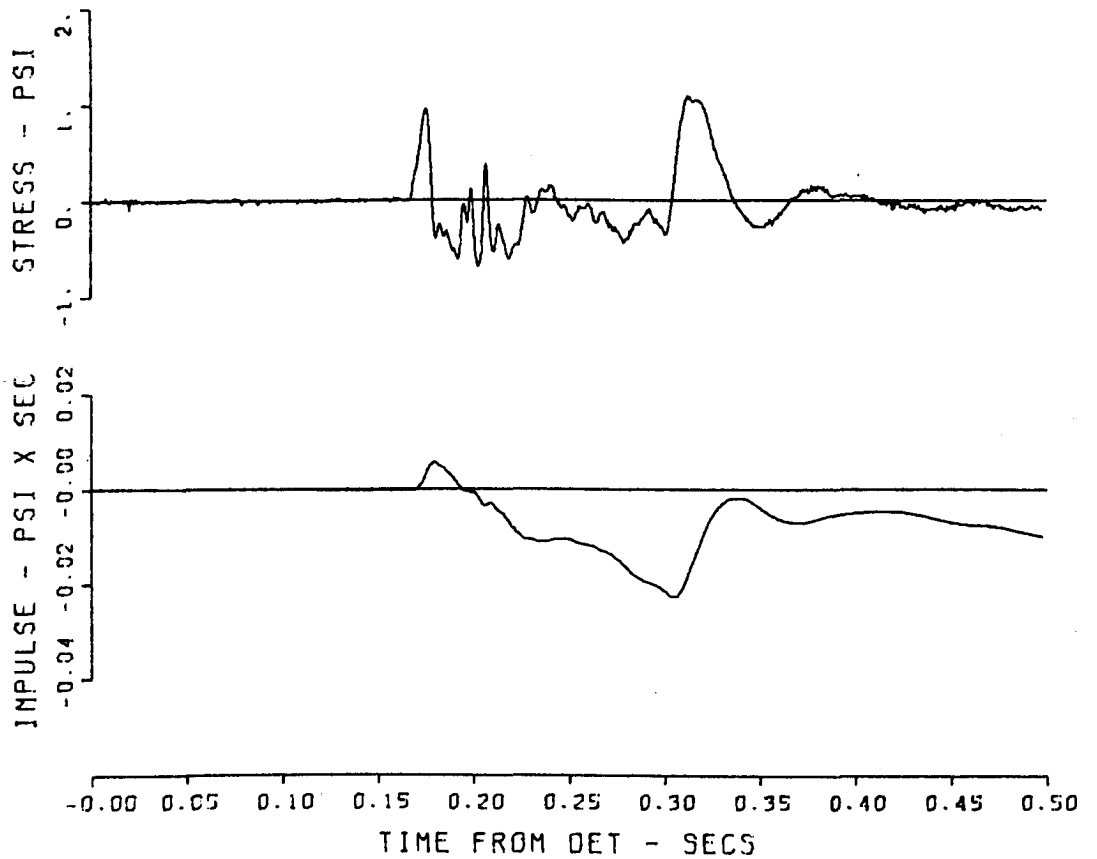

Figure B.26 Motion-time histories, Event Dial Pack (expanded time scale), Gage 840-10-PV.

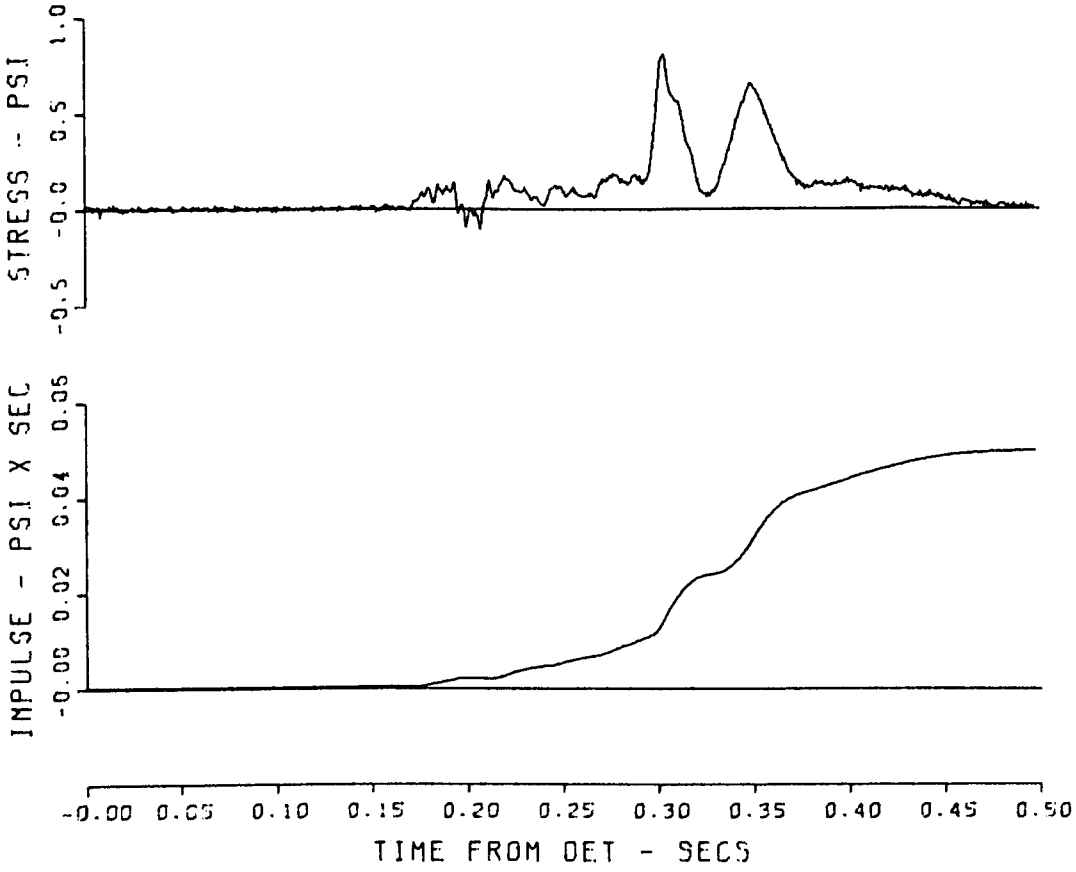

Figure B.27 Motion-time histories, Event Dial Pack (expanded time scale), Gage 840-10-PH.

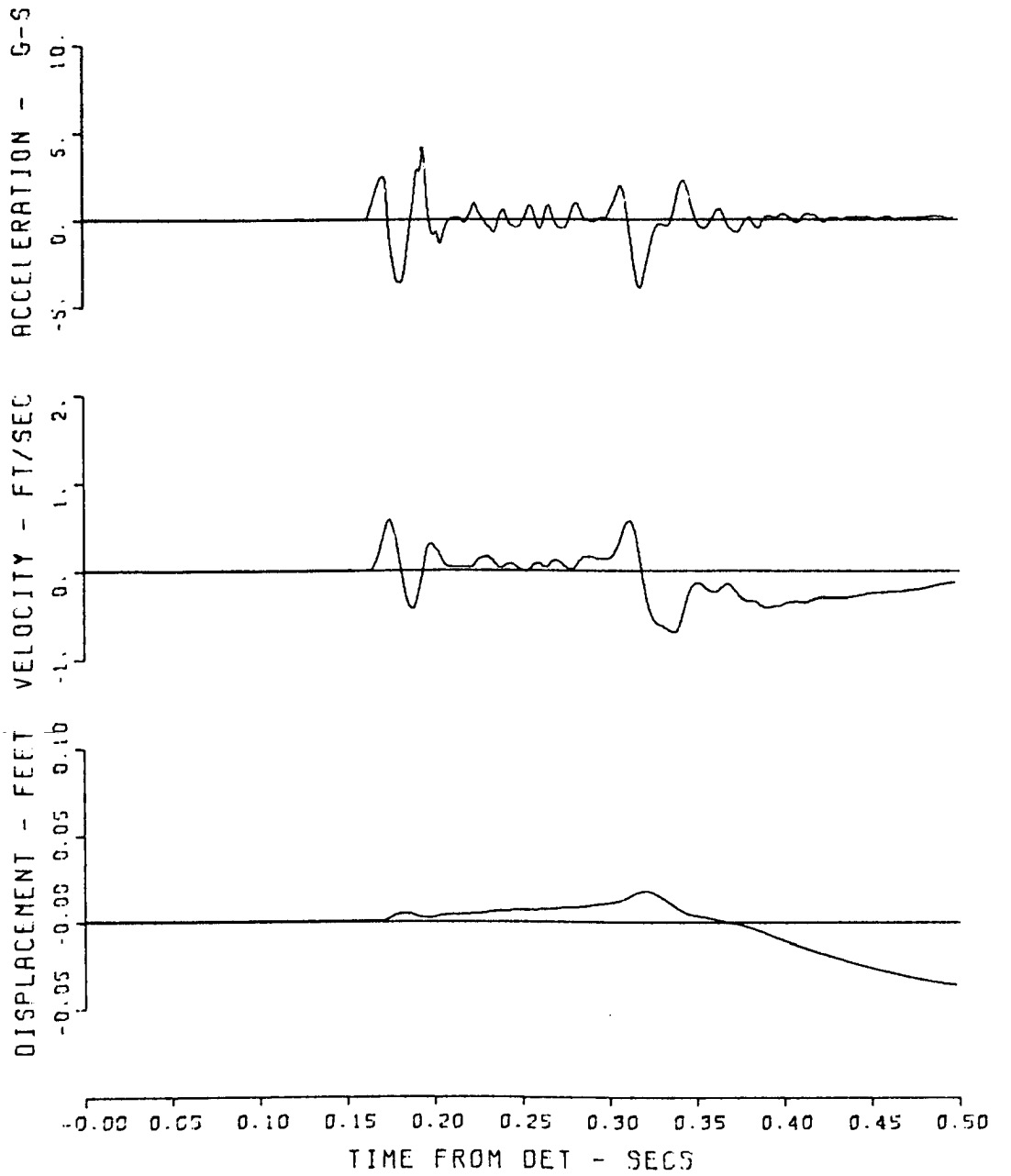

Figure B.28 Motion-time histories, Event Dial Pack (expanded time scale), Gage 840-20-AV.

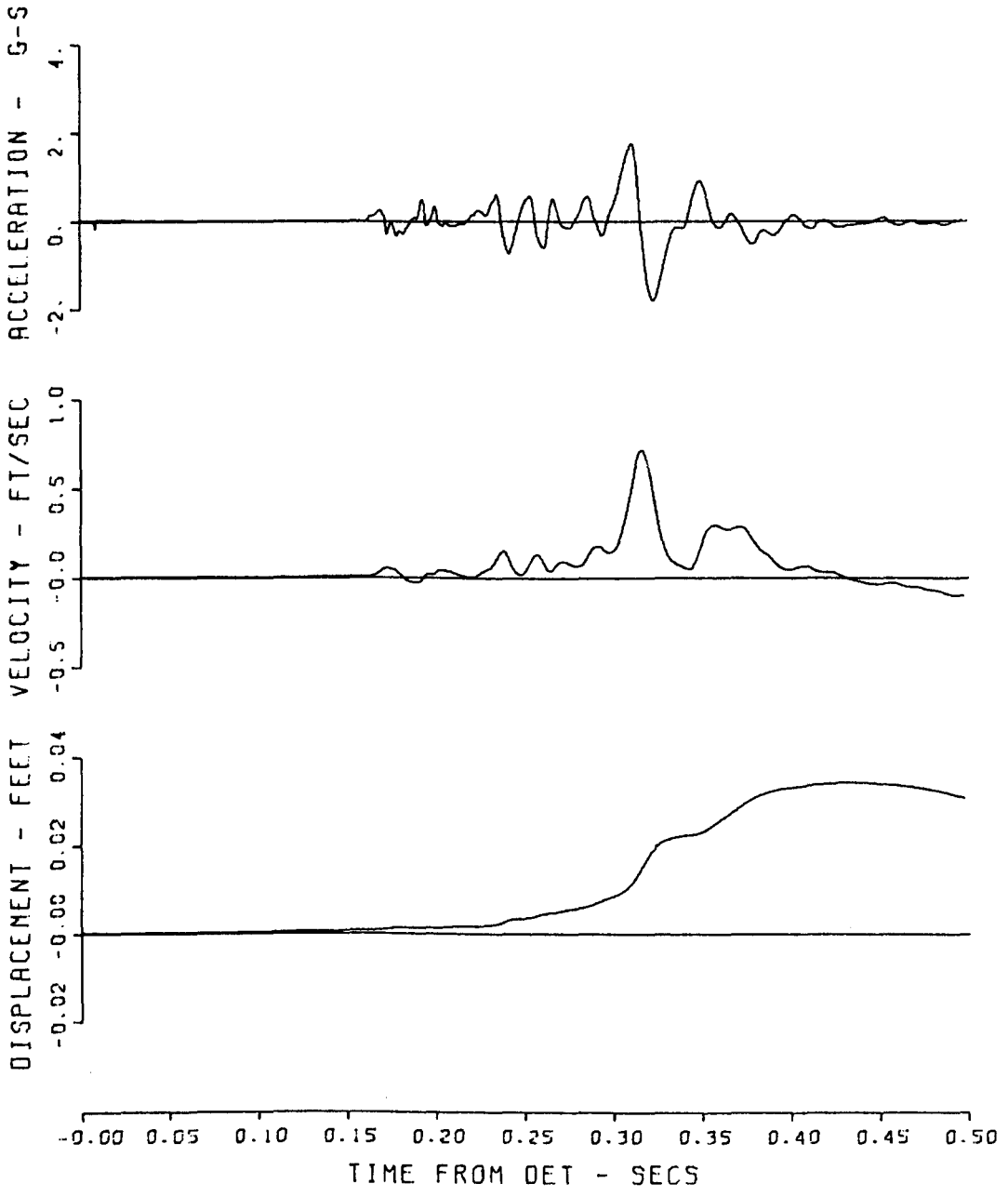

Figure B.29 Motion-time histories, Event Dial Pack (expanded time scale), Gage 840-20-AH.

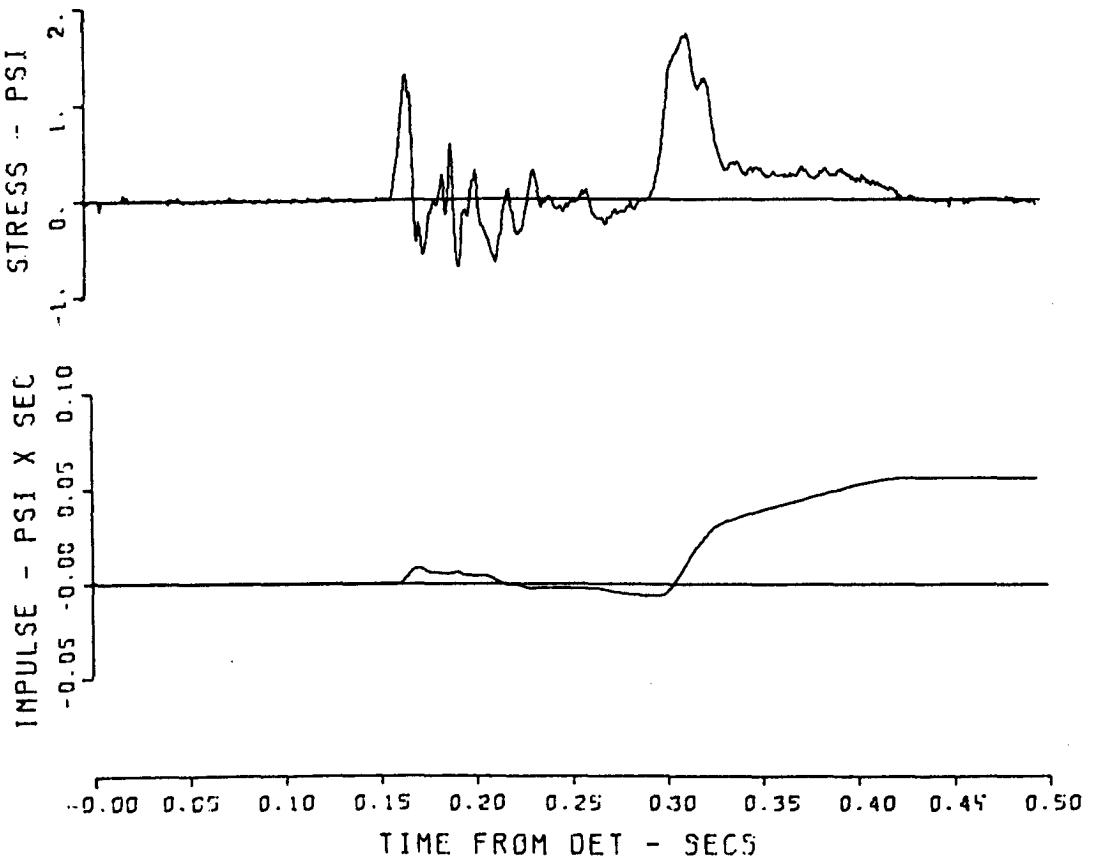

Figure B.30 Motion-time histories, Event Dial Pack (expanded time scale), Gage 840-20-PV.

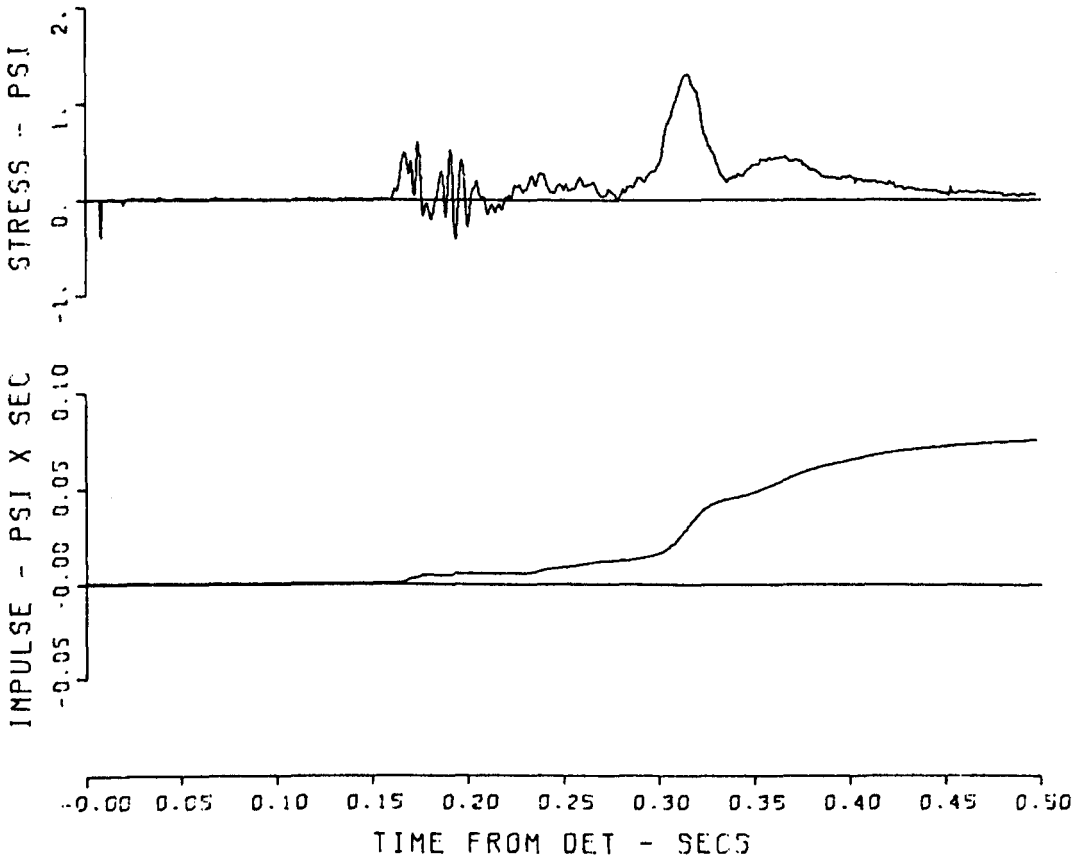

Figure B.31 Motion-time histories, Event Dial Pack (expanded time scale), Gage 840-20-PH.

APPENDIX C

FOURIER SPECTRA

Calculations of the Fourier undamped residual response spectra made for eight of the sixteen acceleration measurements are presented herein.

Peak response amplitudes (pseudovelocity) for both the vertical and horizontal data are noted to be somewhat depth sensitive, occurring at about 10 to 13 Hz for measurements from the 1.5-foot depth and about 30 to 50 Hz for measurements from the 5-, 10-, and 20-foot depths. The horizontal spectrum for the 645-foot range and 10-foot depth (Figure C.4) shows a well-defined maximum at 1.5 Hz, which was the frequency of the late-time motion. Spectra of the other horizontal measurements were not computed to a sufficiently low frequency to enable this maximum to be observed.

Ratios of pseudovelocity to measured peak velocity were calculated for seven of the eight spectra. These ranged from 0.5 to 4.2, and averaged 2.7.

The explanation of the gage numbers in the titles of Figures C.1 through C.8 is the same as that for Appendixes A and B.

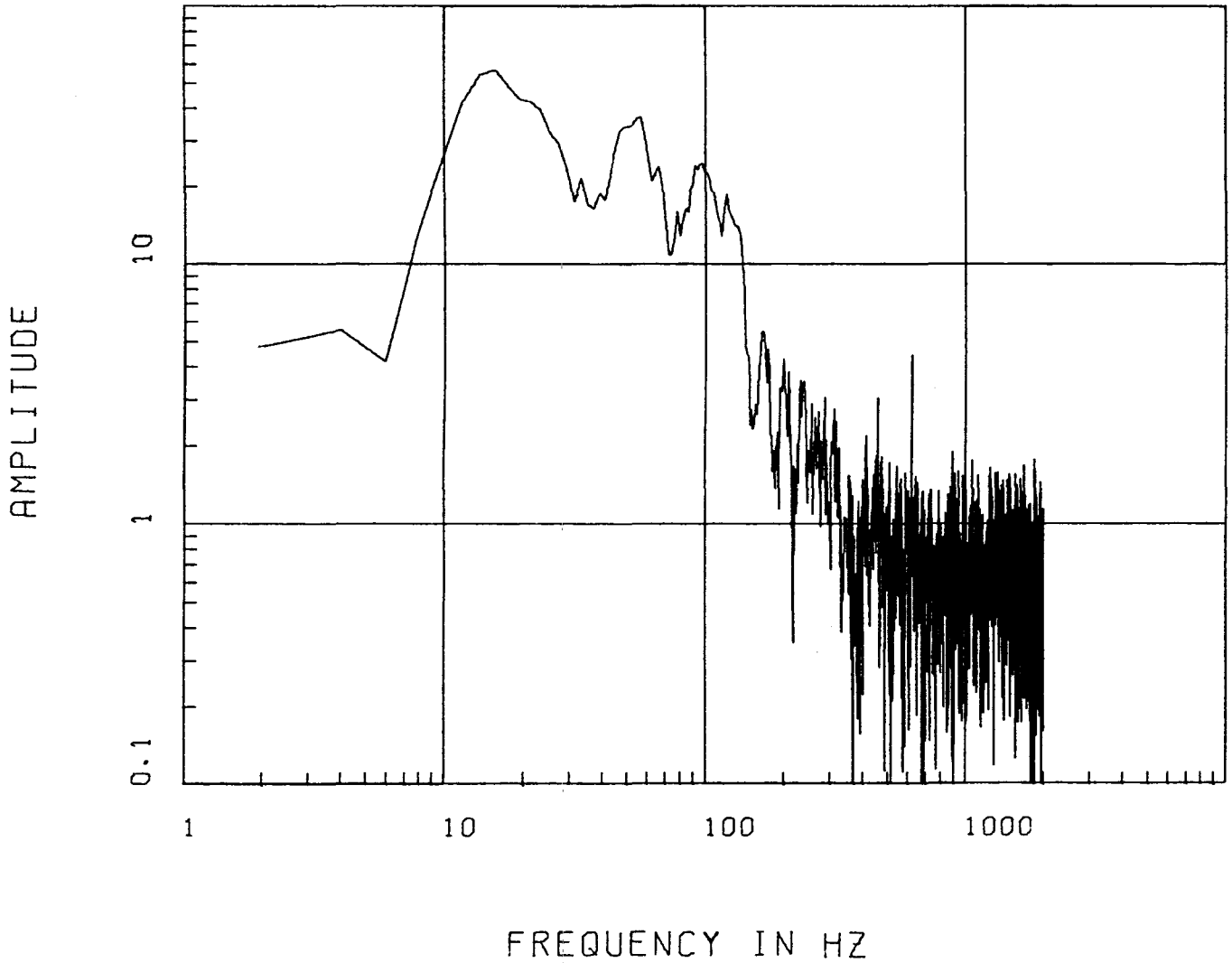

Figure C.1 Frequency response spectrum, Event Dial Pack, Gage 645-1.5-AV.

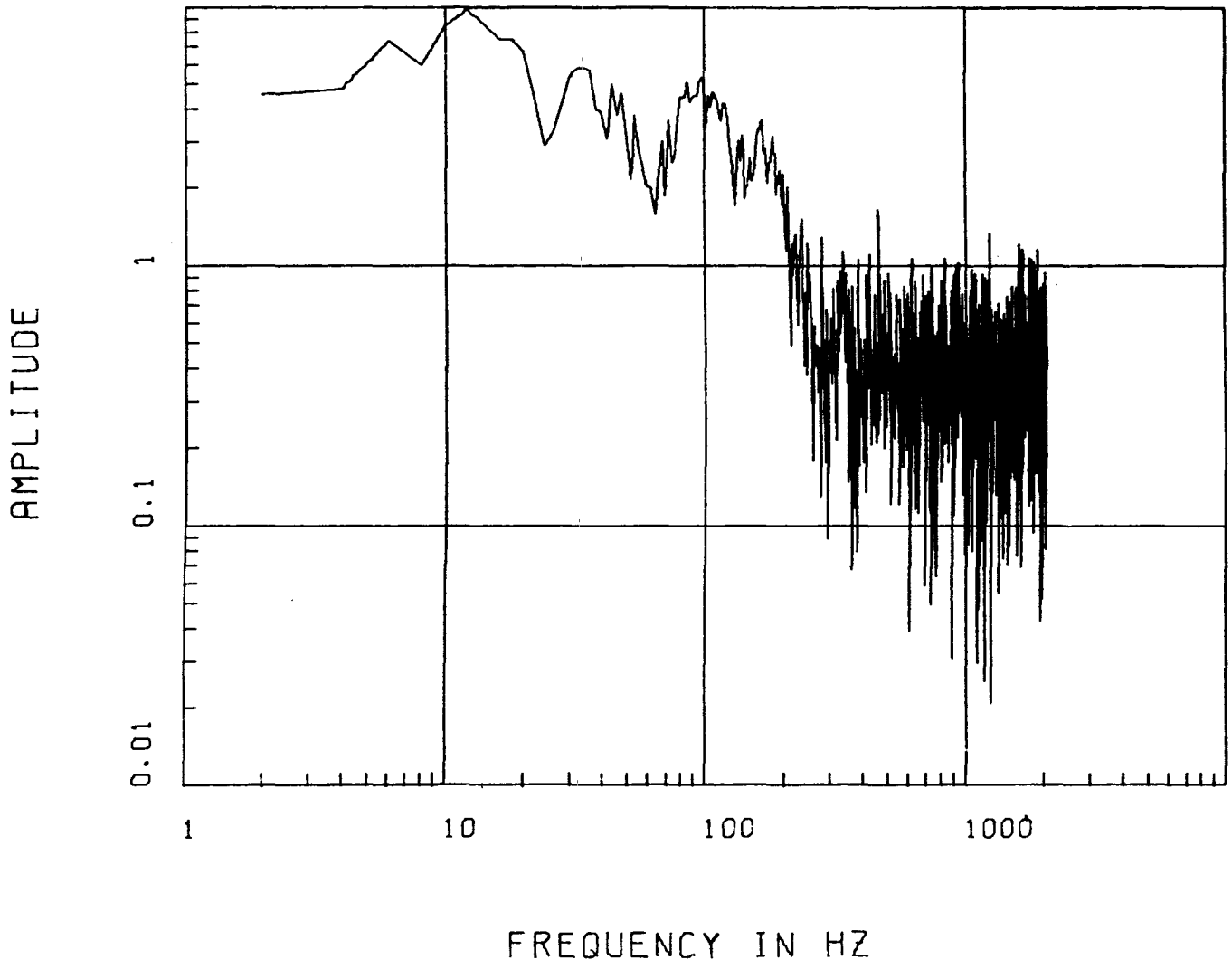

Figure C.2 Frequency response spectrum, Event Dial Pack, Gage 645-1.5-AH.

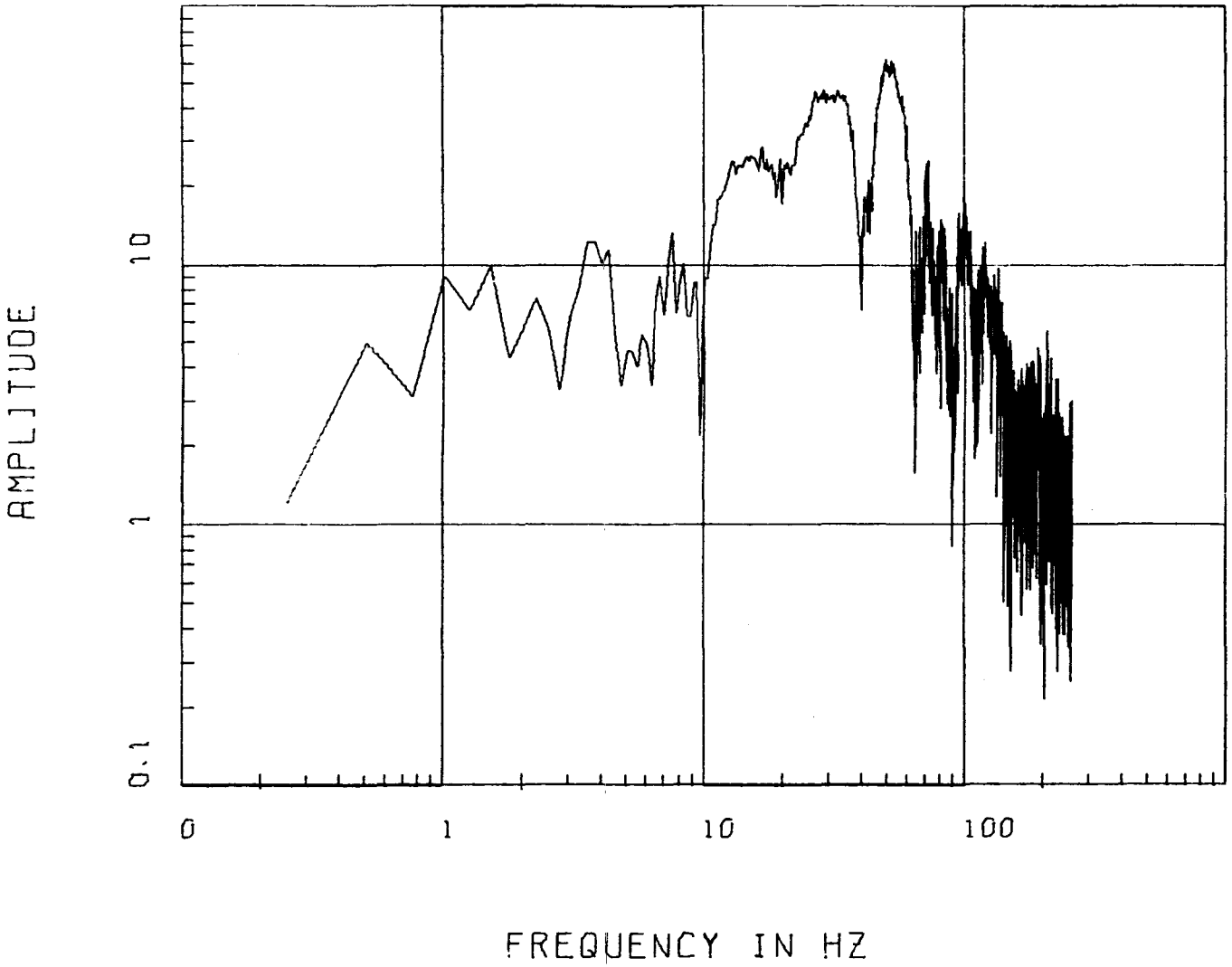

Figure C.3 Frequency response spectrum, Event Dial Pack, Gage 645-10-AV.

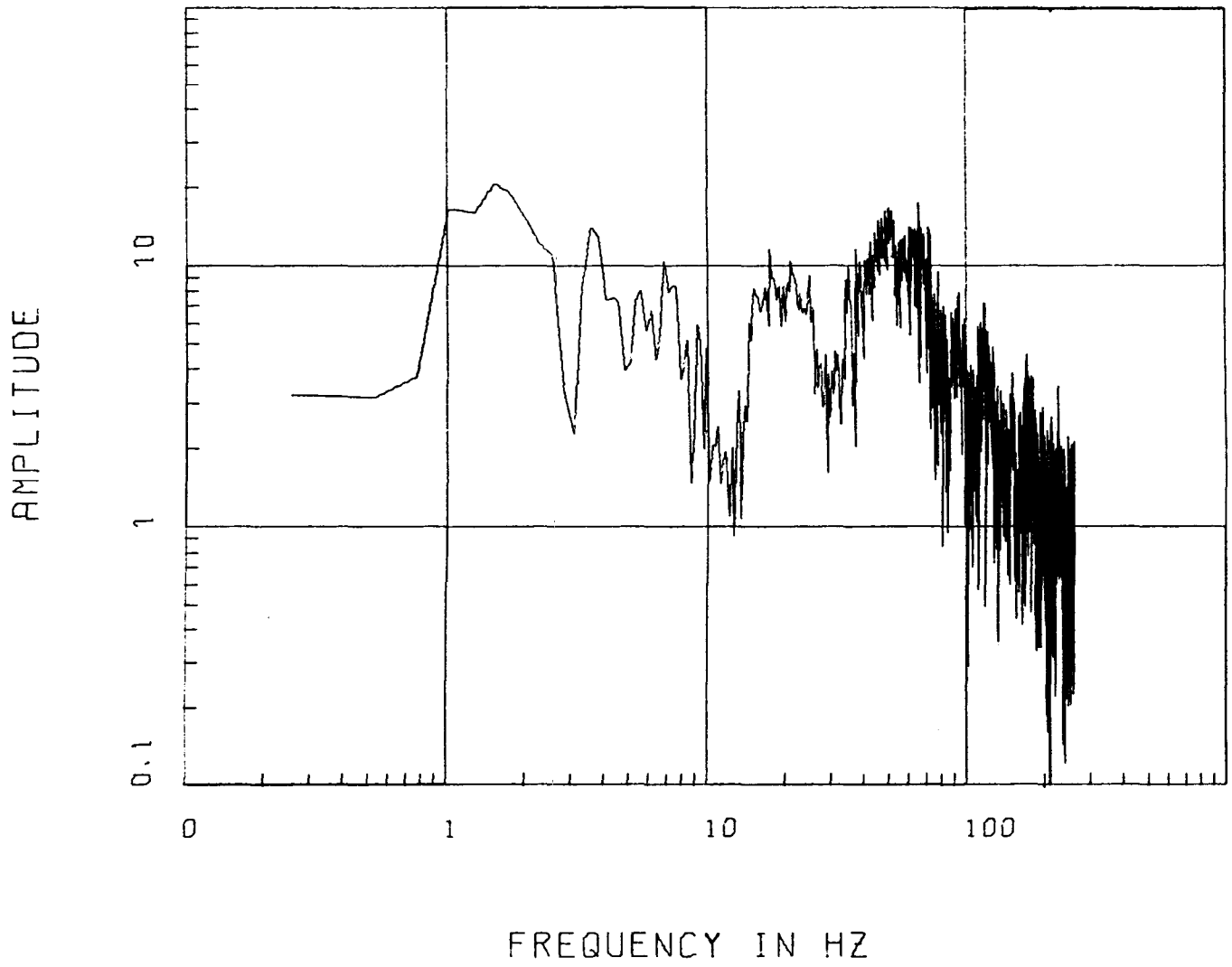

Figure C.4 Frequency response spectrum, Event Dial Pack, Gage 645-10-AH.

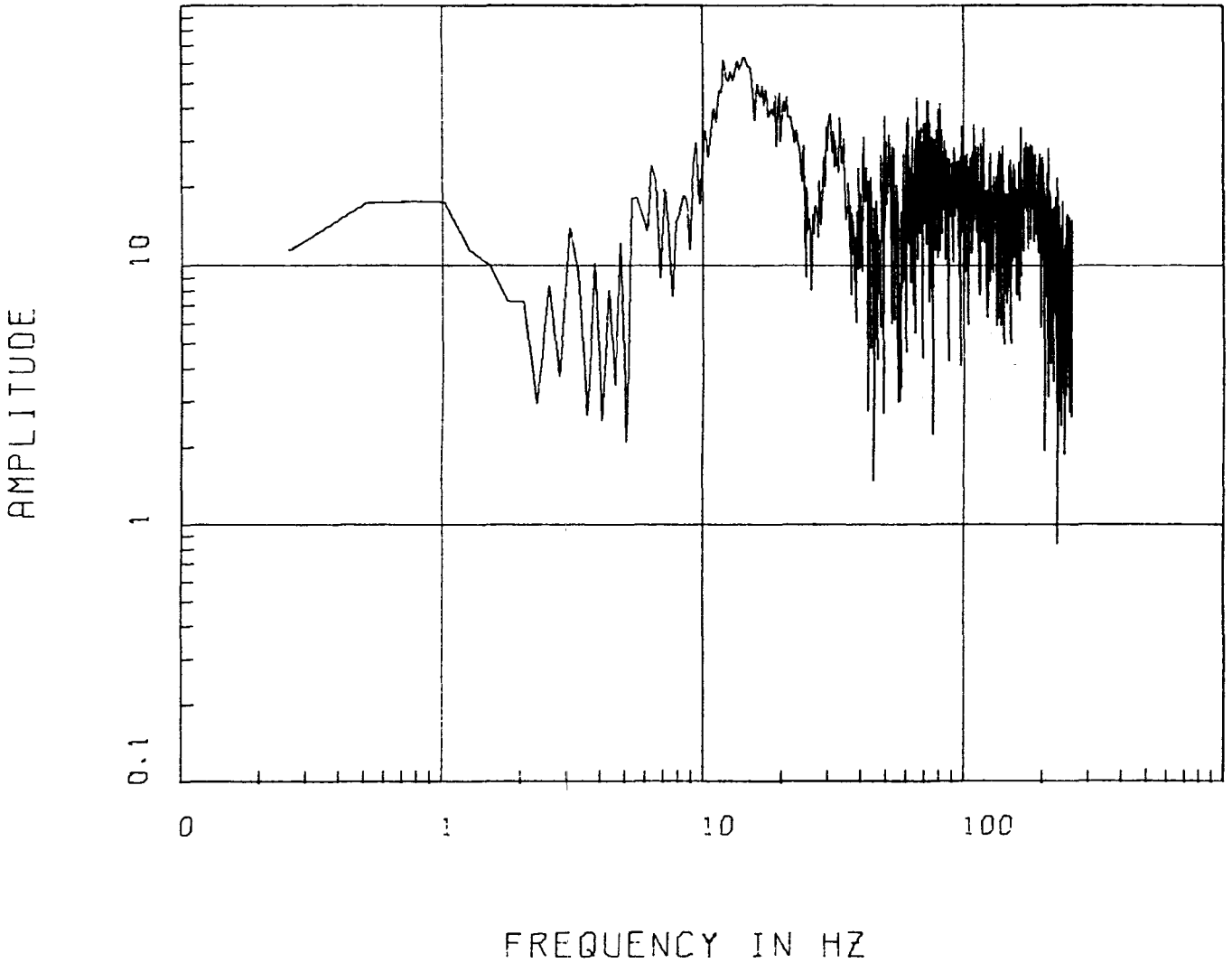

Figure C.5 Frequency response spectrum, Event Dial Pack, Gage 840-1.5-AV.

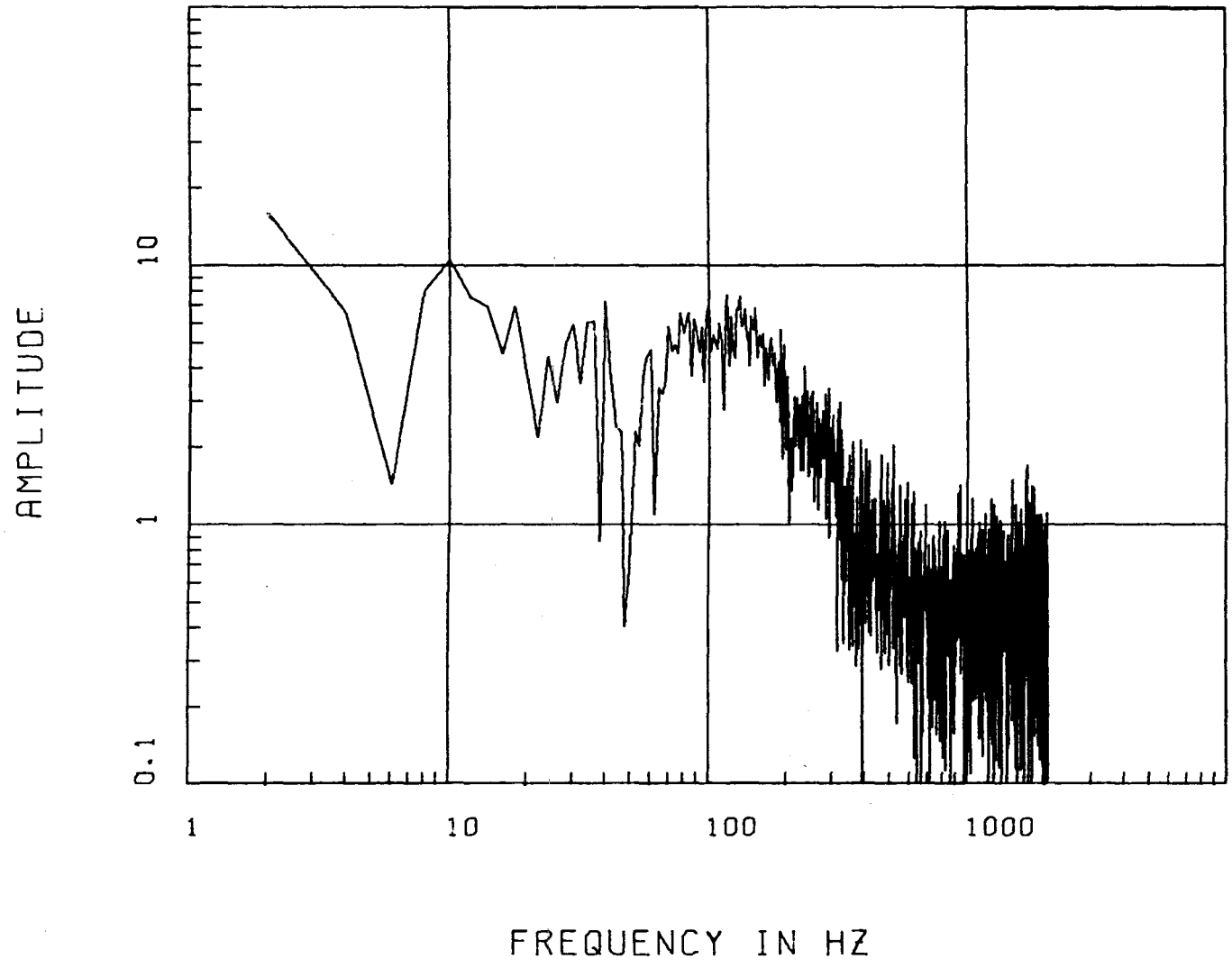

Figure C.6 Frequency response spectrum, Event Dial Pack, Gage 840-1.5-AH.

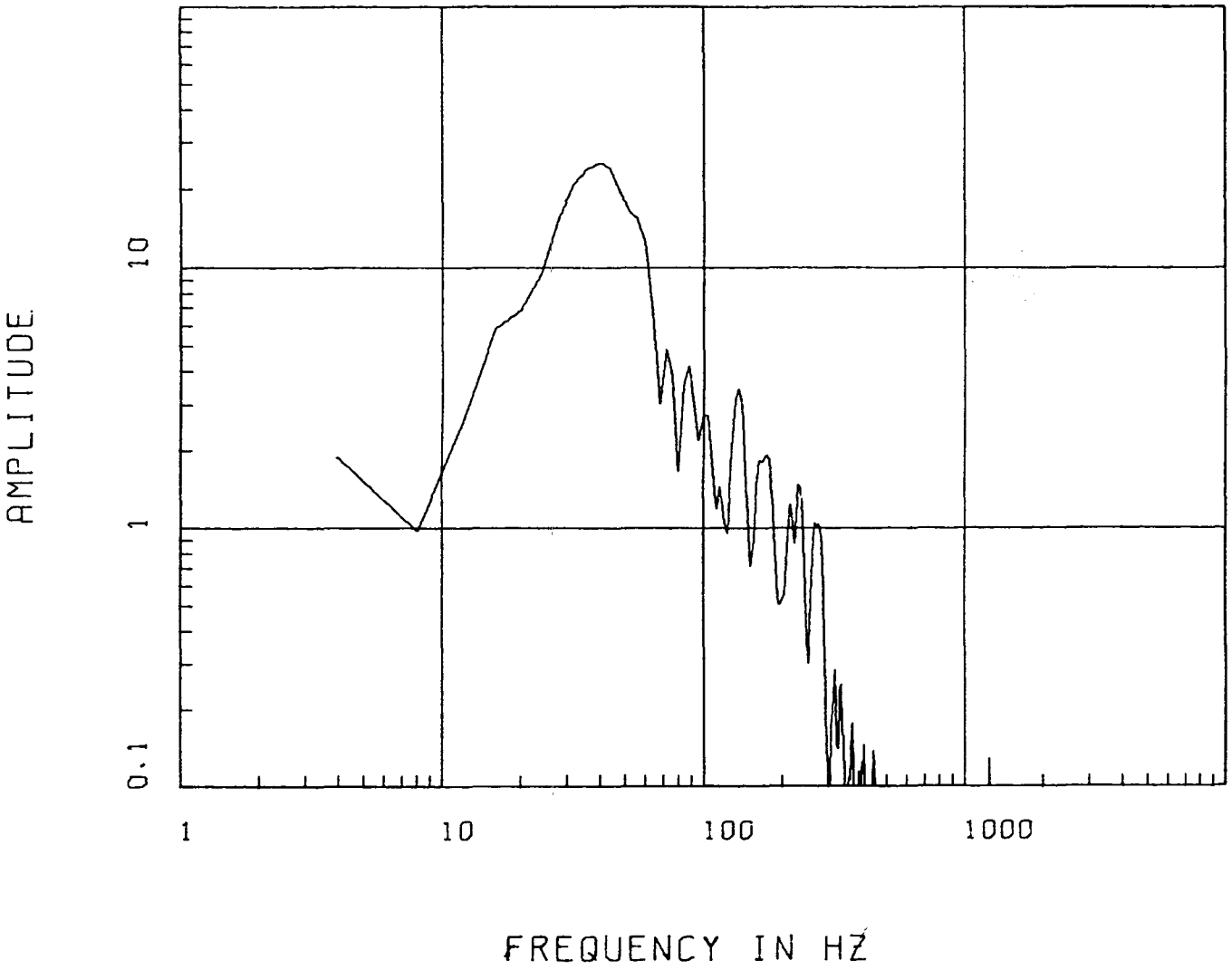

Figure C.7 Frequency response spectrum, Event Dial Pack, Gage 840-20-AV.

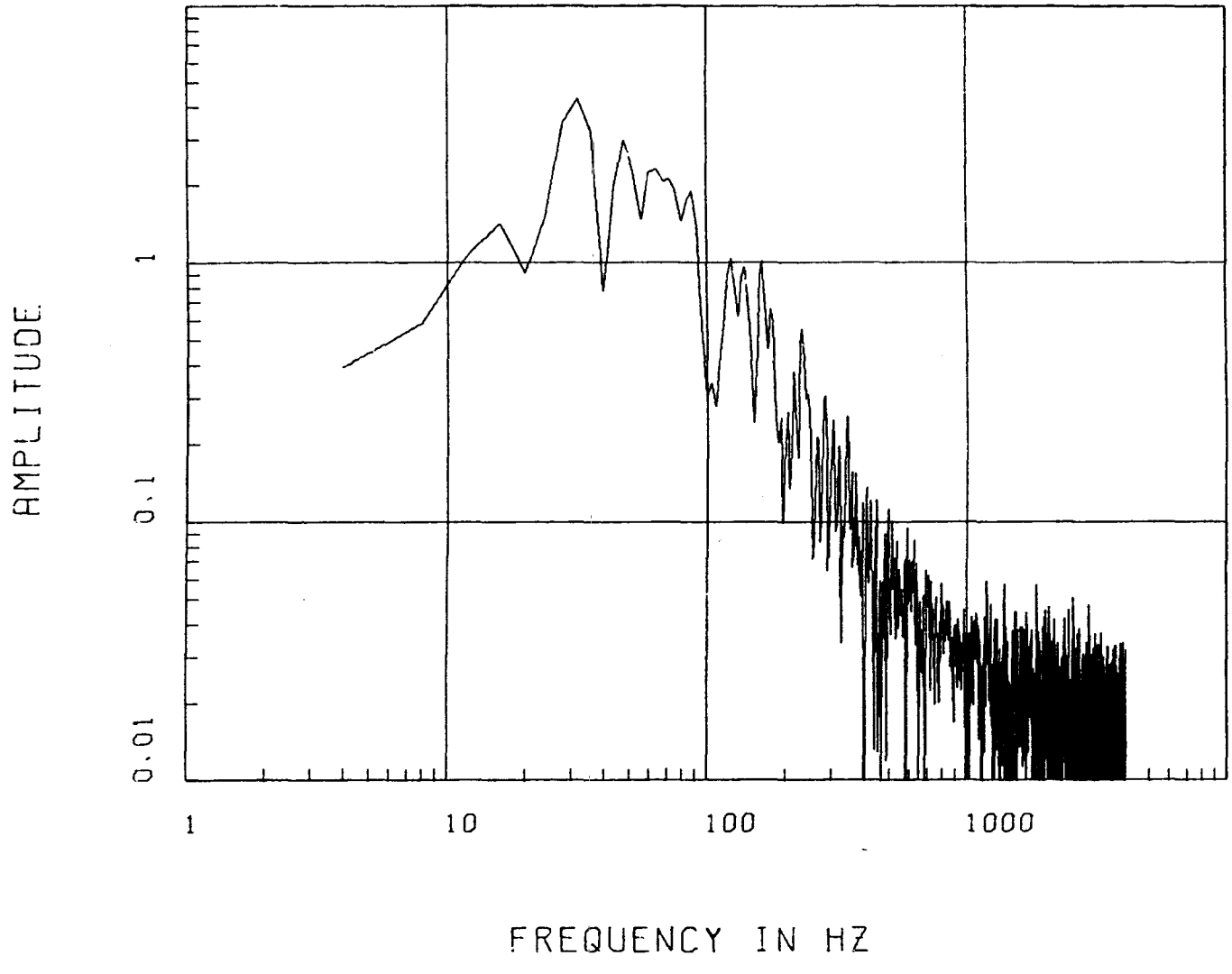

Figure C.8 Frequency response spectrum, Event Dial Pack, Gage 840-20-AH.

Unclassified
Security Classification

DOCUMENT CONTROL DATA - R & D

(Security classification of title, body of abstract and indexing annotation must be entered when the overall report is classified)

1. ORIGINATING ACTIVITY (Corporate author)	2a. REPORT SECURITY CLASSIFICATION
U. S. Army Engineer Waterways Experiment Station Vicksburg, Mississippi	Unclassified
	2b. GROUP

3. REPORT TITLE

OPERATION DIAL PACK, PROJECT LN 305: EARTH MOTION AND STRESS MEASUREMENTS IN THE OUTRUNNING REGION

4. DESCRIPTIVE NOTES (Type of report and inclusive dates)

Final report

5. AUTHOR(S) (First name, middle initial, last name)

Donald W. Murrell

6. REPORT DATE	7a. TOTAL NO. OF PAGES	7b. NO. OF REFS
May 1973	117	10

8a. CONTRACT OR GRANT NO.	9a. ORIGINATOR'S REPORT NUMBER(S)
b. PROJECT NO.	Technical Report N-73-4
c.	9b. OTHER REPORT NO(S) (Any other numbers that may be assigned this report)
d.	

10. DISTRIBUTION STATEMENT

Approved for public release; distribution unlimited.

11. SUPPLEMENTARY NOTES	12. SPONSORING MILITARY ACTIVITY
	U. S. Army Engineer Division, Huntsville Huntsville, Ala.

13. ABSTRACT

The objective of this project was to measure and analyze ground shock in the outrunning region produced by the 500-ton Dial Pack detonation. Motions and stresses were measured at 645- and 840-foot ground ranges at depths of 1.5, 5, 10, and 20 feet. Thirty-one of thirty-two gages produced good records; time histories are included in Appendixes A and B, and frequency response spectra are presented in Appendix C. Peak outrunning accelerations and velocities showed little attenuation over the instrumented range. The vertical peaks did not show any consistent relationship with depth, but the horizontal motions increased with depth. Since the deeper gages were close to the refractive layer, the motions emanating therefrom were stronger at depth. Vertical accelerations were greater than horizontal accelerations by a factor of 4, and vertical velocities showed a tenfold increase over horizontal velocities. Similar patterns of attenuation were noted for the displacements. However, due to additive effects of the airblast-induced motion, horizontal displacements were greater than vertical displacements by a factor of 1.9. Airblast-induced accelerations and velocities were compared with the outrunning motions and were found to be dominant at the 1.5- and 5-foot depths. At the 10- and 20-foot depths, accelerations and velocities from the two sources were about equal.

DD FORM 1 NOV 68 1473 REPLACES DD FORM 1473, 1 JAN 64, WHICH IS OBSOLETE FOR ARMY USE.

Unclassified
Security Classification

14. KEY WORDS	LINK A		LINK B		LINK C	
	ROLE	WT	ROLE	WT	ROLE	WT
Dial Pack (Operation)						
Earth movements						
Explosive effects						
Ground shock calculations						
Stress measurement						